

Nonmyopic Gaussian Process Optimization with Macro-Actions

Dmitrii Kharkovskii, Chun Kai Ling, Bryan Kian Hsiang Low

Abstract—This paper presents a multi-staged approach to nonmyopic adaptive *Gaussian process optimization* (GPO) for *Bayesian optimization* (BO) of unknown, highly complex objective functions that, in contrast to existing nonmyopic adaptive BO algorithms, exploits the notion of macro-actions for scaling up to a further lookahead to match up to a larger available budget. To achieve this, we generalize GP upper confidence bound to a new acquisition function defined w.r.t. a nonmyopic adaptive macro-action policy, which is intractable to be optimized exactly due to an uncountable set of candidate outputs. The contribution of our work here is thus to derive a nonmyopic adaptive ϵ -Bayes-optimal macro-action GPO (ϵ -Macro-GPO) policy. To perform nonmyopic adaptive BO in real time, we then propose an asymptotically optimal anytime variant of our ϵ -Macro-GPO policy with a performance guarantee. We empirically evaluate the performance of our ϵ -Macro-GPO policy and its anytime variant in BO with synthetic and real-world datasets.

Index Terms—Bayesian optimization, Gaussian process.

I. INTRODUCTION

Recent advances in *Bayesian optimization* (BO) have delivered a promising suite of tools for optimizing an unknown (possibly noisy, non-convex, with no closed-form expression/derivative) objective function with a finite budget of function evaluations, as demonstrated in a wide range of applications like automated machine learning, robotics, sensor networks, environmental monitoring, among others [1]. Conventionally, a BO algorithm relies on some choice of acquisition function (e.g., improvement-based such as probability of improvement or *expected improvement* (EI) over currently found maximum, information-based [2], [3], [4], or *upper confidence bound* (UCB) [5]) as a heuristic to guide its search for the global maximum. To do this, the BO algorithm exploits the chosen acquisition function to repeatedly select an input for evaluating the unknown objective function that trades off between observing a likely maximum based on a GP belief of the unknown objective function (exploitation) vs. improving the GP belief (exploration) until the budget is expended.

Unfortunately, such a conventional BO algorithm is greedy/myopic and hence performs suboptimally with respect to the given finite budget¹. To be nonmyopic, its policy to

select the next input has to additionally account for its subsequent selections of inputs for evaluating the unknown objective function². Perhaps surprisingly, this can be partially achieved by batch BO algorithms capable of *jointly*³ optimizing a batch of inputs [12], [13], [14], [15] because their selection of each input has to account for that of all other inputs of the batch⁴. However, since the batch size is typically set to be much smaller than the given budget, they have to repeatedly select the next batch greedily. Furthermore, unlike the conventional BO algorithm described above, their selection of each input is independent of the outputs observed from evaluating the objective function at the other selected inputs of the batch, thus sacrificing some degree of adaptivity. Hence, they also perform suboptimally with respect to the given budget.

Some nonmyopic adaptive BO algorithms [16], [17], [18], [19], [20] have been developed to combine the best of both worlds. But, they have been empirically demonstrated to be effective and tractable for at most a lookahead of 5 observations which is usually much less than the size of the available budget in practice, thus causing them to behave myopically in this case. To increase the lookahead, the work of [21] has proposed a two-staged approach that utilizes a *greedy* batch BO algorithm³ in its second stage to efficiently but myopically optimize all but the first input afforded by the budget. Note that the above works on nonmyopic adaptive BO do not provide theoretical performance guarantees except for that of [18]. The challenge therefore remains in devising a multi-staged approach to nonmyopic adaptive BO that can empirically scale well to a further lookahead (and hence match up to a larger budget) and still be amenable to a theoretical analysis of its performance, which is the focus of our work here.

To address this challenge, we exploit the notion of macro-actions (i.e., each denoting a sequence of primitive actions executed in full without considering any observation taken after performing each primitive action in the sequence) inherent to the structure of several real-world task environments/applications such as environmental sensing and monitoring, mobile sensor networks, and robotics. Some examples are given below and described in detail in Section IV:

- (a) In monitoring of algal bloom in the coastal ocean, an *autonomous underwater vehicle* (AUV) is deployed on

²Fig. 1 shows how a nonmyopic BO algorithm can outperform a myopic one.

³In contrast, a *greedy* batch BO algorithm [8], [9], [10], [11] selects the inputs of a batch one at a time myopically.

⁴Batch BO is traditionally considered when resources are available to evaluate the objective function in parallel. We suggest a further possibility of using batch BO for non-myopic selections of inputs here.

D. Kharkovskii and B. K. H. Low are with the Department of Computer Science, National University of Singapore, Republic of Singapore (email: dmitrkha@comp.nus.edu.sg, lowkh@comp.nus.edu.sg).

C. K. Ling is with the Department of Computer Science, Carnegie Mellon University, Pittsburgh, PA 15213, USA (e-mail: chunkail@cs.cmu.edu).

¹Acquisition functions like EI [6], [7] and UCB [5] offer theoretical guarantees for the convergence rate of their BO algorithms (i.e., in the limit) via regret bounds. In practice, since the budget is limited, such bounds are suboptimal as they cannot be specified to be arbitrarily small.

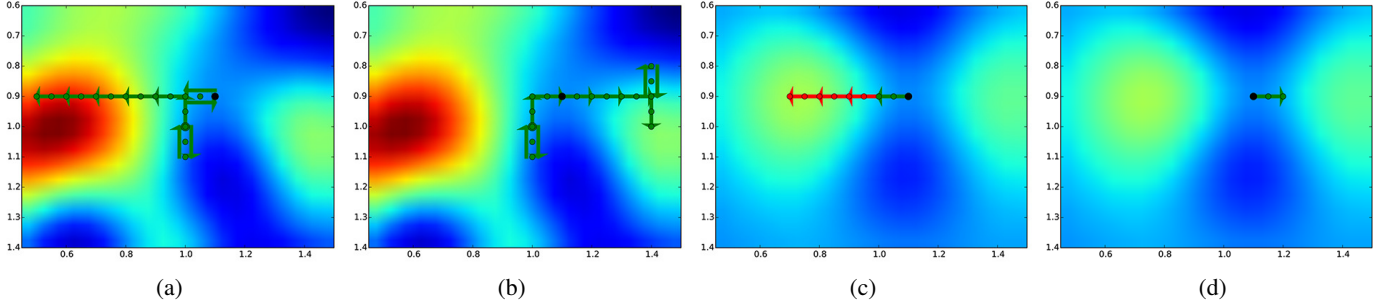


Fig. 1. Illustrating the behaviors of (a) our nonmyopic ϵ -Macro-GPO policy with a lookahead of 8 observations ($H = 4$, $N = 1$) vs. (b) greedy/myopic DB-GP-UCB [13] with macro-action length $\kappa = 2$ and budget of 20 observations in controlling an AUV to gather observations for finding a hotspot (i.e., global maximum) in a simulated plankton density phenomenon (Section IV). Prior observations are at the AUV’s initial starting input location (blue circle) and buoy’s location $(0, 0)$ (not shown here). Up till $t = 5$, both ϵ -Macro-GPO and DB-GP-UCB produce the same trajectories to reach the input location denoted by a black circle. Figs. c & d plot maps of GP posterior mean (1) over the phenomenon at stage $t = 5$. (c) Since ϵ -Macro-GPO is able to look ahead and plan its macro-actions in the later planning stages (red arrows) to reach the region containing the global maximum, it moves the UAV left towards the global maximum. (d) On the other hand, DB-GP-UCB moves the UAV right towards the local maximum. So, by utilizing lookahead, our nonmyopic ϵ -Macro-GPO policy can outperform the myopic DB-GP-UCB.

board a research vessel in search for a hotspot of peak phytoplankton abundance and tasked to take dives from the vessel to gather “Gulper” water samples for on-deck testing that can be cast as macro-actions [22];

- (b) In servicing the mobility demands within an urban city, an autonomous robotic vehicle in a mobility-on-demand system cruises along different road trajectories abstracted as macro-actions to find a hotspot of highest mobility demand to pick up a user [23];
- (c) In monitoring of the indoor environmental quality of an office environment [24], a mobile robot mounted with a weather board is tasked to find a hotspot of peak temperature by exploring different stretches of corridors that can be naturally abstracted into macro-actions. This setting is visually illustrated in Fig. 2;
- (d) In monitoring of algal bloom in the coastal ocean, an underwater glider is tasked to find a hotspot of peak chlorophyll fluorescence by optimizing its search trajectory tractably over simple ellipses of varying sizes [25] that constitute different macro-actions.

Macro-actions have in fact been well-studied and used by the planning community to scale up algorithms for planning under uncertainty to a further lookahead [26], [27], [28], which is realized from a much reduced space of possible sequences of primitive actions (i.e., macro-actions) induced by the structure of the task environment/application. Macro-actions are also studied in reinforcement learning community but named as options instead [29], [30], [31].

The use of macro-actions in the context of nonmyopic adaptive BO poses an interesting research question: *How can an acquisition function be defined with respect to a nonmyopic adaptive macro-action⁵ policy and optimized tractably to yield such a policy with a provable performance guarantee for a given finite budget?*

The main technical difficulty in answering this question stems from the need to account for the correlation of outputs to be observed from evaluating the unknown objective function

⁵In BO, each macro-action denotes a sequence of inputs for evaluating the unknown objective function.

at inputs found within a macro-action and between different macro-actions (Section III). Such a correlation structure is the chief ingredient to be exploited for selecting informative observations to find the global maximum.

This paper presents a principled multi-staged Bayesian sequential decision problem framework for nonmyopic adaptive *GP optimization* (GPO) (Section III) that, in particular, exploits macro-actions inherent to the structure of several real-world task environments/applications for scaling up to a further lookahead (as compared to the existing nonmyopic adaptive BO algorithms discussed above [17], [16], [18], [19], [20]) to match up to a larger available budget. To achieve this, we first generalize GP-UCB [5] to a new acquisition function defined with respect to a nonmyopic adaptive macro-action policy, which, unfortunately, is intractable to be optimized exactly due to an uncountable set of candidate outputs. The key novel contribution of our work here is to show that it is in fact possible to solve for a nonmyopic adaptive ϵ -Bayes-optimal macro-action GPO (ϵ -Macro-GPO) policy given an arbitrarily user-specified loss bound ϵ via stochastic sampling in each planning stage which requires only a polynomial number of samples in the length of macro-actions⁶. To perform nonmyopic adaptive BO in real time, we then propose an asymptotically optimal anytime variant of our ϵ -Macro-GPO policy with a performance guarantee. We empirically evaluate the performance of our nonmyopic adaptive ϵ -Macro-GPO policy and its anytime variant in BO with synthetic and real-world datasets (Section IV).

II. MODELING SPATIALLY VARYING PHENOMENA WITH GAUSSIAN PROCESSES

To simplify exposition of our work here, we will assume the task environment to be a spatially varying phenomenon (e.g., indoor environmental quality of an office environment, plankton bloom in the ocean, mobility demand within an urban

⁶In contrast, though the nonmyopic adaptive BO algorithm of [18] based on deterministic sampling can be naively generalized to exploit macro-actions, it requires an exponential number of samples per planning stage, as detailed in Remark 3.

city, as described in Section I). A mobile sensing agent utilizes our proposed nonmyopic adaptive ϵ -Macro-GPO policy or its anytime variant to select and gather observations from the task environment for finding the global maximum.

A. Notations and Preliminaries

Let \mathcal{S} be the domain of a spatially varying phenomenon corresponding to a set of input locations. In every stage $t > 0$, the agent executes one of the available macro-actions of length κ at its current input location by deterministically moving through a sequence of κ input locations, denoted by a vector $s_t \in \mathcal{A}(s_{t-1})$, and observes the corresponding output measurements $z_t \in \mathbb{R}^\kappa$, where $\mathcal{A}(s_{t-1}) \subseteq \mathcal{S}^\kappa$ denotes a finite set of available macro-actions at the agent's current input location. Note that $\mathcal{A}(s_{t-1})$ depends on the agent's current input location which corresponds to the last component of macro-action s_{t-1} executed in the previous stage $t-1$. These notations are visually illustrated in Fig. 2 and its caption b. The state of the agent at its initial starting input location is represented by prior observations/data $d_0 \triangleq \langle s_0, z_0 \rangle$ available before planning where s_0 and z_0 denote, respectively, vectors comprising input locations visited and corresponding output measurements observed by the agent prior to planning. The agent's initial starting input location is the last component of s_0 . In stage $t > 0$, the state of the agent is represented by observations/data $d_t \triangleq \langle s_t, z_t \rangle$ where $s_t \triangleq s_0 \oplus \dots \oplus s_t$ and $z_t \triangleq z_0 \oplus \dots \oplus z_t$ denote, respectively, vectors comprising input locations visited and corresponding output measurements observed by the agent up till stage t and ' \oplus ' denotes vector concatenation.

B. Gaussian Process (GP)

The spatially varying phenomenon is modeled as a realization of a GP: Each input location $s \in \mathcal{S}$ is associated with an output measurement y_s . Let $y_{\mathcal{S}} \triangleq \{y_s\}_{s \in \mathcal{S}}$ denote a GP, that is, every finite subset of $y_{\mathcal{S}}$ has a multivariate Gaussian distribution. Then, the GP is fully specified by its prior mean $\mu_s \triangleq \mathbb{E}[y_s]$ (we assume w.l.o.g. that $\mu_s = 0$ for all $s \in \mathcal{S}$) and covariance $\sigma_{ss'} \triangleq \text{cov}[y_s, y_{s'}]$ for all $s, s' \in \mathcal{S}$, the latter of which characterizes the spatial correlation structure of the phenomenon. For example, $\sigma_{ss'}$ can be defined by the commonly-used squared exponential covariance function $\sigma_{ss'} \triangleq \sigma_y^2 \exp\{-0.5(s-s')^\top \Gamma^{-2}(s-s')\}$ where σ_y^2 is the signal variance controlling the intensity of output measurements and Γ is a diagonal matrix with length-scale components ℓ_1 and ℓ_2 controlling the spatial correlation or "similarity" between output measurements in the respective east-west and north-south directions of the 2D phenomenon.

All output measurements observed by the agent are corrupted by an additive noise ε , i.e., $z_{i,j} \triangleq y_{s_{i,j}} + \varepsilon$ for stage $i = 0, \dots, t$ and $j = 1, \dots, \kappa$ where $s_{i,j}$ is the j -th input location of macro-action s_i at stage i , $z_{i,j}$ is the corresponding output measurement and $\varepsilon \sim \mathcal{N}(0, \sigma_n^2)$ with the noise variance σ_n^2 . Supposing the agent has gathered observations $d_t = \langle s_t, z_t \rangle$ from stages 0 to t , the GP model can exploit these observations d_t to perform probabilistic regression by providing a Gaussian posterior belief $p(z_{t+1}|s_{t+1}, d_t) = \mathcal{N}(\mu_{s_{t+1}|d_t}, \Sigma_{s_{t+1}|d_t})$ of

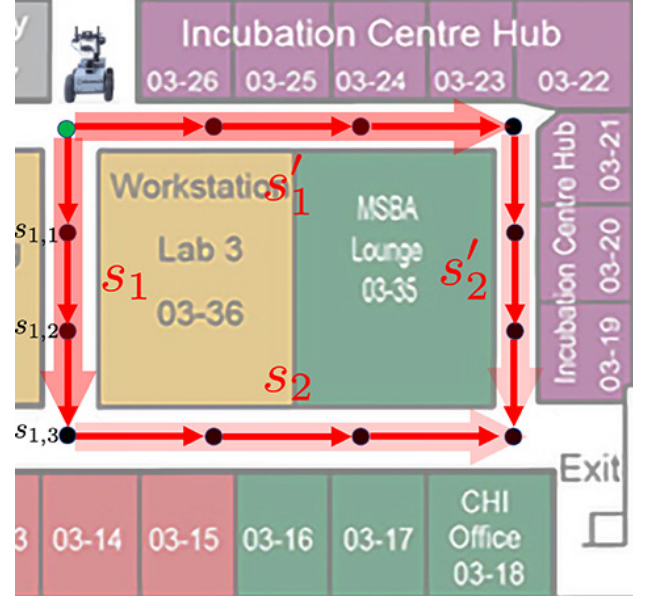


Fig. 2. Example of monitoring indoor environmental quality of an office environment [24]: (a) A mobile robot mounted with a weather board is tasked to find a hotspot of peak temperature by exploring different stretches of corridors that can be naturally abstracted into macro-actions. (b) In stage $t = 1$, the robot is at its initial starting input location (green dot). It can decide to execute macro-action s_1 (translucent red arrow), which is a sequence of $\kappa = 3$ primitive actions (opaque red arrows) moving it through a sequence of $\kappa = 3$ input locations (black dots) to arrive at input location $s_{1,3}$. So, $s_1 \triangleq (s_{1,1}, s_{1,2}, s_{1,3})$. (c) To derive a myopic Macro-GPO or ϵ -Macro-GPO policy with $H = 1$, the last stages of Bellman equations in (5)-(9) require macro-actions s_1 and s_1' as inputs. To derive a nonmyopic one with $H = 2$, they require macro-action sequences $s_1 \oplus s_2$ and $s_1' \oplus s_2'$ as inputs instead.

noisy output measurements for any κ input locations $s_{t+1} \subset \mathcal{S}$ with the following posterior mean vector and covariance matrix, respectively [32]:

$$\begin{aligned} \mu_{s_{t+1}|d_t} &\triangleq \Sigma_{s_{t+1}s_t} \Sigma_{s_t s_t}^{-1} z_t^\top, \\ \Sigma_{s_{t+1}|s_t} &\triangleq \Sigma_{s_{t+1}s_{t+1}} - \Sigma_{s_{t+1}s_t} \Sigma_{s_t s_t}^{-1} \Sigma_{s_t s_{t+1}} \end{aligned} \quad (1)$$

where $\Sigma_{s_{t+1}s_t}$ is a matrix with covariance components $\sigma_{ss'}$ for every input location s of s_{t+1} and s' of s_t , $\Sigma_{s_t s_{t+1}}$ is the transpose of $\Sigma_{s_{t+1}s_t}$, and $\Sigma_{s_t s_t}$ ($\Sigma_{s_{t+1}s_{t+1}}$) is a matrix with covariance components $\sigma_{ss'} + \sigma_n^2 \delta_{ss'}$ for every pair of input locations s, s' of s_t (s_{t+1}) and $\delta_{ss'}$ is a Kronecker delta of value 1 if $s = s'$, and 0 otherwise. A key property of the GP model is that, different from $\mu_{s_{t+1}|d_t}$, $\Sigma_{s_{t+1}|s_t}$ is independent of the output measurements z_t .

III. ϵ -BAYES-OPTIMAL MACRO-GPO

A. Problem Formulation

To cast nonmyopic adaptive macro-action GP optimization (Macro-GPO) as a Bayesian sequential decision problem, we define a nonmyopic adaptive macro-action policy π to sequentially decide in each stage t the next macro-action $\pi(d_t) \in \mathcal{A}(s_t)$ to be executed for gathering κ new observations based on the current observations d_t over a finite planning horizon of H stages (i.e., a lookahead of κH observations). The goal of the agent is to plan/decide its macro-actions to

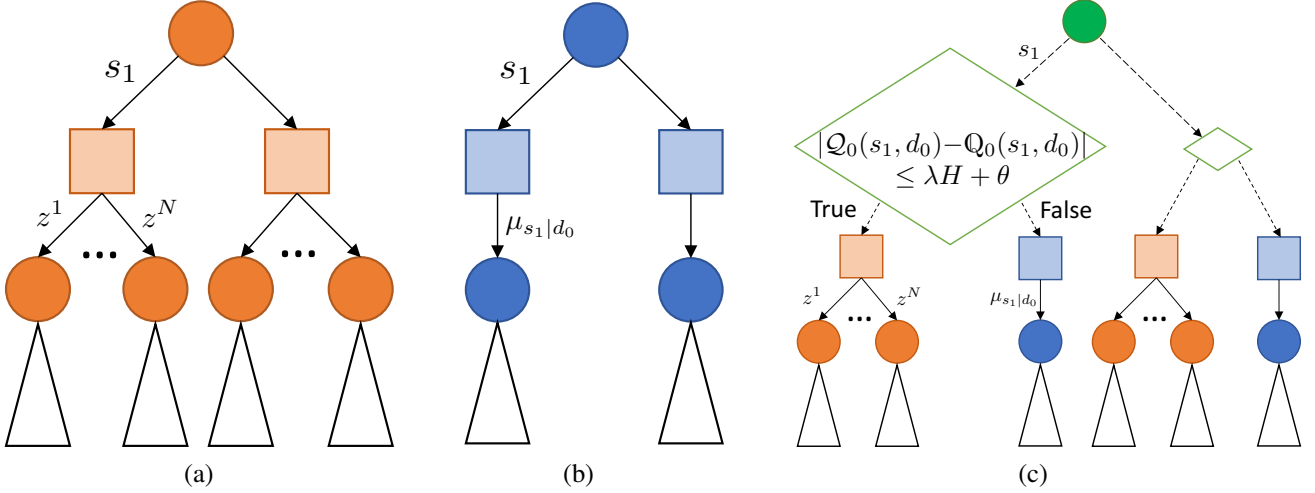


Fig. 3. Visual illustrations of policies induced by (a) stochastic sampling (6), (b) most likely observations (8), and (c) our ϵ -Macro-GPO policy π^ϵ (9). Circles denote nodes d_t and squares denote nodes $\langle s_{t+1}, \mathbf{z}_t \rangle$.

visit input locations $\mathbf{s}_H \triangleq s_1 \oplus \dots \oplus s_H$ with the maximum total corresponding output measurements

$$\mathbf{1}^\top \mathbf{z}_H = \sum_{t=1}^H \mathbf{1}^\top \mathbf{z}_t = \sum_{t=1}^H \sum_{i=1}^{\kappa} z_{t,i}$$

or, equivalently, minimum cumulative regret where $\mathbf{z}_H \triangleq z_1 \oplus \dots \oplus z_H$ and $\mathbf{z}_t \triangleq (z_{t,1}, \dots, z_{t,\kappa})$. However, since only the prior observations/data d_0 are known, the Macro-GPO problem involves finding a nonmyopic adaptive macro-action policy π to select input locations \mathbf{s}_H to be visited by the agent with the maximum *expected* total corresponding output measurements $\mathbb{E}_{\mathbf{z}_H|d_0, \pi}[\mathbf{1}^\top \mathbf{z}_H]$ instead.

Supposing the size of the available budget in a real-world task environment exceeds the lookahead of κH observations, it can afford a *stronger exploration behavior* by including an additional weighted exploration term $\beta \mathbb{I}[y_S; \mathbf{z}_H | d_0, \pi]$; its effect on BO performance is empirically investigated in Section IV. The conditional mutual information $\mathbb{I}[y_S; \mathbf{z}_H | d_0, \pi]$ here can be interpreted as the information gain on the phenomenon over the entire domain \mathcal{S} (i.e., equivalent to y_S) from gathering observations $\langle \mathbf{s}_H, \mathbf{z}_H \rangle$ selected according to the nonmyopic adaptive macro-action policy π given the prior data d_0 . Then, the acquisition function w.r.t. a nonmyopic adaptive macro-action policy π when starting in d_0 and following π thereafter can be defined as

$$V_0^\pi(d_0) \triangleq \mathbb{E}_{\mathbf{z}_H|d_0, \pi}[\mathbf{1}^\top \mathbf{z}_H] + \beta \mathbb{I}[y_S; \mathbf{z}_H | d_0, \pi]. \quad (2)$$

Applying the chain rule for mutual information and a few other information-theoretic results to (2) yields the following H -stage Bellman equations (Appendix F):

$$\begin{aligned} V_t^\pi(d_t) &\triangleq Q_t^\pi(\pi(d_t), d_t), \\ Q_t^\pi(s_{t+1}, d_t) &\triangleq R(s_{t+1}, d_t) + \\ &\quad \mathbb{E}_{\mathbf{z}_{t+1}|s_{t+1}, d_t} [V_{t+1}^\pi(\langle s_{t+1}, \mathbf{z}_{t+1} \rangle)] \end{aligned} \quad (3)$$

for stages $t = 0, \dots, H-1$ where $V_H^\pi(d_H) \triangleq 0$ and

$$R(s_{t+1}, d_t) \triangleq \mathbf{1}^\top \mu_{s_{t+1}|d_t} + 0.5\beta \log |I + \sigma_n^{-2} \Sigma_{s_{t+1}|\mathbf{s}_t}|. \quad (4)$$

To solve the Macro-GPO problem, Bayes-optimality⁷ is exploited to select input locations to be visited by the agent that maximize the expected total corresponding output measurements (and, if the budget can afford, the additional weighted exploration term representing the information gain on the phenomenon) with respect to all possible induced sequences of future GP posterior beliefs $p(z_{t+1}|s_{t+1}, d_t)$ for $t = 0, \dots, H-1$. Formally, this involves choosing a nonmyopic adaptive macro-action policy π to maximize $V_0^\pi(d_0)$, which we call the Bayes-optimal Macro-GPO policy π^* . That is,

$$V_0^*(d_0) \triangleq V_0^{\pi^*}(d_0) = \max_{\pi} V_0^\pi(d_0).$$

Plugging π^* into $V_t^\pi(d_t)$ and $Q_t^\pi(s_{t+1}, d_t)$ (3) gives

$$\begin{aligned} V_t^*(d_t) &\triangleq \max_{s_{t+1} \in \mathcal{A}(s_t)} Q_t^*(s_{t+1}, d_t), \\ Q_t^*(s_{t+1}, d_t) &\triangleq R(s_{t+1}, d_t) + \\ &\quad \mathbb{E}_{\mathbf{z}_{t+1}|s_{t+1}, d_t} [V_{t+1}^*(\langle s_{t+1}, \mathbf{z}_{t+1} \rangle)] \end{aligned} \quad (5)$$

for stages $t = 0, \dots, H-1$ where $V_H^*(d_H) \triangleq 0$.⁸ When the lookahead of κH observations matches up to the available budget, the Bayes-optimal Macro-GPO policy π^* can naturally trade off between exploration vs. exploitation without needing the additional weighted exploration term in (2) or (4) (i.e., $\beta = 0$): Its selected macro-action $\pi^*(d_t) = \operatorname{argmax}_{s_{t+1} \in \mathcal{A}(s_t)} Q_t^*(s_{t+1}, d_t)$ in each stage t has to trade off between exploiting the current GP posterior belief $p(z_{t+1}|\pi^*(d_t), d_t)$ to maximize the expected total corresponding output measurements $R(\pi^*(d_t), d_t) = \mathbf{1}^\top \mu_{\pi^*(d_t)|d_t}$ vs. improving the GP posterior belief of the phenomenon (i.e., exploration) so as to maximize the expected total output

⁷Bayes-optimality is previously studied in discrete *Bayesian reinforcement learning* (BRL) [33] but its assumed discrete-valued output measurements and Markov property do not hold in Macro-GPO. Continuous BRLs [34], [35] assume a known parametric observation function, the reward function to be independent of output measurements and previous input locations, and/or, when using GP, the most likely observations during planning with no performance guarantee.

⁸To understand the effect of H on how much macro-action sequence information are required as inputs to the Bellman equations in (5)-(9), refer to Fig. 2 and its caption c for a visual illustration.

measurements $\mathbb{E}_{z_{t+1}|\pi^*(d_t), d_t} [V_{t+1}^*(\langle \mathbf{s}_t \oplus \pi^*(d_t), \mathbf{z}_t \oplus z_{t+1} \rangle)]$ in the later stages.

When the available budget is larger than the lookahead of κH observations, it can afford a *stronger exploration behavior* by setting a positive weight $\beta > 0$ on the exploration term $0.5 \log |I + \sigma_n^{-2} \Sigma \pi^*(d_t)|_{\mathbf{s}_t}|$ in (4); its effect on BO performance is empirically investigated in Section IV. This exploration term can be interpreted as the information gain $\mathbb{I}[y_S; z_{t+1}|d_t, \pi^*(d_t)]$ on the phenomenon (Appendix F) from executing the macro-action $\pi^*(d_t)$ to gather κ new observations. As such, the macro-action $\pi^*(d_t)$ can gain more information on the phenomenon (larger exploration term) by gathering observations with higher uncertainty (larger individual posterior variance) but lower correlation (smaller magnitude of posterior covariance) between them.

B. ϵ -Bayes-Optimal Macro-GPO (ϵ -Macro-GPO)

In general, the Bayes-optimal Macro-GPO policy π^* cannot be derived exactly because the expectation term in (5) (and hence Q_t^* and V_t^*) often cannot be evaluated in closed form due to an uncountable set of candidate output measurements.

To resolve this issue, we will exploit the following result on the Lipschitz continuity of $R(s_{t+1}, d_t)$ (4) and consequently of $V_t^*(d_t)$ (5) in the realized output measurements \mathbf{z}_t (see Appendices G and H for their respective proofs) to tractably derive a nonmyopic adaptive ϵ -Macro-GPO policy π^ϵ whose expected performance loss is theoretically guaranteed to be not more than an arbitrarily user-specified loss bound ϵ :

Lemma 1. Let $\alpha(s_{t+1}) \triangleq \|\Sigma_{s_{t+1}\mathbf{s}_t} \Sigma_{\mathbf{s}_t\mathbf{s}_t}^{-1}\|_F$ and $d'_t \triangleq \langle \mathbf{s}_t, \mathbf{z}'_t \rangle$. Then,

$$|R(s_{t+1}, d_t) - R(s_{t+1}, d'_t)| \leq \sqrt{\kappa} \alpha(s_{t+1}) \|\mathbf{z}_t - \mathbf{z}'_t\|.$$

Preliminary to the design and construction of our proposed nonmyopic adaptive ϵ -Macro-GPO policy π^ϵ is the approximation of the expectation term in (5) for each candidate macro-action s_{t+1} in every stage using *stochastic* sampling of N i.i.d. multivariate Gaussian vectors z^1, \dots, z^N from the GP posterior belief $p(z_{t+1}|s_{t+1}, d_t)$ (1), as illustrated in Fig. 3a:

$$\begin{aligned} \mathcal{V}_t(d_t) &\triangleq \max_{s_{t+1} \in \mathcal{A}(s_t)} Q_t(s_{t+1}, d_t), \\ Q_t(s_{t+1}, d_t) &\triangleq R(s_{t+1}, d_t) + \frac{1}{N} \sum_{\ell=1}^N \mathcal{V}_{t+1}(\langle \mathbf{s}_{t+1}, \mathbf{z}_t \oplus z^\ell \rangle) \end{aligned} \quad (6)$$

for stages $t = 0, \dots, H-1$ where $\mathcal{V}_H(d_H) \triangleq 0$.⁸ We prove in Appendix I that $Q_t(s_{t+1}, d_t)$ (6) can approximate $Q_t^*(s_{t+1}, d_t)$ (5) arbitrarily closely for all s_{t+1} with a high probability of at least $1-\delta$ requiring only a polynomial number N of samples in the macro-action length κ (10) per planning stage:

Theorem 1. Suppose that the observations d_t , $H \in \mathbb{Z}^+$, a budget of $\kappa(H-t)$ input locations for $t = 0, \dots, H-1$, $\delta \in (0, 1)$, and $\lambda > 0$ are given. Then, the probability of

$$|Q_t(s_{t+1}, d_t) - Q_t^*(s_{t+1}, d_t)| \leq \lambda H$$

for all $s_{t+1} \in \mathcal{A}(s_t)$ is at least $1-\delta$ by setting

$$N = \mathcal{O}((\kappa^{2H}/\lambda^2) \log(\kappa A/(\delta \lambda))) \quad (7)$$

where A is the largest number of candidate macro-actions available in any input location.

Remark 1. Since $|\mathcal{V}_t(d_t) - V_t^*(d_t)| \leq \max_{s_{t+1} \in \mathcal{A}(s_t)} |Q_t(s_{t+1}, d_t) - Q_t^*(s_{t+1}, d_t)|$, it immediately follows from Theorem 1 that the probability of $|\mathcal{V}_t(d_t) - V_t^*(d_t)| \leq \lambda H$ is at least $1-\delta$.

Remark 2. It can be observed from Theorem 1 that the number N (7) of stochastic samples increases¹⁰ with (a) a tighter bound λ on the error $|Q_t(s_{t+1}, d_t) - Q_t^*(s_{t+1}, d_t)|$ due to stochastic sampling, (b) a higher probability $1-\delta$ of Q_t (6) approximating Q_t^* (5) closely, (c) a larger number A of candidate macro-actions, and (d) a greater macro-action length κ .

Deriving the above probabilistic bound usually requires using a concentration inequality involving independent Gaussian random variables. However, the components of the multivariate Gaussian random vector z_{t+1} in (5) are *correlated* output measurements corresponding to the κ input locations found within the candidate macro-action s_{t+1} . To resolve this complication, we exploit a change of variables trick (i.e., to make the components independent) and the Lipschitz continuity of $R(s_{t+1}, d_t)$ (Lemma 1) for enabling the use of the Tsirelson-Ibragimov-Sudakov inequality [36] to prove the probabilistic bound in Theorem 1, as shown in Appendix I.

Theorem 1, however, only entails probabilistic bounds on how far $\mathcal{V}_t(d_t)$ (6) is from $V_t^*(d_t)$ (5) (see Remark 1) and on the resulting policy loss. We will prove a stronger non-trivial result: In the unlikely event (with an arbitrarily small probability of at most δ) that $Q_t(s_{t+1}, d_t)$ (6) is unboundedly far from $Q_t^*(s_{t+1}, d_t)$ (5) for some s_{t+1} , we instead rely on the κ most likely observations⁹ $\mu_{s_{t+1}|d_t}$ for approximating the expectation term in (5) (see Fig. 3b):

$$\begin{aligned} \mathbb{V}_t(d_t) &\triangleq \max_{s_{t+1} \in \mathcal{A}(s_t)} Q_t(s_{t+1}, d_t), \\ Q_t(s_{t+1}, d_t) &\triangleq R(s_{t+1}, d_t) + \mathbb{V}_{t+1}(\langle \mathbf{s}_{t+1}, \mathbf{z}_t \oplus \mu_{s_{t+1}|d_t} \rangle) \end{aligned} \quad (8)$$

for stages $t = 0, \dots, H-1$ where $\mathbb{V}_H(d_H) \triangleq 0$.⁸ Unlike $Q_t(s_{t+1}, d_t)$ (6), the approximation quality of $Q_t(s_{t+1}, d_t)$ (8) can be *deterministically* bounded but cannot be user-specified to be arbitrarily good, as shown in Theorem 2 below (see Appendix J for the proof). To ease understanding, we visually illustrate in Fig. 3 how the policies induced by stochastic sampling (6) vs. most likely observations (8) differ and are used to design our ϵ -Macro-GPO policy π^ϵ (9).

Theorem 2. Suppose that the observations d_t , $H \in \mathbb{Z}^+$, and a budget of $\kappa(H-t)$ input locations for $t = 0, \dots, H-1$ are given. Then,

$$|Q_t(s_{t+1}, d_t) - Q_t^*(s_{t+1}, d_t)| \leq \theta$$

for all $s_{t+1} \in \mathcal{A}(s_t)$ where $\theta \triangleq \mathcal{O}(\kappa^{H+1/2})$.

Remark 3. \mathbb{V}_t (8) can be potentially generalized to resemble \mathcal{V}_t (6) by approximating the expectation term in (5) for each candidate macro-action s_{t+1} in every stage via *deterministic*

⁹Though the nonmyopic BO algorithm of [19] assumes the most likely observations during planning, it does not consider macro-actions nor give a performance guarantee.

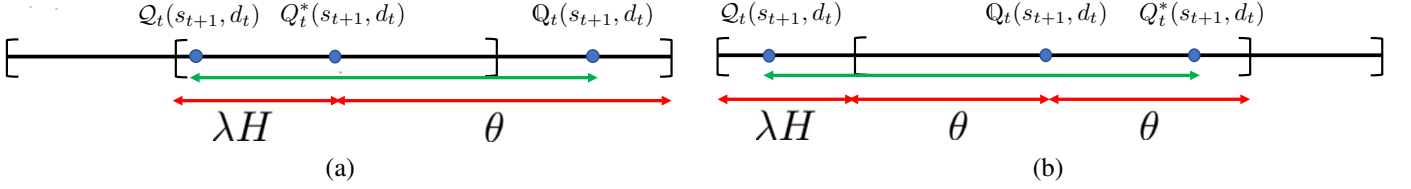


Fig. 4. Implications of specifying conditional policy (9): (a) When $|Q_t(s_{t+1}, d_t) - Q_t^*(s_{t+1}, d_t)| \leq \lambda H$, $|Q_t(s_{t+1}, d_t) - Q_t^ε(s_{t+1}, d_t)|$ (green) is at most $\lambda H + \theta$ (red). (b) When $|Q_t(s_{t+1}, d_t) - Q_t^*(s_{t+1}, d_t)| > \lambda H$ and $|Q_t(s_{t+1}, d_t) - Q_t(s_{t+1}, d_t)| \leq \lambda H + \theta$, $Q_t^ε(s_{t+1}, d_t) = Q_t(s_{t+1}, d_t)$ due to (9) and $|Q_t^ε(s_{t+1}, d_t) - Q_t^*(s_{t+1}, d_t)|$ (green) is at most $\lambda H + 2\theta$ (red). We do not show other cases (e.g., when both $Q_t(s_{t+1}, d_t)$ and $Q_t^*(s_{t+1}, d_t)$ are larger than $Q_t^ε(s_{t+1}, d_t)$ in (a) or $|Q_t(s_{t+1}, d_t) - Q_t^*(s_{t+1}, d_t)| > \lambda H$ and $|Q_t(s_{t+1}, d_t) - Q_t(s_{t+1}, d_t)| > \lambda H + \theta$ in (b), $Q_t^ε(s_{t+1}, d_t) = Q_t(s_{t+1}, d_t)$ due to (9)) which are all covered by our rigorous analysis in the text below (9).

sampling from the GP posterior belief $p(z_{t+1}|s_{t+1}, d_t) = \mathcal{N}(\mu_{s_{t+1}|d_t}, \Sigma_{s_{t+1}|s_t})$ (1) over the κ -dimensional output measurement space of z_{t+1} . To do this, the nonmyopic adaptive BO algorithm of [18] can be extended to handle macro-actions by uniformly partitioning and sampling the κ -dimensional space of z_{t+1} but would consequently incur an *exponential* number of samples (in κ) per planning stage. In contrast, our ϵ -Macro-GPO policy π^ϵ only requires a polynomial number (in κ) of samples per planning stage, as shown in Theorem 3.

The key question remains: Under what condition(s) should our ϵ -Macro-BO policy π^ϵ decide to follow that induced by stochastic sampling (6) and, if so, what is the required number N of samples in (6) such that its *expected* performance loss can be deterministically guaranteed to be within an arbitrarily user-specified bound ϵ ? Ideally, this can be decided if we can directly assess whether $Q_t(s_{t+1}, d_t)$ (6) approximates $Q_t^*(s_{t+1}, d_t)$ (5) closely (i.e., $|Q_t(s_{t+1}, d_t) - Q_t^*(s_{t+1}, d_t)| \leq \lambda H$) for all $s_{t+1} \in \mathcal{A}(s_t)$, which unfortunately is not possible since $Q_t^*(s_{t+1}, d_t)$ cannot be tractably evaluated, as explained previously. To overcome this technical difficulty, we propose a nonmyopic adaptive ϵ -Macro-BO policy π^ϵ that decides to strictly follow that induced by stochastic sampling (6) only if $Q_t(s_{t+1}, d_t)$ (6) is boundedly close to $Q_t(s_{t+1}, d_t)$ (8) for all $s_{t+1} \in \mathcal{A}(s_t)$:

$$\pi^\epsilon(d_t) \triangleq \operatorname{argmax}_{s_{t+1} \in \mathcal{A}(s_t)} Q_t^\epsilon(s_{t+1}, d_t),$$

$$Q_t^\epsilon(s_{t+1}, d_t) \triangleq \begin{cases} Q_t(s_{t+1}, d_t) & \text{if } |Q_t(s_{t+1}, d_t) - Q_t(s_{t+1}, d_t)| \leq \lambda H + \theta, \\ Q_t(s_{t+1}, d_t) & \text{otherwise;} \end{cases} \quad (9)$$

for stages $t = 0, \dots, H-1$.⁸ Like the Macro-GPO policy π^* , π^ϵ can also naturally trade off between exploration vs. exploitation, by the same reasoning as earlier. Unlike the deterministic policy π^* , π^ϵ is stochastic due to its use of stochastic sampling in Q_t (6).

Of noteworthy interest and discussion are the implications of the tractable choice of the if condition in (9) for theoretically guaranteeing the performance of our ϵ -Macro-BO policy π^ϵ , which we illustrate in Fig. 4:

I. In the likely event (with a high probability of at least $1 - \delta$) that $|Q_t(s_{t+1}, d_t) - Q_t^*(s_{t+1}, d_t)| \leq \lambda H$ for all $s_{t+1} \in \mathcal{A}(s_t)$

(Theorem 1),

$$\begin{aligned} & |Q_t(s_{t+1}, d_t) - Q_t(s_{t+1}, d_t)| \\ & \leq |Q_t(s_{t+1}, d_t) - Q_t^*(s_{t+1}, d_t)| \\ & \quad + |Q_t^*(s_{t+1}, d_t) - Q_t(s_{t+1}, d_t)| \\ & \leq \lambda H + \theta \end{aligned}$$

for all $s_{t+1} \in \mathcal{A}(s_t)$ such that the first inequality is due to triangle inequality and the second inequality is due to Theorems 1 and 2. Consequently, according to (9), $Q_t^\epsilon(s_{t+1}, d_t) = Q_t(s_{t+1}, d_t)$ for all $s_{t+1} \in \mathcal{A}(s_t)$ and $\pi^\epsilon(d_t)$ thus selects the same macro-action as the policy induced by stochastic sampling (6).

II. In the unlikely event (with an arbitrarily small probability of at most δ) that $Q_t(s_{t+1}, d_t)$ (6) is unboundedly far from $Q_t^*(s_{t+1}, d_t)$ (5) (i.e., $|Q_t(s_{t+1}, d_t) - Q_t^*(s_{t+1}, d_t)| > \lambda H$) for some $s_{t+1} \in \mathcal{A}(s_t)$, $\pi^\epsilon(d_t)$ (9) guarantees that, for any selected macro-action $s_{t+1} \in \mathcal{A}(s_t)$,

$$\begin{aligned} & |Q_t^\epsilon(s_{t+1}, d_t) - Q_t^*(s_{t+1}, d_t)| \\ & = \begin{cases} |Q_t(s_{t+1}, d_t) - Q_t^*(s_{t+1}, d_t)| & \text{if } |Q_t(s_{t+1}, d_t) - Q_t(s_{t+1}, d_t)| \leq \lambda H + \theta, \\ |Q_t(s_{t+1}, d_t) - Q_t^*(s_{t+1}, d_t)| & \text{otherwise;} \end{cases} \\ & \leq \begin{cases} |Q_t(s_{t+1}, d_t) - Q_t(s_{t+1}, d_t)| & \text{if } |Q_t(s_{t+1}, d_t) - Q_t(s_{t+1}, d_t)| \leq \lambda H + \theta, \\ \theta & \text{otherwise;} \end{cases} \\ & \leq \lambda H + 2\theta, \quad \text{by triangle inequality and Theorem 2.} \end{aligned}$$

The above two implications of our tractable choice of the if condition in (9) are central to establishing our main result deterministically bounding the *expected* performance loss of π^ϵ relative to that of Bayes-optimal Macro-BO policy π^* , that is, policy π^ϵ is ϵ -Bayes-optimal.

To understand the rationale/implications of our choice of if condition in (9), refer to Fig. 4. These implications are central to establishing our main result deterministically bounding the *expected* performance loss of π^ϵ relative to that of π^* , i.e., π^ϵ is ϵ -Bayes-optimal (see proof in Appendix K):

Theorem 3. Suppose that the observations d_0 , $H \in \mathbb{Z}^+$, a budget of κH input locations, and a user-specified loss bound $\epsilon > 0$ are given. Then, $V_0^*(d_0) - \mathbb{E}_{\pi^\epsilon}[V_0^{\pi^\epsilon}(d_0)] \leq \epsilon$ for policy π^ϵ defined in (9), by setting $\theta \triangleq \mathcal{O}(\kappa^{H+1/2})$ according to Theorem 2, $\delta = \epsilon/(8\theta H)$, and $\lambda = \epsilon/(4H^2)$ in Theorem 1 to yield

$$N = \mathcal{O}((\kappa^{2H}/\epsilon^2) \log(\kappa A/\epsilon)) \quad (10)$$

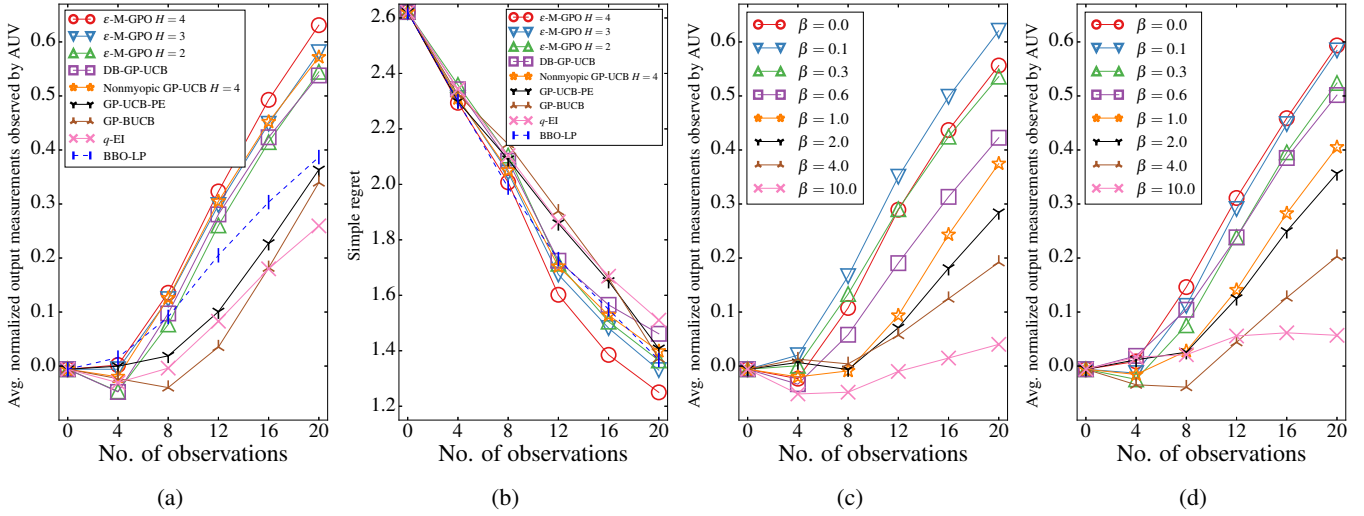


Fig. 5. Graphs of (a) average normalized¹³ output measurements observed by AUV, (b) simple regrets achieved by tested BO algorithms, average normalized output measurements achieved by ϵ -Macro-GPO (ϵ -M-GPO in the graphs) with (c) $H = 2$ and (d) $H = 3$ and varying exploration weights β vs. no. of observations for simulated plankton density phenomena. Standard errors are given in Tables VII and VIII in Appendix B.

where A denotes the largest number of candidate macro-actions available at any input location in \mathcal{S} .

Remark 4. It can be observed from Theorem 3 that the number N of stochastic samples increases¹⁰ with (a) a tighter user-specified loss bound ϵ , (b) a larger number A of candidate macro-actions at any input location in \mathcal{S} , and (c) a greater macro-action length κ .

C. Anytime ϵ -Macro-GPO

Unlike the Bayes-optimal Macro-GPO policy π^* , our ϵ -Macro-GPO policy π^ϵ can be derived exactly since its incurred time does not depend on the size of the uncountable set of candidate output measurements. But, deriving π^ϵ (9) requires expanding an entire search tree of $\mathcal{O}(N^H)$ nodes to solve the H -stage Bellman equations of V_t (6), which incurs time with a $\mathcal{O}(N^H)$ term and is not always needed to achieve ϵ -Bayes optimality in practice. To ease this computational burden (e.g., for real-time planning), we propose an asymptotically optimal anytime variant of our ϵ -Macro-GPO policy that can attain good BO performance quickly and improve its approximation quality over time, as briefly discussed here and detailed along with the pseudocode in Appendix L.

The intuition behind our anytime ϵ -Macro-GPO algorithm is to incrementally expand a search tree by iteratively simulating greedy exploration paths down the partially constructed tree and expanding the sub-trees rooted at nodes with the largest uncertainty of their corresponding values $V_t^*(d_t)$ so as to improve their approximation quality. Such an uncertainty at each encountered node d_t is quantified by the gap between its maintained upper and lower heuristic bounds $\bar{V}_t^*(d_t)$ and $\underline{V}_t^*(d_t)$ that are (a) tightened via backpropagation from the leaves up through node d_t to the root d_0 and (b) subsequently used to refine that at its siblings by exploiting the Lipschitz

¹⁰In fact, N also increases when a larger H is available and the spatial phenomenon varies with more intensity and less noise (larger σ_y^2/σ_n^2) (Appendix I). These constants are omitted from (10) to ease clutter.

continuity of V_t^* (Appendix H). Consequently, each iteration of our anytime ϵ -Macro-GPO algorithm only incurs linear time in N . The formulation of our anytime variant resembles that of ϵ -Macro-GPO policy π^ϵ (9) except that it utilizes the lower heuristic bound instead of \mathcal{Q}_t (6) and a modified if condition to bound its expected performance loss likewise, as detailed in Appendix L.

IV. EXPERIMENTS AND DISCUSSION

This section empirically evaluates the performance of our nonmyopic adaptive ϵ -Macro-GPO policy and its anytime variant for a given finite budget with three datasets featuring simulated plankton density phenomena [22], a real-world traffic phenomenon [23], and a real-world temperature phenomenon over an office environment [24]. The performances of our ϵ -Macro-GPO policy and its anytime variant are compared with that of state-of-the-art (a) nonmyopic GP-UCB [19] generalized to handle macro-actions that coincides with our deterministic policy (8) exploiting the most likely observations during planning, (b) *distributed batch GP-UCB* (DB-GP-UCB) [13] that casts a macro-action as a batch to be optimized and is thus equivalent to ϵ -Macro-GPO with $H = 1$, (c) *q-EI* [12] that does likewise, and (d) greedy batch BO algorithms¹¹ such as GP-BUCB [10], GP-UCB-PE [9], and BBO-LP [11] whose implementations are detailed in Appendix A.¹²

¹¹Unlike DB-GP-UCB and *q-EI*, a greedy batch BO algorithm cannot exploit the full informativeness of any candidate macro-action for its macro-action selection: Since it selects the inputs of a batch one at a time myopically³, its first few selected input locations immediately decide its chosen macro-action and consequently the remaining sequence of input locations found within.

¹²It is not obvious to us how GLASSES [21] and Rollout [17] can be modified to handle macro-actions and are thus not empirically compared here. However, since Rollout [17] also exploits Bellman equations, it is compared with our ϵ -Macro-GPO by setting macro-action length to $\kappa = 1$ (i.e., primitive action).

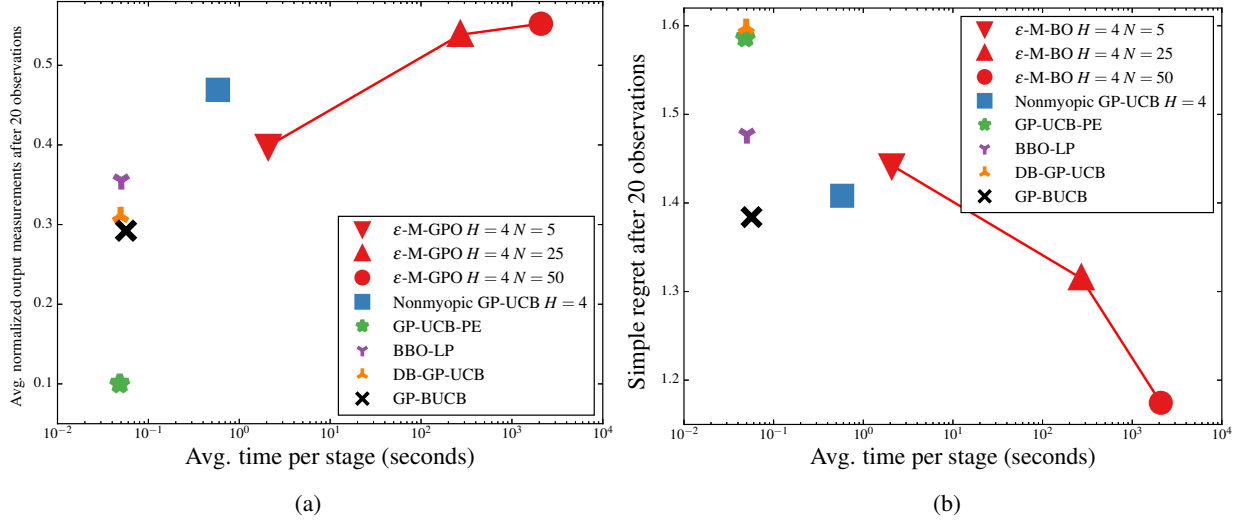


Fig. 6. Graphs of (a) average normalized¹³ output measurements observed by AUV and (b) simple regrets achieved by tested BO algorithms vs. average time per stage for simulated plankton density phenomena.

Four performance metrics are used: (a) average normalized¹³ output measurements observed by the agent (larger average output measurements imply less average/cumulative regret (Section III)), (b) simple regret (i.e., difference between global maximum and currently found maximum), (c) no. of explored nodes in all constructed search trees (more nodes incur more time), and (d) average runtime per stage.

A. Simulated plankton density phenomena

An *autonomous underwater vehicle* (AUV) is deployed on board of a *research vessel* (RV) in search for a hotspot of peak phytoplankton abundance (i.e., algal bloom) in coastal ocean. The AUV and RV are initially positioned near the center of the plankton density (mg/m^3) phenomenon spatially distributed over a 5 km by 5 km region that is discretized into a 50×50 grid of input locations. The phenomenon is modeled as a realization of a GP and simulated using the GP hyperparameters $\mu_s = 0$, $\ell_1 = \ell_2 = 0.5$ km, $\sigma_y^2 = 1$, and $\sigma_n^2 = 10^{-5}$. The AUV is tasked to execute the selected macro-action of a straight dive (due to limited maneuverability) along one of the 4 cardinal directions from the RV to gather ‘‘Gulper’’ water samples/observations over $\kappa = 4$ input locations for precise on-deck testing [22]; given a budget of 20 observations, this will be repeated for 5 times (i.e. 5 stages) from the input location that it has previously surfaced. Figs. 5a and 5b show

TABLE I
NO. OF EXPLORED NODES BY ϵ -MACRO-GPO (WHEN $H = 1$, IT CORRESPONDS TO DB-GP-UCB) FOR SIMULATED PLANKTON DENSITY PHENOMENA.

$H = 1$	$H = 2$	$H = 3$	$H = 4$
2.50×10	8.01×10^3	2.40×10^6	6.41×10^8

results of the performances of ϵ -Macro-GPO with $H = 2, 3, 4$ (lookahead of, respectively, 8, 12, 16 observations), $\beta = 0$, and

$N = 100$,¹⁴ and the other tested BO algorithms averaged over 250 independent realizations of the simulated phenomena. It can be observed that as the number of observations increases, the nonmyopic adaptive BO algorithms generally outperform the myopic ones. In particular, the performance of ϵ -Macro-GPO improves considerably by increasing H : ϵ -Macro-GPO with the furthest lookahead (i.e., $H = 4$) achieves the largest average normalized output measurements observed by the AUV and smallest simple regret after 20 observations at the cost of a larger number of explored nodes (see Table I). For example, the nonmyopic ϵ -Macro-GPO with $H = 4$ achieves $0.093\sigma_y$ ($0.059\sigma_y$) more average output measurements and $0.211\sigma_y$ ($0.148\sigma_y$) less simple regret than myopic DB-GP-UCB (nonmyopic GP-UCB with the same horizon $H = 4$ but assuming most likely observations during planning), which are expected.

Figs. 5c and 5d show the effect of varying exploration weights β on the performance of ϵ -Macro-GPO with $H = 2$ and $H = 3$, respectively. It can be observed from Fig. 5c that when $H = 2$, ϵ -Macro-GPO with $\beta = 0.1$ achieves $0.064\sigma_y$ more average normalized output measurements than that with $\beta = 0$ after 20 observations, which indicates the need of a slightly stronger exploration behavior. Fig. 5d shows that by increasing to a lookahead of 12 observations (i.e., $H = 3$), ϵ -Macro-GPO no longer needs the additional weighted exploration term in (4) (i.e., $\beta = 0$) since it can naturally trade off between exploration vs. exploitation, as explained previously (Section III). It can also be observed from Figs. 5c and 5d that $\beta = 10$ greatly hurts its performance due to an overly aggressive exploration.

We also investigate the effect of varying the number N of stochastic samples on the behavior of ϵ -Macro-GPO. To this end, ϵ -Macro-GPO with a fixed horizon H offers an advantage of being able to trade off its performance for time efficiency

¹³To ease interpretation of results, the prior mean is subtracted from each output measurement to normalize it.

¹⁴Specifying the value of N (instead of ϵ) may yield a loose ϵ based on Theorem 3. Nevertheless, the resulting ϵ -Macro-GPO with $H = 3, 4$ empirically outperforms other tested BO algorithms.

by decreasing N . This observation is theoretically validated in Theorem 3 and empirically illustrated in Fig. 6.

Figs. 6a and 6b show results of the performances of ϵ -Macro-GPO with $H = 4$ (lookahead of 16 observations), $\beta = 0$, and $N = 5, 25, 50$, and the other tested BO algorithms averaged over 35 independent realizations of the simulated plankton density phenomena. It can be observed that the performance of ϵ -Macro-GPO improves considerably by increasing N : ϵ -Macro-GPO with the largest number of samples (i.e., $N = 50$) achieves the largest average normalized output measurements and smallest simple regret after 20 observations at the cost of larger average time per iteration. For example, ϵ -Macro-GPO with $N = 50$ achieves $0.26\sigma_y$ more average output measurements and $0.21\sigma_y$ less simple regret than myopic GP-BUCB, but needs 2085.37 more seconds per iteration.

B. Real-world traffic phenomenon

To service the mobility demands within the central business district of an urban city, an *autonomous vehicle* (AV) in a mobility-on-demand system cruises along different road trajectories to find a hotspot of highest mobility demand to pick up a user. The 29.4 km by 11.9 km service area is gridded into 100×50 input regions, of which only 2506 input regions are accessible to the AV via the road network. The AV can cruise from input region s to an adjacent input region s' using one primitive action iff at least one road segment in the road network starts in s and ends in s' ; the maximum outdegree from any input region is 8. In any input region, a surrogate demand measurement is obtained by counting the number of pickups¹⁵ from all historic taxi trajectories generated by a major taxi company during 9:30-10 p.m. on August 2, 2010 [23]; the resulting mobility demand pattern is visualized in Fig. 8. The original demand measurements are log-transformed to remove skewness and extremity for stabilizing the GP covariance structure and the GP hyperparameters $\mu_s = 1.5673$, $\ell_1 = 0.1689$ km, $\ell_2 = 0.1275$ km, $\sigma_y^2 = 0.7486$, and $\sigma_n^2 = 0.0111$ are then learned using maximum likelihood estimation [32]; note that the length-scales and signal-to-noise ratio are relatively smaller than that of the simulated plankton density phenomena. The AV is tasked to execute the selected macro-action of a cruising trajectory along $\kappa = 5$ adjacent input regions to observe their corresponding demand measurements; given a budget of 20 observations, this will be repeated for 4 times (i.e. 4 stages) from the input region that it has previously cruised to. Since every input region s has a large number of available macro-actions (i.e., with an average of 178 and maximum of 1193 macro-actions), 20 of them are randomly¹⁶ selected to form its representative set of candidate macro-actions.

¹⁵A distributed gossip-based protocol can be used to aggregate these pickup information from the AVs in the input region that are connected via an ad hoc wireless communication network [23]. Any AV entering the input region can then access its pickup count by joining its ad hoc network.

¹⁶The BO performance of ϵ -Macro-GPO and its anytime variant can be potentially improved by using macro-action generation algorithms [27] instead of random selection.

TABLE II
NO. OF EXPLORED NODES BY ANYTIME ϵ -MACRO-GPO (WHEN $H = 1$, IT CORRESPONDS TO DB-GP-UCB) FOR THE REAL-WORLD TRAFFIC PHENOMENON (I.E., MOBILITY DEMAND PATTERN).

$H = 1$	$H = 2$	$H = 3$	$H = 4$
8.29×10	9.52×10^4	1.29×10^6	1.34×10^7

Figs. 7a and 7b show results of the performances of *anytime* ϵ -Macro-GPO with $H = 2, 3, 4$ (a lookahead of, respectively, 10, 15, 20 observations), $\beta = 0$, and $N = 300$ after running for 1500 iterations¹⁴, and the other tested BO algorithms averaged over 35 random starting input regions of the AV. Similar to the results for simulated plankton density phenomena, it can be observed that the performance of anytime ϵ -Macro-GPO improves considerably by increasing H : Anytime ϵ -Macro-GPO with the furthest lookahead (i.e., $H = 4$) achieves the largest average normalized output measurements observed by the AV and among the least simple regret after 20 observations at the cost of a larger number of explored nodes (see Table II). For example, the nonmyopic anytime ϵ -Macro-GPO with $H = 4$ achieves $0.069\sigma_y$ ($0.05\sigma_y$) more average output measurements and $0.188\sigma_y$ ($0.219\sigma_y$) less simple regret than myopic DB-GP-UCB (nonmyopic GP-UCB with $H = 4$), which are expected. Interestingly, GP-BUCB and GP-UCB-PE can achieve simple regret comparable to that of anytime ϵ -Macro-GPO with $H = 4$ even though they perform very poorly in terms of average output measurements.

Figs. 7c and 7d show the effect of varying exploration weights β on the performance of anytime ϵ -Macro-GPO with $H = 2$ and $H = 3$, respectively. It can be observed from Fig. 7c that when $H = 2$, anytime ϵ -Macro-GPO with $\beta = 0.2$ achieves $0.022\sigma_y$ more average normalized output measurements than that with $\beta = 0$ after 20 observations, which indicates the need of a slightly stronger exploration behavior. Fig. 7d shows that by increasing to a lookahead of 15 observations (i.e., $H = 3$), anytime ϵ -Macro-GPO no longer needs the additional weighted exploration term in (4) (i.e., $\beta = 0$) since it can naturally trade off between exploration vs. exploitation, as explained previously (Section III). It can also be observed from Figs. 7c and 7d that $\beta \geq 0.5$ hurts its performance due to overly aggressive exploration.

Lastly, we investigate the effect of downsampling the number of available macro-actions per input region to 20 on the performance of anytime ϵ -Macro-GPO. To do this, the performances of anytime ϵ -Macro-GPO with $H = 2, 4$ and 20 randomly selected macro-actions per input region are compared with that of anytime ϵ -Macro-GPO with $H = 2$ and all available macro-actions as well as myopic EI [1] with all available macro-actions of length 1. It can be observed from Figs. 9a and 9b that when $H = 2$, downsampling the number of available macro-actions per input region to 20 decreases average normalized output measurements by $0.032\sigma_y$ and increases simple regret by $0.112\sigma_y$ after 20 observations, but also reduces the number of explored nodes by more than 1 order of magnitude (see Table III). By increasing to a lookahead of 20 observations, anytime ϵ -Macro-GPO with $H = 4$ and 20 randomly selected macro-actions per

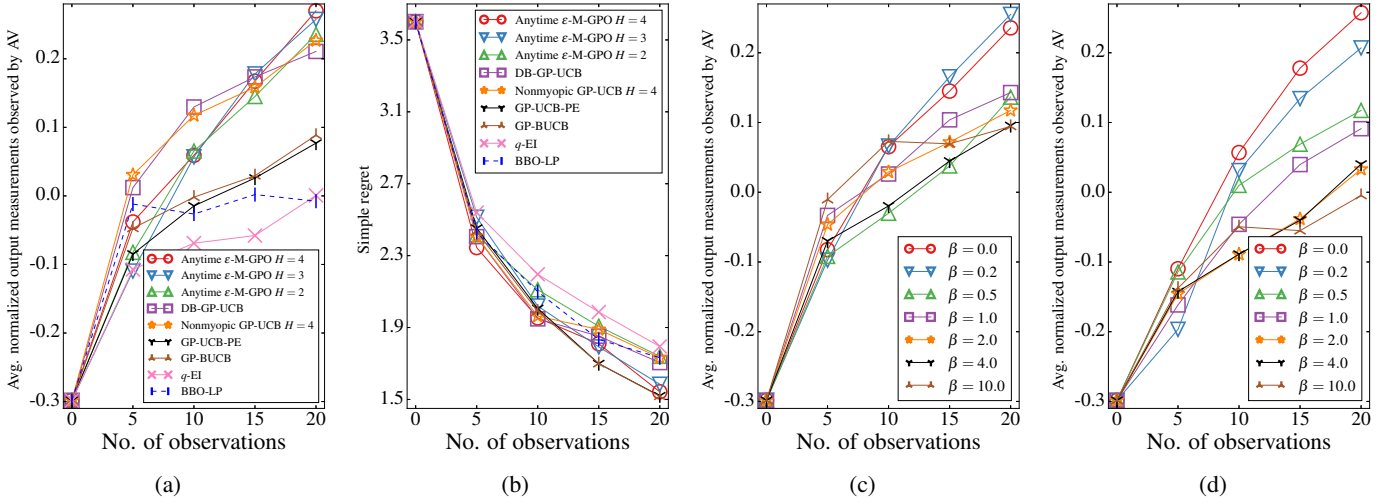


Fig. 7. Graphs of (a) average normalized¹³ output measurements observed by the AV and (b) simple regrets achieved by the tested BO algorithms, and average normalized output measurements achieved by *anytime* ϵ -Macro-GPO with (c) $H = 2$ and (d) $H = 3$ and varying exploration weights β vs. no. of observations for real-world traffic phenomenon. The standard errors are given in Tables IX and X in Appendix C.

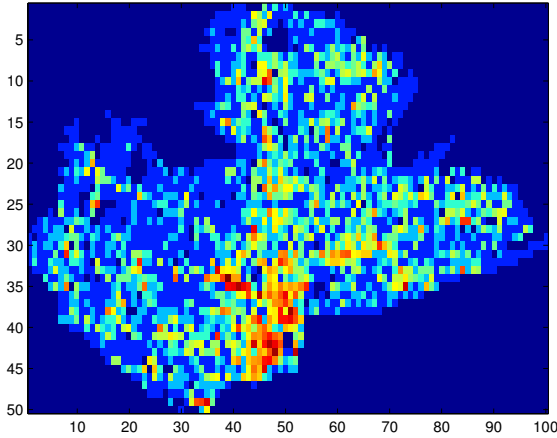


Fig. 8. Mobility demand pattern spatially distributed over the central business district of an urban city during 9:30-10 p.m. on August 2, 2010: “Hotter” regions indicate larger numbers of pickups (Image courtesy of [23]).

input region achieves $0.008\sigma_y$ more average normalized output measurements and $0.116\sigma_y$ less simple regret than that with $H = 2$ and all available macro-actions at the cost of a larger number of explored nodes. Though EI can access all available macro-actions of length 1 (i.e., no restriction on action space of AV), it obtains much less average normalized output measurements and more simple regret than *anytime* ϵ -Macro-GPO with $H = 4$ and 20 randomly selected macro-actions per input region due to its myopia.

C. Real-world temperature phenomenon

In monitoring of the indoor environmental quality of an office environment [24], a mobile robot mounted with a weather board is tasked to find a hotspot of peak temperature by exploring different stretches of corridors that can be

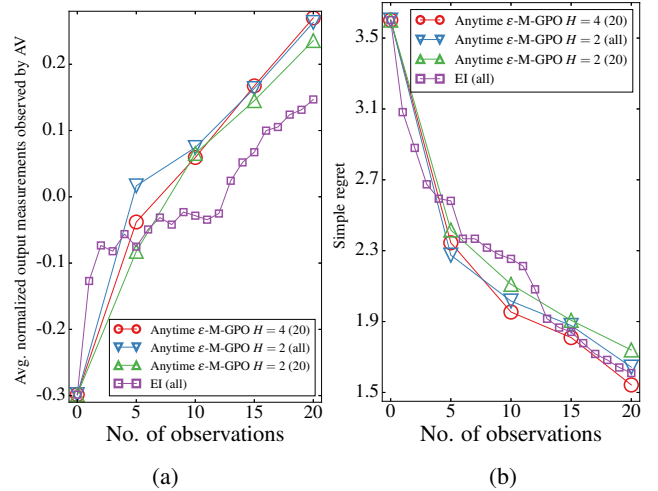


Fig. 9. Graphs of (a) average normalized output measurements observed by the AV and (b) simple regrets achieved by *anytime* ϵ -Macro-GPO with $H = 2, 4$ and 20 randomly selected macro-actions per input region, *anytime* ϵ -Macro-GPO with $H = 2$ and all available macro-actions (the no. of available macro-actions per input region is enclosed in brackets), and EI with all available macro-actions of length 1 vs. no. of observations for real-world traffic phenomenon. Standard errors are given in Table XI in Appendix C.

TABLE III
NO. OF EXPLORED NODES BY *ANYTIME* ϵ -MACRO-GPO (THE NO. OF AVAILABLE MACRO-ACTIONS PER INPUT REGION IS ENCLOSED IN BRACKETS) FOR THE REAL-WORLD TRAFFIC PHENOMENON (I.E., MOBILITY DEMAND PATTERN).

$H = 2$ (20)	$H = 2$ (all)	$H = 4$ (20)
0.95×10^5	1.26×10^6	1.34×10^7

naturally abstracted into macro-actions. The temperature ($^{\circ}\text{C}$) phenomenon is spatially distributed over the Intel Berkeley Research Lab (of about 41 m by 32 m in size) with 41 deployed temperature sensors (see Fig. 11) and modeled as a realization of a GP. Using the observations/data gathered

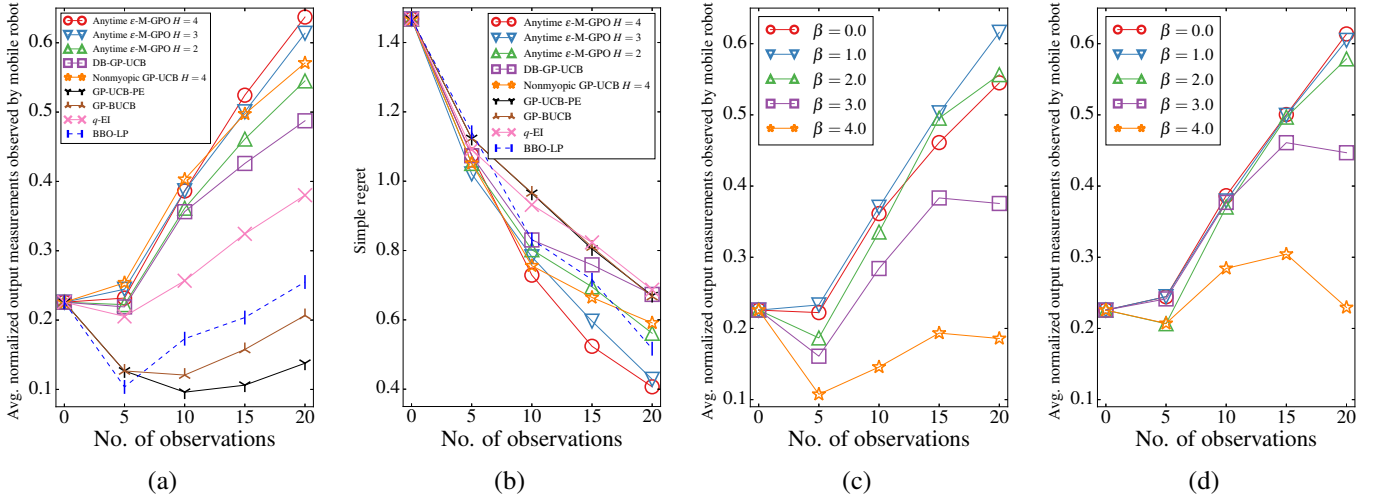


Fig. 10. Graphs of (a) average normalized¹³ output measurements observed by the mobile robot and (b) simple regrets achieved by the tested BO algorithms vs. no. of observations, and average normalized output measurements achieved by *anytime* ϵ -Macro-GPO with (c) $H = 2$ and (d) $H = 3$ and varying exploration weights β vs. no. of observations for the real-world temperature phenomenon over the Intel Berkeley Research Lab. The standard errors are given in Tables XII and XIII in Appendix D.

by the 41 temperature sensors¹⁷, the GP hyperparameters $\mu_s = 17.8513$, $\ell_1 = 4.0058$ m, $\ell_2 = 11.3811$ m, $\sigma_y^2 = 0.5964$, and $\sigma_n^2 = 0.0597$ are learned using maximum likelihood estimation [32]. Then, using these learned hyperparameters and the observations/data gathered by the 41 temperature sensors, we exploit the GP posterior mean (1) to predict the temperature measurements at the 104 input locations shown in Fig. 11; these predictions together with the data obtained from the 41 sensors serve as the dataset for the experiment here. The mobile robot is tasked to execute the selected macro-action of a motion path along a stretch of $\kappa = 5$ input locations on one of the corridors in the lab to observe their corresponding temperature measurements; given a budget of 20 observations, this will be repeated for 4 times from the input location that it has previously moved to. Since every input location s has a large number of available macro-actions (i.e., with an average of 27 and maximum of 114 macro-actions), 20 of them are randomly¹⁶ selected to form its representative set of candidate macro-actions.

Figs. 10a and 10b show results of the performances of *anytime* ϵ -Macro-GPO with $H = 2, 3, 4$ (lookahead of, respectively, 10, 15, 20 observations), $\beta = 0$, and $N = 300$ after running for 1500 iterations¹⁴, and the other tested BO algorithms averaged over 35 random initial starting input locations of the mobile robot. Similar to the results for simulated plankton density phenomena and real-world traffic phenomenon, it can be observed that as the number of observations increases, the nonmyopic adaptive BO algorithms generally outperform the myopic ones. In particular, the performance of *anytime* ϵ -Macro-GPO improves considerably by increasing H such that *anytime* ϵ -Macro-GPO with the furthest lookahead (i.e., $H = 4$) achieves the largest average normalized output measurements observed by the mobile robot and smallest simple regret after 20 observations at the cost of a larger number

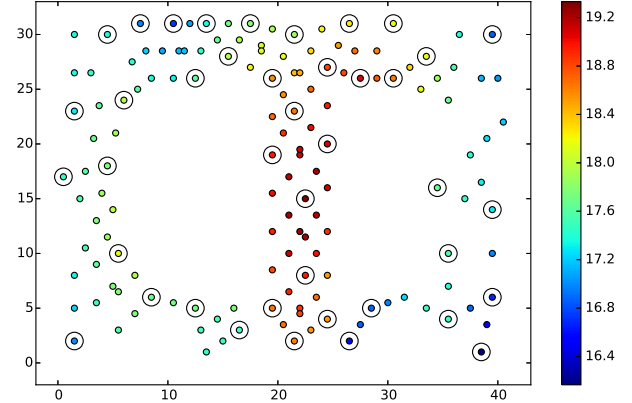


Fig. 11. The temperature measurements at the 104 input locations (not circled) in the Intel Berkeley Research lab are predicted using the GP posterior mean (1) based on the data gathered by the 41 temperature sensors (circled); these predictions together with the data obtained from the 41 sensors serve as the dataset for the experiment here.

of explored nodes (see Table IV). For example, the nonmyopic *anytime* ϵ -Macro-GPO with $H = 4$ achieves $0.194\sigma_y$ ($0.086\sigma_y$) more average normalized output measurements and $0.345\sigma_y$ ($0.239\sigma_y$) less simple regret than the myopic DB-GP-UCB (nonmyopic GP-UCB with the same horizon $H = 4$ but assuming most likely observations during planning), which are expected.

TABLE IV
NO. OF EXPLORED NODES BY ANYTIME ϵ -MACRO-GPO (WHEN $H = 1$, IT CORRESPONDS TO DB-GP-UCB) FOR THE REAL-WORLD TEMPERATURE PHENOMENON OVER THE INTEL BERKELEY RESEARCH LAB.

$H = 1$	$H = 2$	$H = 3$	$H = 4$
7.51×10	8.88×10^4	1.13×10^6	1.12×10^7

Figs. 10c and 10d show the effect of varying exploration weights β on the performance of *anytime* ϵ -Macro-GPO with

¹⁷<http://db.csail.mit.edu/labdata/labdata.html>

$H = 2$ and $H = 3$, respectively. It can be observed from Fig. 10c that when $H = 2$, anytime ϵ -Macro-GPO with $\beta = 1$ achieves $0.092\sigma_y$ more average normalized output measurements than that with $\beta = 0$ after 20 observations, which indicates the need of a slightly stronger exploration behavior. Fig. 10d shows that by increasing to a lookahead of 15 observations (i.e., $H = 3$), anytime ϵ -Macro-GPO no longer needs the additional weighted exploration term in (4) (i.e., $\beta = 0$) since it can naturally trade off between exploration vs. exploitation, as explained previously (Section III). It can also be observed from Figs. 10c and 10d that $\beta \geq 3$ hurts its performance due to overly aggressive exploration.

Lastly, we investigate the effect of downsampling the number of available macro-actions per input location to 20 on the performance of anytime ϵ -Macro-GPO. Similar to that for the real-world traffic phenomenon, the performances of anytime ϵ -Macro-GPO with $H = 2, 4$ and 20 randomly selected macro-actions per input location are compared with that of anytime ϵ -Macro-GPO with $H = 2$ and all available macro-actions as well as myopic EI [1] with all available macro-actions of length 1. It can be observed from Figs. 12a and 12b that when $H = 2$, downsampling the number of available macro-actions per input location to 20 decreases average normalized output measurements by $0.106\sigma_y$ and increases simple regret by $0.064\sigma_y$ after 20 observations, but also reduces the number of explored nodes (see Table V). By increasing to a lookahead of 20 observations, anytime ϵ -Macro-GPO with $H = 4$ and 20 randomly selected macro-actions per input location achieves average normalized output measurements comparable to that with $H = 2$ and all available macro-actions, but $0.136\sigma_y$ less simple regret at the cost of a larger number of explored nodes. Though EI can access all available macro-actions of length 1 (i.e., no restriction on action space of the mobile robot), it obtains much less average normalized output measurements and considerably more simple regret than anytime ϵ -Macro-GPO with $H = 4$ and 20 randomly selected macro-actions per input location due to its myopia.

TABLE V

NO. OF EXPLORED NODES BY ANYTIME ϵ -MACRO-GPO (THE NO. OF AVAILABLE MACRO-ACTIONS PER INPUT REGION IS ENCLOSED IN BRACKETS) FOR THE REAL-WORLD TEMPERATURE PHENOMENON OVER THE INTEL BERKELEY RESEARCH LAB.

$H = 2$ (20)	$H = 2$ (all)	$H = 4$ (20)
8.88×10^4	2.49×10^5	1.12×10^7

D. Comparison with Rollout [17]

Our proposed algorithms are not benchmarked against Rollout [17] because Rollout [17] is not designed to handle macro-actions that are inherent to the structure of the task environments/applications considered in our work and experiments. So, such a comparison would not be fair. For a fair comparison with Rollout [17], we set the macro-action length to $\kappa = 1$ (i.e., primitive action) for our ϵ -Macro-GPO and evaluate their performances using the metrics of average normalized output measurements observed by the agent and simple regret, and the synthetic dataset featuring the simulated plankton density phenomena in Section IV.

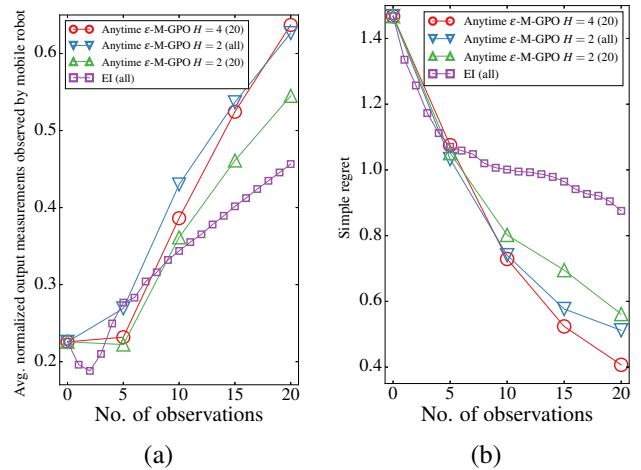


Fig. 12. Graphs of (a) average normalized¹³ output measurements observed by the mobile robot and (b) simple regrets achieved by anytime ϵ -Macro-GPO with $H = 2, 4$ and 20 randomly selected macro-actions per input region, anytime ϵ -Macro-GPO with $H = 2$ and all available macro-actions (the no. of available macro-actions per input region is enclosed in brackets), and EI with all available macro-actions of length 1 vs. no. of observations for the real-world temperature phenomenon over the Intel Berkeley Research Lab. The standard errors are given in Table XIV in Appendix D.

Figs. 13a and 13b show results of the performances of ϵ -Macro-GPO ($H = 4$, $\beta = 0$, and $N = 20$) and the best-performing Rollout ($H = 4$, $\gamma = 1.0$, base policy: greedy EI-based policy defined in equations 22 and 23 in [17]) reported on page 7 in [17] averaged over 107 independent realizations of the simulated phenomena. It can be observed that ϵ -Macro-GPO achieves $0.143\sigma_y$ more average normalized output measurement and $0.173\sigma_y$ less simple regret than Rollout [17]. To explain this, ϵ -Macro-GPO considers all available actions from each input location during planning (equations 6, 8, and 9) while Rollout utilizes only the action selected by the base policy (e.g., greedy EI) and ignores all the other available actions during planning, thus resulting in its suboptimal behavior.

V. CONCLUSION

This paper describes ϵ -Macro-GPO and its anytime variant for nonmyopic adaptive BO that have been empirically shown to scale up to a lookahead of 20 observations by exploiting macro-actions and consequently achieve superior BO performance. Different from the asymptotic no-regret performance¹ typical of GP-UCB and its variants, we theoretically guarantee the *expected* performance loss of ϵ -Macro-GPO and its anytime variant that can be specified to be arbitrarily small given a *limited* budget. Though this requires a polynomial number of stochastic samples in the macro-action length κ in each planning stage (Theorem 3), our experiments reveal that a relatively small sample size ($N=100-300$) is needed for ϵ -Macro-GPO and its anytime variant to outperform state-of-the-art BO algorithms. Though a sufficiently large exploration weight β is usually needed to guarantee asymptotic no-regret performance¹ for GP-UCB and its variants, we have observed in our experiments that their performances are highly sensitive to the chosen value of β given a finite/limited budget and can

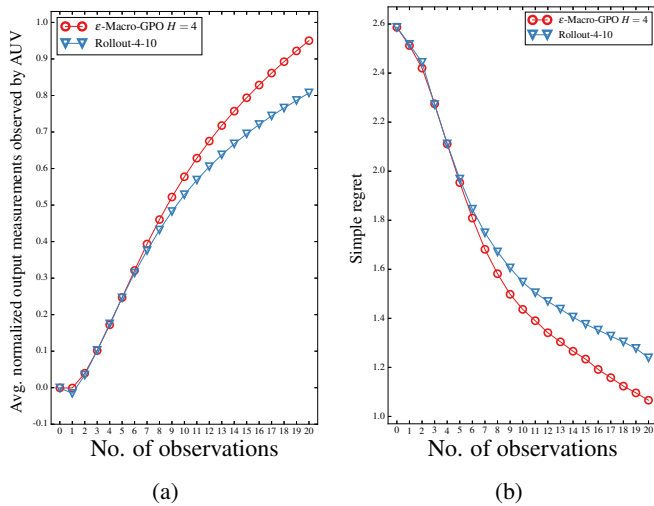


Fig. 13. Graphs of (a) average normalized¹³ output measurements observed by AUV and (b) simple regrets achieved by ϵ -Macro-GPO with $H = 4$ and Rollout-4-10 vs. no. of observations for simulated plankton density phenomena. Standard errors are given in Table XV in Appendix E.

be greatly hurt by an often unknowingly “large” value of β due to excessive exploration. To sidestep this, ϵ -Macro-GPO can eliminate the need of the additional weighted exploration term (i.e., $\beta = 0$) by utilizing a further lookahead, that is, if computational resources permit or are more affordable than the cost of function evaluations.

ACKNOWLEDGMENT

This research is supported by the Singapore Ministry of Education Academic Research Fund Tier 2, MOE2016-T2-2-156.

REFERENCES

- [1] B. Shahriari, K. Swersky, Z. Wang, R. Adams, and N. de Freitas, “Taking the human out of the loop: A review of Bayesian optimization,” *Proceedings of the IEEE*, vol. 104, no. 1, pp. 148–175, 2016.
- [2] P. Hennig and C. J. Schuler, “Entropy search for information-efficient global optimization,” *JMLR*, vol. 13, pp. 1809–1837, 2012.
- [3] J. M. Hernández-Lobato, M. W. Hoffman, and Z. Ghahramani, “Predictive entropy search for efficient global optimization of black-box functions,” in *Proc. NIPS*, 2014, pp. 918–926.
- [4] J. Villemonteix, E. Vazquez, and E. Walter, “An informational approach to the global optimization of expensive-to-evaluate functions,” *J. Glob. Optim.*, vol. 44, no. 4, pp. 509–534, 2009.
- [5] N. Srinivas, A. Krause, S. Kakade, and M. Seeger, “Gaussian process optimization in the bandit setting: No regret and experimental design,” in *Proc. ICML*, 2010, pp. 1015–1022.
- [6] A. D. Bull, “Convergence rates of efficient global optimization algorithms,” *JMLR*, vol. 12, pp. 2879–2904, 2011.
- [7] E. Vazquez and J. Bect, “Convergence properties of the expected improvement algorithm with fixed mean and covariance functions,” *J. Statistical Planning and Inference*, vol. 140, no. 11, pp. 3088–3095, 2010.
- [8] J. Azimi, A. Fern, and X. Z. Fern, “Batch Bayesian optimization via simulation matching,” in *Proc. NIPS*, 2010, pp. 109–117.
- [9] E. Contal, D. Buffoni, A. Robicquet, and N. Vayatis, “Parallel Gaussian process optimization with upper confidence bound and pure exploration,” in *Proc. ECML/PKDD*, 2013, pp. 225–240.
- [10] T. Desautels, A. Krause, and J. W. Burdick, “Parallelizing exploration-exploitation tradeoffs in Gaussian process bandit optimization,” *JMLR*, vol. 15, pp. 4053–4103, 2014.
- [11] J. González, Z. Dai, P. Hennig, and N. D. Lawrence, “Batch Bayesian optimization via local penalization,” in *Proc. AISTATS*, 2016, pp. 648–657.
- [12] C. Chevalier and D. Ginsbourger, “Fast computation of the multi-points expected improvement with applications in batch selection,” in *Proc. 7th International Conference on Learning and Intelligent Optimization*, 2013, pp. 59–69.
- [13] E. A. Daxberger and K. H. Low, “Distributed batch Gaussian process optimization,” in *Proc. ICML*, 2017, pp. 951–960.
- [14] A. Shah and Z. Ghahramani, “Parallel predictive entropy search for batch global optimization of expensive objective functions,” in *Proc. NIPS*, 2015, pp. 3312–3320.
- [15] J. Wu and P. Frazier, “The parallel knowledge gradient method for batch Bayesian optimization,” in *Proc. NIPS*, 2016, pp. 3126–3134.
- [16] R. R. Lam and K. E. Willcox, “Lookahead Bayesian optimization with inequality constraints,” in *Proc. NIPS*, 2017.
- [17] R. R. Lam, K. E. Willcox, and D. H. Wolpert, “Bayesian optimization with a finite budget: An approximate dynamic programming approach,” in *Proc. NIPS*, 2016.
- [18] C. K. Ling, K. H. Low, and P. Jaillet, “Gaussian process planning with Lipschitz continuous reward functions: Towards unifying Bayesian optimization, active learning, and beyond,” in *Proc. AAAI*, 2016, pp. 1860–1866.
- [19] R. Marchant, F. Ramos, and S. Sanner, “Sequential Bayesian optimisation for spatial-temporal monitoring,” in *Proc. UAI*, 2014, pp. 553–562.
- [20] M. A. Osborne, R. Garnett, and S. J. Roberts, “Gaussian processes for global optimization,” in *Proc. 3rd International Conference on Learning and Intelligent Optimization*, 2009.
- [21] J. González, M. Osborne, and N. D. Lawrence, “GLASSES: Relieving the myopia of Bayesian optimisation,” in *Proc. AISTATS*, 2016, pp. 790–799.
- [22] J. T. Pennington, M. Blum, and F. P. Chavez, “Seawater sampling by an autonomous underwater vehicle: “Gulper” sample validation for nitrate, chlorophyll, phytoplankton, and primary production,” *Limnol. Oceanogr.: Methods*, vol. 14, no. 1, pp. 14–23, 2016.
- [23] J. Chen, K. H. Low, P. Jaillet, and Y. Yao, “Gaussian process decentralized data fusion and active sensing for spatiotemporal traffic modeling and prediction in mobility-on-demand systems,” *IEEE T-ASE*, vol. 12, no. 3, pp. 901–921, 2015.
- [24] J.-H. Choi, V. Loftness, and A. Aziz, “Post-occupancy evaluation of 20 office buildings as basis for future IEQ standards and guidelines,” *Energy and Buildings*, vol. 46, pp. 167–175, 2012.
- [25] N. E. Leonard, D. A. Paley, F. Lekien, R. Sepulchre, D. M. Fratantoni, and R. E. Davis, “Collective motion, sensor networks, and ocean sampling,” *Proceedings of the IEEE*, vol. 95, no. 1, pp. 48–74, 2007.
- [26] R. He, E. Brunskill, and N. Roy, “PUMA: Planning under uncertainty with macro-actions,” in *Proc. AAAI*, 2010, pp. 1089–1095.
- [27] —, “Efficient planning under uncertainty with macro-actions,” *JAIR*, vol. 40, pp. 523–570, 2011.
- [28] Z. Lim, W. S. Lee, and D. Hsu, “Monte Carlo value iteration with macro-actions,” in *Proc. NIPS*, 2011, pp. 1287–1295.
- [29] A. G. Barto and S. Mahadevan, “Recent advances in hierarchical reinforcement learning,” *Discrete Event Dynamic Systems*, vol. 13, no. 4, pp. 341–379, 2003.
- [30] G. Konidaris and A. G. Barto, “Building portable options: Skill transfer in reinforcement learning,” in *Proc. IJCAI*, 2007, pp. 895–900.
- [31] M. Stolle and D. Precup, “Learning options in reinforcement learning,” in *Proc. International Symposium on Abstraction, Reformulation, and Approximation*, 2002, pp. 212–223.
- [32] C. E. Rasmussen and C. K. I. Williams, *Gaussian Processes for Machine Learning*. MIT Press, 2006.
- [33] P. Poupart, N. Vlassis, J. Hoey, and K. Regan, “An analytic solution to discrete Bayesian reinforcement learning,” in *Proc. ICML*, 2006, pp. 697–704.
- [34] P. Dallaire, C. Besse, S. Ross, and B. Chaib-draa, “Bayesian reinforcement learning in continuous POMDPs with Gaussian processes,” in *Proc. IEEE/RSJ IROS*, 2009, pp. 2604–2609.
- [35] S. Ross, B. Chaib-draa, and J. Pineau, “Bayesian reinforcement learning in continuous POMDPs with application to robot navigation,” in *Proc. IEEE ICRA*, 2008, pp. 2845–2851.
- [36] S. Boucheron, G. Lugosi, and P. Massart, *Concentration inequalities: A nonasymptotic theory of independence*. Oxford University Press, 2013.
- [37] T. M. Cover and J. A. Thomas, *Elements of information theory*, 2nd ed. Wiley-Interscience, 2006.
- [38] G. H. Golub and C.-F. Van Loan, *Matrix Computations*, 3rd ed. Johns Hopkins Univ. Press, 1996.

- [39] G. W. Stewart and J.-G. Sun, *Matrix Perturbation Theory*. Academic Press, 1990.
- [40] M. Taboga, *Lectures on probability theory and mathematical statistics*. CreateSpace Independent Publishing Platform, 2017, <http://www.statlect.com>.
- [41] K. B. Petersen and M. S. Pedersen, *The Matrix Cookbook*, 2012.
- [42] V. Chandrasekaran, B. Recht, P. A. Parrilo, and A. S. Willsky, “The convex geometry of linear inverse problems,” *Foundations of Computational Mathematics*, vol. 12, no. 6, pp. 805–849, 2012.

APPENDIX A

DETAILS ON THE IMPLEMENTATIONS OF BATCH BO ALGORITHMS

See Table VI.

TABLE VI

DETAILS ON THE AVAILABLE IMPLEMENTATIONS OF THE BATCH BO ALGORITHMS FOR COMPARISON WITH ϵ -MACRO-GPO IN OUR EXPERIMENTS.

BO Algorithm	Language	URL of Source Code
GP-BUCB	MATLAB	http://www.gatsby.ucl.ac.uk/~tdesauteis/
GP-UCB-PE	MATLAB	http://econtal.perso.math.cnrs.fr/software/
q -EI	Python	https://github.com/oxfordcontrol/Bayesian-Optimization
BBO-LP	Python	http://sheffieldml.github.io/GPyOpt/

APPENDIX B

ADDITIONAL EXPERIMENTAL RESULTS FOR SIMULATED PLANKTON DENSITY PHENOMENA

See Table VII and Table VIII.

TABLE VII

AVERAGE NORMALIZED¹³ OUTPUT MEASUREMENTS OBSERVED BY THE AUV AND SIMPLE REGRETS ACHIEVED BY THE TESTED BO ALGORITHMS AFTER 20 OBSERVATIONS.

BO Algorithm	Average normalized output measurements	Simple regret
ϵ -Macro-GPO $H = 4$	0.6310 ± 0.0458	1.2500 ± 0.0541
ϵ -Macro-GPO $H = 3$	0.5809 ± 0.0486	1.3303 ± 0.0542
ϵ -Macro-GPO $H = 2$	0.5446 ± 0.0464	1.3651 ± 0.0550
DB-GP-UCB	0.5379 ± 0.0462	1.4612 ± 0.0572
Nonmyopic GP-UCB $H = 4$	0.5719 ± 0.0467	1.3984 ± 0.0537
GP-UCB-PE	0.3635 ± 0.0467	1.4079 ± 0.0568
GP-BUCB	0.3396 ± 0.0486	1.3717 ± 0.0573
q -EI	0.2595 ± 0.0444	1.5104 ± 0.0544
BBO-LP	0.3868 ± 0.0444	1.3666 ± 0.0547

TABLE VIII

AVERAGE NORMALIZED¹³ OUTPUT MEASUREMENTS ACHIEVED BY ϵ -MACRO-GPO WITH $H = 2$ AND $H = 3$ AFTER 20 OBSERVATIONS.

Value of β	$H = 2$	$H = 3$
$\beta = 0.0$	0.5563 ± 0.0446	0.5935 ± 0.0461
$\beta = 0.1$	0.6207 ± 0.0458	0.5842 ± 0.0438
$\beta = 0.3$	0.5357 ± 0.0459	0.5240 ± 0.0446
$\beta = 0.6$	0.4226 ± 0.0471	0.5016 ± 0.0470
$\beta = 1.0$	0.3746 ± 0.0460	0.4052 ± 0.0489
$\beta = 2.0$	0.2843 ± 0.0478	0.3566 ± 0.0491
$\beta = 4.0$	0.1919 ± 0.0498	0.2026 ± 0.0441
$\beta = 10.0$	0.0402 ± 0.0468	0.0569 ± 0.0453

APPENDIX C

ADDITIONAL EXPERIMENTAL RESULTS FOR REAL-WORLD TRAFFIC PHENOMENON (I.E., MOBILITY DEMAND PATTERN) OVER THE CENTRAL BUSINESS DISTRICT OF AN URBAN CITY

See Tables IX, X and XI.

TABLE IX

AVERAGE NORMALIZED¹³ OUTPUT MEASUREMENTS OBSERVED BY THE AV AND SIMPLE REGRETS ACHIEVED BY THE TESTED BO ALGORITHMS AFTER 20 OBSERVATIONS FOR THE REAL-WORLD TRAFFIC PHENOMENON (I.E., MOBILITY DEMAND PATTERN).

BO Algorithm	Average normalized output measurements	Simple regret
Anytime ϵ -Macro-GPO $H = 4$	0.2700 ± 0.1014	1.5423 ± 0.1047
Anytime ϵ -Macro-GPO $H = 3$	0.2574 ± 0.1019	1.5843 ± 0.0994
Anytime ϵ -Macro-GPO $H = 2$	0.2357 ± 0.1109	1.7396 ± 0.1179
DB-GP-UCB	0.2108 ± 0.1081	1.7050 ± 0.1212
Nonmyopic GP-UCB $H = 4$	0.2267 ± 0.1134	1.7314 ± 0.1158
GP-UCB-PE	0.0770 ± 0.0808	1.5203 ± 0.1247
GP-BUCB	0.0884 ± 0.0819	1.5177 ± 0.1262
q -EI	0.0007 ± 0.0945	1.7945 ± 0.1515
BBO-LP	-0.0077 ± 0.0957	1.7320 ± 0.1149

TABLE X

AVERAGE NORMALIZED¹³ OUTPUT MEASUREMENTS ACHIEVED BY *anytime* ϵ -MACRO-GPO WITH $H = 2, 3$ AND VARYING EXPLORATION WEIGHTS β AFTER 20 OBSERVATIONS FOR THE REAL-WORLD TRAFFIC PHENOMENON (I.E., MOBILITY DEMAND PATTERN).

Value of β	$H = 2$	$H = 3$
$\beta = 0.0$	0.2357 ± 0.1109	0.2574 ± 0.1019
$\beta = 0.2$	0.2550 ± 0.1032	0.2069 ± 0.0987
$\beta = 0.5$	0.1364 ± 0.0967	0.1174 ± 0.0893
$\beta = 1.0$	0.1429 ± 0.0967	0.0911 ± 0.0772
$\beta = 2.0$	0.1174 ± 0.0843	0.0330 ± 0.0755
$\beta = 4.0$	0.0957 ± 0.0841	0.0403 ± 0.0765
$\beta = 10.0$	0.0944 ± 0.0768	-0.0046 ± 0.0756

TABLE XI

AVERAGE NORMALIZED OUTPUT MEASUREMENTS OBSERVED BY THE AV AND SIMPLE REGRETS ACHIEVED BY *anytime* ϵ -MACRO-GPO WITH $H = 2, 4$ AND 20 RANDOMLY SELECTED MACRO-ACTIONS PER INPUT REGION, ANYTIME ϵ -MACRO-GPO WITH $H = 2$ AND ALL AVAILABLE MACRO-ACTIONS (THE NO. OF AVAILABLE MACRO-ACTIONS PER INPUT REGION IS ENCLOSED IN BRACKETS), AND EI WITH ALL AVAILABLE MACRO-ACTIONS OF LENGTH 1 AFTER 20 OBSERVATIONS FOR THE REAL-WORLD TRAFFIC PHENOMENON (I.E., MOBILITY DEMAND PATTERN).

BO Algorithm	Average normalized output measurements	Simple regret
Anytime ϵ -Macro-GPO $H = 4$ (20)	0.2700 ± 0.1014	1.5423 ± 0.1047
Anytime ϵ -Macro-GPO $H = 2$ (all)	0.2631 ± 0.0918	1.6427 ± 0.0792
Anytime ϵ -Macro-GPO $H = 2$ (20)	0.2357 ± 0.1109	1.7396 ± 0.1179
EI (all)	0.1469 ± 0.1084	1.6094 ± 0.0946

APPENDIX D

ADDITIONAL EXPERIMENTAL RESULTS FOR REAL-WORLD TEMPERATURE PHENOMENON OVER AN OFFICE ENVIRONMENT

See Table XII, Table XIII and Table XIV.

TABLE XII

AVERAGE NORMALIZED¹³ OUTPUT MEASUREMENTS OBSERVED BY THE MOBILE ROBOT AND SIMPLE REGRETS ACHIEVED BY THE TESTED BO ALGORITHMS AFTER 20 OBSERVATIONS FOR THE REAL-WORLD TEMPERATURE PHENOMENON OVER THE INTEL BERKELEY RESEARCH LAB.

BO Algorithm	Average normalized output measurements	Simple regret
Anytime ϵ -Macro-GPO $H = 4$	0.6371 ± 0.0797	0.4069 ± 0.0723
Anytime ϵ -Macro-GPO $H = 3$	0.6137 ± 0.0829	0.4285 ± 0.0678
Anytime ϵ -Macro-GPO $H = 2$	0.5450 ± 0.0951	0.5613 ± 0.0834
DB-GP-UCB	0.4874 ± 0.1017	0.6734 ± 0.0934
Nonmyopic GP-UCB $H = 4$	0.5708 ± 0.0908	0.5911 ± 0.0886
GP-UCB-PE	0.1377 ± 0.0734	0.6700 ± 0.0758
GP-BUCB	0.2067 ± 0.0758	0.6670 ± 0.0762
q -EI	0.3801 ± 0.1044	0.6868 ± 0.1116
BBO-LP	0.2549 ± 0.0833	0.5168 ± 0.0733

TABLE XIII

AVERAGE NORMALIZED¹³ OUTPUT MEASUREMENTS ACHIEVED BY ϵ -MACRO-GPO WITH $H = 2, 3$ AND VARYING EXPLORATION WEIGHTS β AFTER 20 OBSERVATIONS FOR THE REAL-WORLD TEMPERATURE PHENOMENON OVER THE INTEL BERKELEY RESEARCH LAB.

Value of β	$H = 2$	$H = 3$
$\beta = 0.0$	0.5450 ± 0.0951	0.6137 ± 0.0829
$\beta = 1.0$	0.6160 ± 0.0820	0.6047 ± 0.0764
$\beta = 2.0$	0.5565 ± 0.0765	0.5787 ± 0.0786
$\beta = 3.0$	0.3755 ± 0.0670	0.4468 ± 0.0645
$\beta = 4.0$	0.1859 ± 0.0608	0.2294 ± 0.0472

APPENDIX E

ADDITIONAL EXPERIMENTAL RESULTS FOR COMPARISON WITH ROLLOUT [17]

See Table XV.

APPENDIX F

DERIVATION OF (3)

The second summand on RHS of (2) can be re-written as

$$\mathbb{I}[y_S; \mathbf{z}_H | d_0, \pi] = \sum_{t=1}^H \mathbb{I}[y_S; z_t | \langle \mathbf{s}_{t-1}, z_0 \oplus \mathbf{z}_{t-1} \rangle, \pi] = 0.5 \sum_{t=0}^{H-1} \log |I + \sigma_n^{-2} \Sigma_{s_{t+1} | \mathbf{s}_t, \pi}|. \quad (11)$$

TABLE XIV

AVERAGE NORMALIZED OUTPUT MEASUREMENTS OBSERVED BY THE MOBILE ROBOT AND SIMPLE REGRETS ACHIEVED BY *anytime* ϵ -MACRO-GPO WITH $H = 2, 4$ AND 20 RANDOMLY SELECTED MACRO-ACTIONS PER INPUT REGION, ANYTIME ϵ -MACRO-GPO WITH $H = 2$ AND ALL AVAILABLE MACRO-ACTIONS (THE NO. OF AVAILABLE MACRO-ACTIONS PER INPUT REGION IS ENCLOSED IN BRACKETS), AND EI WITH ALL AVAILABLE MACRO-ACTIONS OF LENGTH 1 AFTER 20 OBSERVATIONS FOR THE REAL-WORLD TEMPERATURE PHENOMENON OVER THE INTEL BERKELEY RESEARCH LAB.

BO Algorithm	Average normalized output measurements	Simple regret
Anytime ϵ -Macro-GPO $H = 4$ (20)	0.6371 ± 0.0797	0.4069 ± 0.0723
Anytime ϵ -Macro-GPO $H = 2$ (all)	0.6265 ± 0.0861	0.5119 ± 0.0807
Anytime ϵ -Macro-GPO $H = 2$ (20)	0.5450 ± 0.0951	0.5613 ± 0.0834
EI (all)	0.4565 ± 0.1051	0.8754 ± 0.0941

TABLE XV

AVERAGE NORMALIZED¹³ OUTPUT MEASUREMENTS OBSERVED BY AUV AND (B) SIMPLE REGRETS ACHIEVED BY ϵ -MACRO-GPO WITH $H = 4$ AND ROLLOUT-4-10 VS. NO. OF OBSERVATIONS FOR SIMULATED PLANKTON DENSITY PHENOMENA.

BO Algorithm	Average normalized output measurements	Simple regret
ϵ -Macro-GPO $H = 4$	0.9501 ± 0.0659	1.066 ± 0.0783
Rollout-4-10	0.8071 ± 0.0637	1.2389 ± 0.0808

The first equality is due to the chain rule for mutual information [37]. Let $s_{t-1} \triangleq (s_{t-1,1}, \dots, s_{t-1,\kappa})$. The last equality follows from

$$\begin{aligned}
& \mathbb{I}[y_S; z_t | \langle \mathbf{s}_{t-1}, z_0 \oplus \mathbf{z}_{t-1} \rangle, \pi] \\
&= \mathbb{H}[z_t | \langle \mathbf{s}_{t-1}, z_0 \oplus \mathbf{z}_{t-1} \rangle, \pi] - \mathbb{H}[z_t | \langle \mathbf{s}_{t-1}, z_0 \oplus \mathbf{z}_{t-1} \rangle, y_S, \pi] \\
&= \mathbb{H}[z_t | \langle \mathbf{s}_{t-1}, z_0 \oplus \mathbf{z}_{t-1} \rangle, \pi] - \mathbb{H}[z_t | (y_{s_{t-1,1}}, \dots, y_{s_{t-1,\kappa}}), \pi] \\
&= 0.5\kappa \log(2\pi e) + 0.5 \log |\sigma_n^2 I + \Sigma_{s_t | s_{t-1}, \pi}| - 0.5\kappa \log(2\pi e) - 0.5 \log |\sigma_n^2 I| \\
&= 0.5 \log (|\sigma_n^2 I + \Sigma_{s_t | s_{t-1}, \pi}| |\sigma_n^2 I|^{-1}) \\
&= 0.5 \log (|\sigma_n^2 I + \Sigma_{s_t | s_{t-1}, \pi}| |\sigma_n^{-2} I|) \\
&= 0.5 \log |I + \sigma_n^{-2} \Sigma_{s_t | s_{t-1}, \pi}|
\end{aligned} \tag{12}$$

where the first equality is due to the definition of conditional mutual information, the third equality is due to the definition of Gaussian entropy, that is, $\mathbb{H}[z_t | \langle \mathbf{s}_{t-1}, z_0 \oplus \mathbf{z}_{t-1} \rangle, \pi] \triangleq 0.5\kappa \log(2\pi e) + 0.5 \log |\sigma_n^2 I + \Sigma_{s_t | s_{t-1}, \pi}|$ and $\mathbb{H}[z_t | (y_{s_{t-1,1}}, \dots, y_{s_{t-1,\kappa}}), \pi] \triangleq 0.5\kappa \log(2\pi e) + 0.5 \log |\sigma_n^2 I|$, the latter of which follows from $\varepsilon = z_{t,i} - y_{s_{t,i}} \sim \mathcal{N}(0, \sigma_n^2)$ for stage $t = 0, \dots, H-1$ and $i = 1, \dots, \kappa$, and hence $p(z_t | (y_{s_{t-1,1}}, \dots, y_{s_{t-1,\kappa}}), \pi) = \mathcal{N}(\mathbf{0}, \sigma_n^2 I)$. So, (2) can be re-expressed as

$$V_0^\pi(d_0) = \mathbb{E}_{\mathbf{z}_H | d_0, \pi} [\mathbf{1}^\top \mathbf{z}_H] + 0.5\beta \sum_{t=0}^{H-1} \log |I + \sigma_n^{-2} \Sigma_{s_{t+1} | s_t, \pi}|. \tag{13}$$

Given an arbitrary positive integer H' and denoting $\mathbf{z}_{\tau+1:H'}$ as a vector of realized output measurements from stage $\tau+1$ to stage H' , (13) for $H = 1, \dots, H'$ are, respectively, equivalent to

$$V_\tau^\pi(d_\tau) = \mathbb{E}_{\mathbf{z}_{\tau+1:H'} | d_\tau, \pi} [\mathbf{1}^\top \mathbf{z}_{\tau+1:H'}] + 0.5\beta \sum_{t=\tau}^{H'-1} \log |I + \sigma_n^{-2} \Sigma_{s_{t+1} | s_t, \pi}| \tag{14}$$

for $\tau = H' - 1, \dots, 0$ by simply adding τ to the indices denoting the planning stage in (13). From (14),

$$\begin{aligned}
& V_\tau^\pi(d_\tau) \\
&= \mathbb{E}_{\mathbf{z}_{\tau+1:H'}|d_\tau, \pi}[\mathbf{1}^\top \mathbf{z}_{\tau+1:H'}] + 0.5\beta \sum_{t=\tau}^{H'-1} \log |I + \sigma_n^{-2} \Sigma_{s_{t+1}|\mathbf{s}_t, \pi}| \\
&= \int \mathbf{1}^\top \mathbf{z}_{\tau+1:H'} p(\mathbf{z}_{\tau+1:H'}|d_\tau, \pi) d\mathbf{z}_{\tau+1:H'} + 0.5\beta \sum_{t=\tau}^{H'-1} \log |I + \sigma_n^{-2} \Sigma_{s_{t+1}|\mathbf{s}_t, \pi}| \\
&= \int (\mathbf{1}^\top \mathbf{z}_{\tau+1} + \mathbf{1}^\top \mathbf{z}_{\tau+2:H'}) p(\mathbf{z}_{\tau+2:H'}|d_{\tau+1}, \pi) d\mathbf{z}_{\tau+2:H'} p(\mathbf{z}_{\tau+1}|d_\tau, \pi) d\mathbf{z}_{\tau+1} \\
&\quad + 0.5\beta \sum_{t=\tau}^{H'-1} \log |I + \sigma_n^{-2} \Sigma_{s_{t+1}|\mathbf{s}_t, \pi}| \\
&= \int \mathbf{1}^\top \mathbf{z}_{\tau+1} \int p(\mathbf{z}_{\tau+2:H'}|d_{\tau+1}, \pi) d\mathbf{z}_{\tau+2:H'} p(\mathbf{z}_{\tau+1}|d_\tau, \pi) d\mathbf{z}_{\tau+1} \\
&\quad + 0.5\beta \log |I + \sigma_n^{-2} \Sigma_{s_{\tau+1}|\mathbf{s}_\tau, \pi}| \\
&\quad + \int \mathbf{1}^\top \mathbf{z}_{\tau+2:H'} p(\mathbf{z}_{\tau+2:H'}|d_{\tau+1}, \pi) d\mathbf{z}_{\tau+2:H'} p(\mathbf{z}_{\tau+1}|d_\tau, \pi) d\mathbf{z}_{\tau+1} \\
&\quad + 0.5\beta \sum_{t=\tau+1}^{H'-1} \log |I + \sigma_n^{-2} \Sigma_{s_{t+1}|\mathbf{s}_t, \pi}| \\
&= \int \mathbf{1}^\top \mathbf{z}_{\tau+1} p(\mathbf{z}_{\tau+1}|d_\tau, \pi) d\mathbf{z}_{\tau+1} + 0.5\beta \log |I + \sigma_n^{-2} \Sigma_{s_{\tau+1}|\mathbf{s}_\tau, \pi}| \\
&\quad + \int \int \mathbf{1}^\top \mathbf{z}_{\tau+2:H'} p(\mathbf{z}_{\tau+2:H'}|d_{\tau+1}, \pi) d\mathbf{z}_{\tau+2:H'} + 0.5\beta \sum_{t=\tau+1}^{H'-1} \log |I + \sigma_n^{-2} \Sigma_{s_{t+1}|\mathbf{s}_t, \pi}| p(\mathbf{z}_{\tau+1}|d_\tau, \pi) d\mathbf{z}_{\tau+1} \\
&= \mathbf{1}^\top \mu_{\mathbf{s}_{\tau+1}|d_\tau, \pi} + 0.5\beta \log |I + \sigma_n^{-2} \Sigma_{s_{\tau+1}|\mathbf{s}_\tau, \pi}| \\
&\quad + \int \mathbb{E}_{\mathbf{z}_{\tau+2:H'}|d_{\tau+1}, \pi}[\mathbf{1}^\top \mathbf{z}_{\tau+2:H'}] + 0.5\beta \sum_{t=\tau+1}^{H'-1} \log |I + \sigma_n^{-2} \Sigma_{s_{t+1}|\mathbf{s}_t, \pi}| p(\mathbf{z}_{\tau+1}|d_\tau, \pi) d\mathbf{z}_{\tau+1} \\
&= \mathbf{1}^\top \mu_{\pi(d_\tau)|d_\tau} + 0.5\beta \log |I + \sigma_n^{-2} \Sigma_{\pi(d_\tau)|\mathbf{s}_\tau}| + \int V_{\tau+1}^\pi(d_{\tau+1}) p(\mathbf{z}_{\tau+1}|d_\tau, \pi) d\mathbf{z}_{\tau+1} \\
&= R(\pi(d_\tau), d_\tau) + \mathbb{E}_{z_{t+1}|\pi(d_\tau), d_\tau}[V_{\tau+1}^\pi(\langle \mathbf{s}_t \oplus \pi(d_\tau), \mathbf{z}_t \oplus z_{t+1} \rangle)] \\
&= Q_\tau^\pi(\pi(d_\tau), d_\tau)
\end{aligned}$$

for stages $\tau = 0, \dots, H' - 1$ where the third last equality is due to (14) and the last two equalities follow from the definitions of R and Q_τ^π in (4) and (3), respectively.

APPENDIX G PROOF OF LEMMA 1

Proof.

$$\begin{aligned}
& |R(s_{t+1}, d_t) - R(s_{t+1}, d'_t)| \\
&= |\mathbf{1}^\top (\mu_{s_{t+1}|d_t} - \mu_{s_{t+1}|d'_t})| \\
&\leq \|\mu_{s_{t+1}|d_t} - \mu_{s_{t+1}|d'_t}\|_1 \\
&= \|\Sigma_{s_{t+1}|\mathbf{s}_t}^{-1} (\mathbf{z}_t - \mathbf{z}'_t)^\top\|_1 \\
&\leq \sqrt{\kappa} \|\Sigma_{s_{t+1}|\mathbf{s}_t}^{-1} (\mathbf{z}_t - \mathbf{z}'_t)^\top\| \\
&= \sqrt{\kappa} \|\Sigma_{s_{t+1}|\mathbf{s}_t}^{-1} (\mathbf{z}_t - \mathbf{z}'_t)^\top\|_F \\
&\leq \sqrt{\kappa} \|\Sigma_{s_{t+1}|\mathbf{s}_t}^{-1}\|_F \|\mathbf{z}_t - \mathbf{z}'_t\|_F \\
&= \sqrt{\kappa} \|\Sigma_{s_{t+1}|\mathbf{s}_t}^{-1}\|_F \|\mathbf{z}_t - \mathbf{z}'_t\| \\
&= \sqrt{\kappa} \alpha(\mathbf{s}_{t+1}) \|\mathbf{z}_t - \mathbf{z}'_t\|.
\end{aligned}$$

The first equality is due to (4). The first inequality is due to triangle inequality. The second equality is due to (1). The second inequality follows from a property of vector norms (see Section 2.2.2 in [38]). The last inequality is due to the submultiplicativity of the Frobenius norm (see Section II.2.1 in [39]). The last equality follows from the definition of $\alpha(\mathbf{s}_{t+1})$. \square

APPENDIX H LIPSCHITZ CONTINUITY OF $V_t^*(d_t)$ (5)

Definition 1. Let $L_H(\mathbf{s}_H) \triangleq 0$. Define

$$L_t(\mathbf{s}_t) \triangleq \max_{s_{t+1} \in \mathcal{A}(\mathbf{s}_t)} \sqrt{\kappa} \alpha(\mathbf{s}_{t+1}) + L_{t+1}(\mathbf{s}_{t+1}) \sqrt{1 + \alpha(\mathbf{s}_{t+1})^2}$$

for $t = 0, \dots, H-1$ where the function α is previously defined in Lemma 1.

The following result shows that $V_t^*(d_t)$ (5) is Lipschitz continuous in the realized output measurements \mathbf{z}_t with Lipschitz constant $L_t(\mathbf{s}_t)$:

Theorem 4. For $t = 0, \dots, H$,

$$|V_t^*(d_t) - V_t^*(d'_t)| \leq L_t(\mathbf{s}_t) \|\mathbf{z}_t - \mathbf{z}'_{0:t}\| \quad (15)$$

where d'_t is previously defined in Lemma 1.

Proof. We give a proof by induction on t . When $t = H$ (i.e., base case), $V_H^*(d_H) = 0$ for any d_H . So, $|V_H^*(d_H) - V_H^*(d'_H)| = 0 \leq L_H(\mathbf{s}_H) \|\mathbf{z}_H - \mathbf{z}'_{0:H}\|$. Supposing (15) holds for $t+1$ (i.e., induction hypothesis), we will prove that it holds for $t = 0, \dots, H-1$. Let $s_{t+1}^* \triangleq \pi^*(d_t)$ and $\Delta_{t+1} \triangleq \mu_{s_{t+1}^*|d_t} - \mu_{s_{t+1}^*|d'_t}$. Using (1), the submultiplicativity of the Frobenius norm (see Section II.2.1 in [39]), and the definition of $\alpha(\mathbf{s}_{t+1})$,

$$\|\Delta_{t+1}\| \leq \alpha(\mathbf{s}_t \oplus s_{t+1}^*) \|\mathbf{z}_t - \mathbf{z}'_t\|. \quad (16)$$

Without loss of generality, assume that $V_t^*(d_t) \geq V_t^*(d'_t)$. From (5),

$$\begin{aligned} & V_t^*(d_t) - V_t^*(d'_t) \\ & \leq Q_t^*(s_{t+1}^*, d_t) - Q_t^*(s_{t+1}^*, d'_t) \\ & \leq |Q_t^*(s_{t+1}^*, d_t) - Q_t^*(s_{t+1}^*, d'_t)| \\ & \leq |R(s_{t+1}^*, d_t) - R(s_{t+1}^*, d'_t)| + \left| \int p(z_{t+1}|s_{t+1}^*, d_t) V_{t+1}^*(\langle \mathbf{s}_t \oplus s_{t+1}^*, \mathbf{z}_{t+1} \rangle) d\mathbf{z}_{t+1} \right. \\ & \quad \left. - \int p(z'_{t+1}|s_{t+1}^*, d'_t) V_{t+1}^*(\langle \mathbf{s}_t \oplus s_{t+1}^*, \mathbf{z}'_{t+1} \rangle) d\mathbf{z}'_{t+1} \right| \\ & \leq \sqrt{\kappa} \alpha(\mathbf{s}_t \oplus s_{t+1}^*) \|\mathbf{z}_t - \mathbf{z}'_t\| + \int p(z_{t+1}|s_{t+1}^*, d_t) L_{t+1}(\mathbf{s}_t \oplus s_{t+1}^*) \|(\mathbf{z}_t - \mathbf{z}'_t) \oplus \Delta_{t+1}\| d\mathbf{z}_{t+1} \\ & = \sqrt{\kappa} \alpha(\mathbf{s}_t \oplus s_{t+1}^*) \|\mathbf{z}_t - \mathbf{z}'_t\| + L_{t+1}(\mathbf{s}_t \oplus s_{t+1}^*) \|(\mathbf{z}_t - \mathbf{z}'_t) \oplus \Delta_{t+1}\| \\ & \leq \sqrt{\kappa} \alpha(\mathbf{s}_t \oplus s_{t+1}^*) \|\mathbf{z}_t - \mathbf{z}'_t\| + L_{t+1}(\mathbf{s}_t \oplus s_{t+1}^*) \sqrt{1 + \alpha(\mathbf{s}_t \oplus s_{t+1}^*)^2} \|\mathbf{z}_t - \mathbf{z}'_t\| \\ & \leq L_t(\mathbf{s}_t) \|\mathbf{z}_t - \mathbf{z}'_t\| \end{aligned} \quad (17)$$

where the third inequality follows from (5) and triangle inequality, the fourth inequality follows from Lemma 1, change of variable $\mathbf{z}'_{t+1} \triangleq \mathbf{z}_{t+1} - \Delta_{t+1}$, and the induction hypothesis, the second last inequality in (17) is due to

$$\|(\mathbf{z}_t - \mathbf{z}'_t) \oplus \Delta_{t+1}\| = \sqrt{\|\mathbf{z}_t - \mathbf{z}'_t\|^2 + \|\Delta_{t+1}\|^2} \leq \sqrt{1 + \alpha(\mathbf{s}_t \oplus s_{t+1}^*)^2} \|\mathbf{z}_t - \mathbf{z}'_t\|$$

with the inequality following from (16), and the last inequality in (17) is due to the definition of L_t (Definition 1). \square

APPENDIX I PROOF OF THEOREM 1

Proof. There are two sources of error arising in using $Q_t(s_{t+1}, d_t)$ to approximate $Q_t^*(s_{t+1}, d_t)$: (a) Every stage-wise expectation term in (5) is approximated via stochastic sampling (6) of a finite number N of i.i.d. multivariate Gaussian vectors z^1, \dots, z^N from the GP posterior belief $p(z_{t+1}|s_{t+1}, d_t) = \mathcal{N}(\mu_{s_{t+1}|d_t}, \Sigma_{s_{t+1}|s_t})$ (1), and (b) evaluating $Q_t(s_{t+1}, d_t)$ does not involve utilizing the values of V_{t+1}^* but rather that of its approximation \mathcal{V}_{t+1} . To facilitate capturing the error due to finite stochastic sampling described in (a), the following intermediate function is introduced:

$$\mathcal{U}_t(s_{t+1}, d_t) \triangleq R(s_{t+1}, d_t) + \frac{1}{N} \sum_{\ell=1}^N V_{t+1}^*(\langle \mathbf{s}_{t+1}, \mathbf{z}_t \oplus z^\ell \rangle) \quad (18)$$

for $t = 0, \dots, H-1$. The following lemma shows that $\mathcal{U}_t(s_{t+1}, d_t)$ can approximate $Q_t^*(s_{t+1}, d_t)$ arbitrarily closely:

Lemma 2. Suppose that the observations $d_{t'}$, $H \in \mathbb{Z}^+$, a budget of $\kappa(H - t')$ input locations for $t' = 0, \dots, H-1$, $\lambda > 0$, and $N \in \mathbb{Z}^+$ are given. For all tuples $\langle t, s_{t+1}, d_t \rangle$ generated at stage $t = t', \dots, H-1$ by (6) to compute $\mathcal{V}_{t'}(d_{t'})$,

$$P(|\mathcal{U}_t(s_{t+1}, d_t) - Q_t^*(s_{t+1}, d_t)| \leq \lambda) \geq 1 - 2 \exp\left(-\frac{N\lambda^2}{2K^2}\right)$$

where $K \triangleq \mathcal{O}(\kappa^H \sqrt{H!} \sigma_n(1 + \sigma_y^2/\sigma_n^2)^H)$.

Proof. For any tuple $\langle t, s_{t+1}, d_t \rangle$, define the following auxiliary function:

$$\begin{aligned} \mathcal{G}(z^1, \dots, z^N) &\triangleq \frac{1}{N} \sum_{\ell=1}^N V_{t+1}^*(\langle \mathbf{s}_{t+1}, \mathbf{z}_t \oplus z^\ell \rangle) \\ &= \mathcal{U}_t(s_{t+1}, d_t) - R(s_{t+1}, d_t) \end{aligned} \quad (19)$$

which follows from (18). Taking an expectation of (19) with respect to GP posterior belief $p(z_{t+1}|s_{t+1}, d_t) = \mathcal{N}(\mu_{s_{t+1}|d_t}, \Sigma_{s_{t+1}|s_t})$ gives

$$\begin{aligned} &\mathbb{E}_{z^1, \dots, z^N \sim \mathcal{N}(\mu_{s_{t+1}|d_t}, \Sigma_{s_{t+1}|s_t})} [\mathcal{G}(z^1, \dots, z^N)] \\ &= \mathbb{E}_{z^1, \dots, z^N \sim \mathcal{N}(\mu_{s_{t+1}|d_t}, \Sigma_{s_{t+1}|s_t})} \left[\frac{1}{N} \sum_{\ell=1}^N V_{t+1}^*(\langle \mathbf{s}_{t+1}, \mathbf{z}_t \oplus z^\ell \rangle) \right] \\ &= \frac{1}{N} \sum_{\ell=1}^N \mathbb{E}_{z^1, \dots, z^N \sim \mathcal{N}(\mu_{s_{t+1}|d_t}, \Sigma_{s_{t+1}|s_t})} [V_{t+1}^*(\langle \mathbf{s}_{t+1}, \mathbf{z}_t \oplus z^\ell \rangle)] \\ &= \frac{1}{N} \sum_{\ell=1}^N \mathbb{E}_{z^\ell \sim \mathcal{N}(\mu_{s_{t+1}|d_t}, \Sigma_{s_{t+1}|s_t})} [V_{t+1}^*(\langle \mathbf{s}_{t+1}, \mathbf{z}_t \oplus z^\ell \rangle)] \\ &= \frac{1}{N} \sum_{\ell=1}^N \mathbb{E}_{z_{t+1}|s_{t+1}, d_t} [V_{t+1}^*(\langle \mathbf{s}_{t+1}, \mathbf{z}_t \oplus z_{t+1} \rangle)] \\ &= \mathbb{E}_{z_{t+1}|s_{t+1}, d_t} [V_{t+1}^*(\langle \mathbf{s}_{t+1}, \mathbf{z}_t \oplus z_{t+1} \rangle)] \\ &= Q_t^*(s_{t+1}, d_t) - R(s_{t+1}, d_t) \end{aligned} \quad (20)$$

such that the last equality is due to (5). From (19) and (20),

$$|\mathcal{U}_t(s_{t+1}, d_t) - Q_t^*(s_{t+1}, d_t)| = \left| \mathcal{G}(z^1, \dots, z^N) - \mathbb{E}_{z^1, \dots, z^N \sim \mathcal{N}(\mu_{s_{t+1}|d_t}, \Sigma_{s_{t+1}|s_t})} [\mathcal{G}(z^1, \dots, z^N)] \right|. \quad (21)$$

The RHS of (21) can usually be bounded using a concentration inequality that involves independent Gaussian random variables. However, the components of the multivariate Gaussian vector z^ℓ are correlated. To resolve this complication, we exploit a change of variables trick to make the components independent:

$$z^\ell = \mu_{s_{t+1}|d_t} + \Psi \mathbf{x}^\ell \quad (22)$$

for $\ell = 1, \dots, N$ where Ψ is a $\kappa \times \kappa$ lower triangular matrix satisfying the Cholesky decomposition of the symmetric and positive definite $\Sigma_{s_{t+1}|s_t} = \Psi \Psi^\top$ and \mathbf{x}^ℓ is a standard multivariate Gaussian vector with independent components (see Section 53.2.2 in [40]).

Define a new auxiliary function G in terms of \mathcal{G} by plugging (22) into (19):

$$G(\mathbf{x}^1, \dots, \mathbf{x}^N) \triangleq \mathcal{G}(z^1, \dots, z^N). \quad (23)$$

We will first prove that G is Lipschitz continuous in $\mathbf{x}^1 \oplus \dots \oplus \mathbf{x}^N$ with Lipschitz constant $L_{t+1}(s_{t+1}) \sqrt{\text{Tr}(\Sigma_{s_{t+1}|s_t})/N}$, which is a sufficient condition for using the Tsirelson-Ibragimov-Sudakov inequality [36] to prove the probabilistic bound in Lemma 2. To simplify notations, let $\bar{\mathbf{x}} \triangleq \mathbf{x}^1 \oplus \dots \oplus \mathbf{x}^N$ and $\bar{\mathbf{x}}' \triangleq \mathbf{x}'^1 \oplus \dots \oplus \mathbf{x}'^N$. Then,

$$\begin{aligned} &|G(\mathbf{x}^1, \dots, \mathbf{x}^N) - G(\mathbf{x}'^1, \dots, \mathbf{x}'^N)| \\ &= |\mathcal{G}(z^1, \dots, z^N) - \mathcal{G}(z'^1, \dots, z'^N)| \\ &\leq \frac{1}{N} \sum_{\ell=1}^N |V_{t+1}^*(\langle \mathbf{s}_{t+1}, \mathbf{z}_t \oplus z^\ell \rangle) - V_{t+1}^*(\langle \mathbf{s}_{t+1}, \mathbf{z}_t \oplus z'^\ell \rangle)| \\ &\leq \frac{L_{t+1}(s_{t+1})}{N} \sum_{\ell=1}^N \|z^\ell - z'^\ell\| \\ &\leq \frac{L_{t+1}(s_{t+1})}{N} \sqrt{N} \|\Psi\|_F \|\bar{\mathbf{x}} - \bar{\mathbf{x}}'\| \\ &= \frac{L_{t+1}(s_{t+1})}{\sqrt{N}} \|\Psi\|_F \|\bar{\mathbf{x}} - \bar{\mathbf{x}}'\| \\ &= L_{t+1}(s_{t+1}) \sqrt{\frac{\text{Tr}(\Sigma_{s_{t+1}|s_t})}{N}} \|\bar{\mathbf{x}} - \bar{\mathbf{x}}'\| \end{aligned} \quad (24)$$

where the first equality is due to (23), the last equality follows from a property of Frobenius norm (see Section 10.4.3 in [41]), the first inequality is due to (19) and triangle inequality, the second inequality is a direct consequence of Theorem 4 in Appendix H, and the third inequality follows from

$$\begin{aligned}
& \sum_{\ell=1}^N \|z^\ell - z'^\ell\| \\
&= \sum_{\ell=1}^N \|\Psi(\mathbf{x}^\ell - \mathbf{x}'^\ell)\| \\
&= \sum_{\ell=1}^N \|\Psi(\mathbf{x}^\ell - \mathbf{x}'^\ell)\|_F \\
&\leq \sum_{\ell=1}^N \|\Psi\|_F \|\mathbf{x}^\ell - \mathbf{x}'^\ell\|_F \\
&= \|\Psi\|_F \sum_{\ell=1}^N \|\mathbf{x}^\ell - \mathbf{x}'^\ell\| \\
&\leq \sqrt{N} \|\Psi\|_F \|\bar{\mathbf{x}} - \bar{\mathbf{x}}'\|
\end{aligned}$$

where the first equality is due to (22), the first inequality is due to the submultiplicativity of the Frobenius norm (see Section II.2.1 in [39]), and the last inequality is due to Cauchy-Schwarz inequality. Since conditioning does not increase GP posterior variance,

$$\text{Tr}(\Sigma_{s_{t+1}|s_t}) \leq \text{Tr}(\Sigma_{s_{t+1}s_{t+1}}) = \kappa(\sigma_y^2 + \sigma_n^2). \quad (25)$$

From (25) and Lemma 9,

$$\begin{aligned}
& L_{t+1}(\mathbf{s}_{t+1}) \sqrt{\text{Tr}(\Sigma_{s_{t+1}|s_t})} \\
&= \mathcal{O}(\kappa^{H-t-1/2} \sqrt{H!/(t+1)!} (1 + \sigma_y^2/\sigma_n^2)^{H-t-1}) \mathcal{O}(\kappa^{1/2}(\sigma_y^2 + \sigma_n^2)^{1/2}) \\
&= \mathcal{O}(\kappa^{H-t} \sqrt{H!/(t+1)!} \sigma_n (1 + \sigma_y^2/\sigma_n^2)^{H-t-1/2}).
\end{aligned} \quad (26)$$

It follows from (26) that

$$K \triangleq \max_{\langle t, s_{t+1}, d_t \rangle} L_{t+1}(\mathbf{s}_{t+1}) \sqrt{\text{Tr}(\Sigma_{s_{t+1}|s_t})} = \mathcal{O}(\kappa^H \sqrt{H!} \sigma_n (1 + \sigma_y^2/\sigma_n^2)^H). \quad (27)$$

Finally,

$$\begin{aligned}
& P(|\mathcal{U}_t(s_{t+1}, d_t) - Q_t^*(s_{t+1}, d_t)| > \lambda) \\
&= P(|\mathcal{G}(z^1, \dots, z^N) - \mathbb{E}_{z^1, \dots, z^N}[\mathcal{G}(z^1, \dots, z^N)]| > \lambda) \\
&= P(|G(\mathbf{x}^1, \dots, \mathbf{x}^N) - \mathbb{E}_{\mathbf{x}^1, \dots, \mathbf{x}^N}[G(\mathbf{x}^1, \dots, \mathbf{x}^N)]| > \lambda) \\
&\leq 2 \exp\left(-\frac{N\lambda^2}{2L_{t+1}^2(\mathbf{s}_{t+1})\text{Tr}(\Sigma_{s_{t+1}|s_t})}\right) \\
&\leq 2 \exp\left(-\frac{N\lambda^2}{2K^2}\right)
\end{aligned}$$

where the first equality is due to (21), the second equality is due to (23) above and (28) below, the first inequality is due to the Tsirelson-Ibragimov-Sudakov inequality that requires G to be Lipschitz continuous in $\mathbf{x}^1 \oplus \dots \oplus \mathbf{x}^N$ which is shown in (24) (see Section 5.4 on page 125 in [36]), and the last inequality is due to (27).

$$\begin{aligned}
& \mathbb{E}_{z^1, \dots, z^N}[\mathcal{G}(z^1, \dots, z^N)] \\
&= \mathbb{E}_{z_{t+1}|s_{t+1}, d_t}[V_{t+1}^*(\langle \mathbf{s}_{t+1}, \mathbf{z}_t \oplus z_{t+1} \rangle)] \\
&= \int_{\mathbb{R}^\kappa} V_{t+1}^*(\langle \mathbf{s}_{t+1}, \mathbf{z}_t \oplus z_{t+1} \rangle) p(z_{t+1}|s_{t+1}, d_t) dz_{t+1} \\
&= \int_{\mathbb{R}^\kappa} V_{t+1}^*(\langle \mathbf{s}_{t+1}, \mathbf{z}_t \oplus (\mu_{s_{t+1}|d_t} + \Psi \mathbf{x}_{t+1}) \rangle) \frac{1}{|\Psi|} p(\mathbf{x}_{t+1}) \left| \frac{\partial z_{t+1}}{\partial \mathbf{x}_{t+1}} \right| d\mathbf{x}_{t+1} \\
&= \int_{\mathbb{R}^\kappa} V_{t+1}^*(\langle \mathbf{s}_{t+1}, \mathbf{z}_t \oplus (\mu_{s_{t+1}|d_t} + \Psi \mathbf{x}_{t+1}) \rangle) p(\mathbf{x}_{t+1}) d\mathbf{x}_{t+1} \\
&= \mathbb{E}_{\mathbf{x}_{t+1}}[V_{t+1}^*(\langle \mathbf{s}_{t+1}, \mathbf{z}_t \oplus (\mu_{s_{t+1}|d_t} + \Psi \mathbf{x}_{t+1}) \rangle)] \\
&= \mathbb{E}_{\mathbf{x}^1, \dots, \mathbf{x}^N} \left[\frac{1}{N} \sum_{\ell=1}^N V_{t+1}^*(\langle \mathbf{s}_{t+1}, \mathbf{z}_t \oplus (\mu_{s_{t+1}|d_t} + \Psi \mathbf{x}^\ell) \rangle) \right] \\
&= \mathbb{E}_{\mathbf{x}^1, \dots, \mathbf{x}^N}[G(\mathbf{x}^1, \dots, \mathbf{x}^N)]
\end{aligned} \quad (28)$$

where the first equality is due to (20), the third equality follows from (22), $p(z_{t+1}|s_{t+1}, d_t) = p(\mathbf{x}_{t+1} = \Psi^{-1}(z_{t+1} - \mu_{s_{t+1}|d_t}))/|\Psi|$ (see Section 35.1.2 in [40]), and an integration by substitution for multiple variables, the fourth equality is due to $|\partial z_{t+1}/\partial \mathbf{x}_{t+1}| = |\Psi|$, and the last two equalities can be derived in a similar manner as (20) using (23). \square

Lemma 3. Suppose that the observations $d_{t'}$, $H \in \mathbb{Z}^+$, a budget of $\kappa(H - t')$ input locations for $t' = 0, \dots, H - 1$, $\lambda > 0$, and $N \in \mathbb{Z}^+$ are given. The probability of $|\mathcal{U}_t(s_{t+1}, d_t) - Q_t^*(s_{t+1}, d_t)| \leq \lambda$ for all tuples $\langle t, s_{t+1}, d_t \rangle$ generated at stage $t = t', \dots, H - 1$ by (6) to compute $\mathcal{V}_{t'}(d_{t'})$ is at least

$$1 - 2(NA)^H \exp\left(-\frac{N\lambda^2}{2K^2}\right)$$

where K is previously defined in Lemma 2.

Proof. From Lemma 2,

$$P(|\mathcal{U}_t(s_{t+1}, d_t) - Q_t^*(s_{t+1}, d_t)| > \lambda) \leq 2 \exp\left(-\frac{N\lambda^2}{2K^2}\right)$$

for each tuple $\langle t, s_{t+1}, d_t \rangle$ generated at stage $t = t', \dots, H - 1$ by (6) to compute $\mathcal{V}_{t'}(d_{t'})$. Since there will be no more than $(NA)^H$ tuples $\langle t, s_{t+1}, d_t \rangle$ generated at stage $t = t', \dots, H - 1$ by (6) to compute $\mathcal{V}_{t'}(d_{t'})$, the probability of $|\mathcal{U}_t(s_{t+1}, d_t) - Q_t^*(s_{t+1}, d_t)| > \lambda$ for some generated tuple $\langle t, s_{t+1}, d_t \rangle$ is at most $2(NA)^H \exp(-N\lambda^2/(2K^2))$ by applying the union bound. Lemma 3 directly follows. \square

Lemma 4. Suppose that the observations $d_{t'}$, $H \in \mathbb{Z}^+$, a budget of $\kappa(H - t')$ input locations for $t' = 0, \dots, H - 1$, $\lambda > 0$, and $N \in \mathbb{Z}^+$ are given. If

$$|\mathcal{U}_t(s_{t+1}, d_t) - Q_t^*(s_{t+1}, d_t)| \leq \lambda \quad (29)$$

for all tuples $\langle t, s_{t+1}, d_t \rangle$ generated at stage $t = t', \dots, H - 1$ by (6) to compute $\mathcal{V}_{t'}(d_{t'})$, then, for all $s_{t'+1} \in \mathcal{A}(s_{t'})$,

$$|\mathcal{Q}_{t'}(s_{t'+1}, d_{t'}) - Q_{t'}^*(s_{t'+1}, d_{t'})| \leq \lambda(H - t'). \quad (30)$$

Proof. We will give a proof by induction on t that $|\mathcal{Q}_t(s_{t+1}, d_t) - Q_t^*(s_{t+1}, d_t)| \leq \lambda(H - t)$ for all tuples $\langle t, s_{t+1}, d_t \rangle$ generated at stage $t = t' \dots, H - 1$ by (6) to compute $\mathcal{V}_{t'}(d_{t'})$.

When $t = H - 1$, $\mathcal{U}_t(s_{t+1}, d_t) = \mathcal{Q}_t(s_{t+1}, d_t)$ in (29), by definition. So, (30) holds for the base case. Supposing (30) holds for $t + 1$ (i.e. induction hypothesis), we will prove that it holds for $t = t', \dots, H - 2$:

$$\begin{aligned} & |\mathcal{Q}_t(s_{t+1}, d_t) - Q_t^*(s_{t+1}, d_t)| \\ & \leq |\mathcal{Q}_t(s_{t+1}, d_t) - \mathcal{U}_t(s_{t+1}, d_t)| + |\mathcal{U}_t(s_{t+1}, d_t) - Q_t^*(s_{t+1}, d_t)| \\ & \leq |\mathcal{Q}_t(s_{t+1}, d_t) - \mathcal{U}_t(s_{t+1}, d_t)| + \lambda \\ & \leq \lambda(H - t - 1) + \lambda \\ & = \lambda(H - t) \end{aligned}$$

where the first and the second inequalities follow, respectively, from the triangle inequality and (29), and the last inequality is due to

$$\begin{aligned} & |\mathcal{Q}_t(s_{t+1}, d_t) - \mathcal{U}_t(s_{t+1}, d_t)| \\ & \leq \frac{1}{N} \sum_{\ell=1}^N |\mathcal{V}_{t+1}(\langle s_{t+1}, \mathbf{z}_t \oplus z^\ell \rangle) - V_{t+1}^*(\langle s_{t+1}, \mathbf{z}_t \oplus z^\ell \rangle)| \\ & \leq \frac{1}{N} \sum_{\ell=1}^N \max_{s_{t+2} \in \mathcal{A}(s_{t+1})} |\mathcal{Q}_{t+1}(s_{t+2}, \langle s_{t+1}, \mathbf{z}_t \oplus z^\ell \rangle) - Q_{t+1}^*(s_{t+2}, \langle s_{t+1}, \mathbf{z}_t \oplus z^\ell \rangle)| \\ & \leq \lambda(H - t - 1) \end{aligned} \quad (31)$$

where the first inequality is due to triangle inequality and the last inequality follows from induction hypothesis.

Finally, when $t = t'$, $|\mathcal{Q}_{t'}(s_{t'+1}, d_{t'}) - Q_{t'}^*(s_{t'+1}, d_{t'})| \leq \lambda(H - t')$ (30) for all $s_{t'+1} \in \mathcal{A}(s_{t'})$ since $d_t = d_{t'}$. \square

Main proof. It follows immediately from Lemmas 3 and 4 that the probability of $|\mathcal{Q}_t(s_{t+1}, d_t) - Q_t^*(s_{t+1}, d_t)| \leq \lambda H$ for all $s_{t+1} \in \mathcal{A}(s_t)$ is at least $1 - 2(NA)^H \exp(-N\lambda^2/(2K^2))$ where K is previously defined in Lemma 2.

To guarantee that the probability of $|\mathcal{Q}_t(s_{t+1}, d_t) - Q_t^*(s_{t+1}, d_t)| \leq \lambda H$ for all $s_{t+1} \in \mathcal{A}(s_t)$ is at least $1 - \delta$, the value of N has to satisfy the following inequality:

$$1 - 2(NA)^H \exp\left(-\frac{N\lambda^2}{2K^2}\right) \geq 1 - \delta,$$

which is equivalent to

$$N \geq \frac{2K^2}{\lambda^2} \left(H \log N + H \log(A) + \log \frac{2}{\delta} \right). \quad (32)$$

Using the identity $\log N \leq \nu N - \log \nu - 1$ for $\nu = \lambda^2/(4K^2H)$, the RHS of (32) can be bounded from above by

$$\frac{N}{2} + \frac{2K^2}{\lambda^2} \left(H \log \left(\frac{4K^2HA}{e\lambda^2} \right) + \log \frac{2}{\delta} \right).$$

Therefore, to satisfy (32), it suffices to determine the value of N such that

$$N \geq \frac{N}{2} + \frac{2K^2}{\lambda^2} \left(H \log \left(\frac{4K^2HA}{e\lambda^2} \right) + \log \frac{2}{\delta} \right)$$

by setting

$$N = \frac{4K^2}{\lambda^2} \left(H \log \left(\frac{4K^2HA}{e\lambda^2} \right) + \log \frac{2}{\delta} \right)$$

where K is previously defined in Lemma 2. By assuming H , σ_y^2 , and σ_n^2 as constants,

$$N = \mathcal{O} \left(\frac{\kappa^{2H}}{\lambda^2} \log \left(\frac{\kappa A}{\delta \lambda} \right) \right).$$

□

APPENDIX J PROOF OF THEOREM 2

Proof. Similar to (18), the following intermediate function is introduced:

$$\mathbb{U}_t(s_{t+1}, d_t) \triangleq R(s_{t+1}, d_t) + V_{t+1}^*(\langle \mathbf{s}_{t+1}, \mathbf{z}_t \oplus \mu_{s_{t+1}|d_t} \rangle). \quad (33)$$

for $t = 0, \dots, H-1$.

We will first bound $|Q_t^*(s_{t+1}, d_t) - \mathbb{U}_t(s_{t+1}, d_t)|$:

$$\begin{aligned} & |Q_t^*(s_{t+1}, d_t) - \mathbb{U}_t(s_{t+1}, d_t)| \\ &= \left| \int_{\mathbb{R}^\kappa} (V_{t+1}^*(\langle \mathbf{s}_{t+1}, \mathbf{z}_t \oplus z_{t+1} \rangle) - V_{t+1}^*(\langle \mathbf{s}_{t+1}, \mathbf{z}_t \oplus \mu_{s_{t+1}|d_t} \rangle)) p(z_{t+1}|s_{t+1}, d_t) \, dz_{t+1} \right| \\ &\leq L_{t+1}(\mathbf{s}_{t+1}) \int_{\mathbb{R}^\kappa} \|z_{t+1} - \mu_{s_{t+1}|d_t}\| p(z_{t+1}|s_{t+1}, d_t) \, dz_{t+1} \\ &= L_{t+1}(\mathbf{s}_{t+1}) \int_{\mathbb{R}^\kappa} \|\Psi \mathbf{x}_{t+1}\| \frac{1}{|\Psi|} p(\mathbf{x}_{t+1}) \left| \frac{\partial z_{t+1}}{\partial \mathbf{x}_{t+1}} \right| \, d\mathbf{x}_{t+1} \\ &= L_{t+1}(\mathbf{s}_{t+1}) \int_{\mathbb{R}^\kappa} \|\Psi \mathbf{x}_{t+1}\| p(\mathbf{x}_{t+1}) \, d\mathbf{x}_{t+1} \\ &\leq L_{t+1}(\mathbf{s}_{t+1}) \|\Psi\|_F \mathbb{E}_{\mathbf{x}_{t+1}} [\|\mathbf{x}_{t+1}\|] \\ &= L_{t+1}(\mathbf{s}_{t+1}) \sqrt{\text{Tr}(\Sigma_{s_{t+1}|s_t})} \mathbb{E}_{\mathbf{x}_{t+1}} [\|\mathbf{x}_{t+1}\|] \\ &= \mathcal{O}(\kappa^{H-t} \sqrt{H!/(t+1)!} \sigma_n (1 + \sigma_y^2/\sigma_n^2)^{H-t-1/2}) \mathbb{E}_{\mathbf{x}_{t+1}} [\|\mathbf{x}_{t+1}\|] \\ &= \mathcal{O}(\kappa^{H-t+1/2} \sqrt{H!/(t+1)!} \sigma_n (1 + \sigma_y^2/\sigma_n^2)^{H-t-1/2}) \end{aligned} \quad (34)$$

where the first equality is due to (5) and (33), the first inequality is a direct consequence of Theorem 4 in Appendix H, the second equality follows from (22), $p(z_{t+1}|s_{t+1}, d_t) = p(\mathbf{x}_{t+1} = \Psi^{-1}(z_{t+1} - \mu_{s_{t+1}|d_t}))/|\Psi|$ (see Section 35.1.2 in [40]), and an integration by substitution for multiple variables, the third equality is due to $|\partial z_{t+1}/\partial \mathbf{x}_{t+1}| = |\Psi|$, the second inequality is due to the submultiplicativity of the Frobenius norm (see Section II.2.1 in [39]), the fourth equality follows from a property of Frobenius norm (see Section 10.4.3 in [41]), the second last equality is due to (26), and the last equality follows from $\mathbb{E}_{\mathbf{x}_{t+1}} [\|\mathbf{x}_{t+1}\|] \leq \sqrt{\kappa}$ (see Section 3.1 in [42]).

We will now give a proof by induction on t that

$$|Q_t^*(s_{t+1}, d_t) - \mathbb{Q}_t(s_{t+1}, d_t)| \leq \theta_t \quad (35)$$

for all $s_{t+1} \in \mathcal{A}(s_t)$ where

$$\theta_t \triangleq \mathcal{O}(\kappa^{H-t+1/2} \sqrt{H!/(t+1)!} \sigma_n (1 + \sigma_y^2/\sigma_n^2)^{H-t-1/2}). \quad (36)$$

When $t = H - 1$, $Q_t^*(s_{t+1}, d_t) - Q_t(s_{t+1}, d_t) = 0$. So, (35) holds for the base case. Supposing (35) holds for $t + 1$ (i.e. induction hypothesis), we will prove that it holds for $t = 0, \dots, H - 2$:

$$\begin{aligned}
& |Q_t^*(s_{t+1}, d_t) - Q_t(s_{t+1}, d_t)| \\
& \leq |Q_t^*(s_{t+1}, d_t) - U_t(s_{t+1}, d_t)| + |U_t(s_{t+1}, d_t) - Q_t(s_{t+1}, d_t)| \\
& \leq \mathcal{O}(\kappa^{H-t+1/2} \sqrt{H!/(t+1)!} \sigma_n (1 + \sigma_y^2/\sigma_n^2)^{H-t-1/2}) \\
& \quad + |V_{t+1}^*(\langle s_{t+1}, \mathbf{z}_t \oplus \mu_{s_{t+1}|d_t} \rangle) - V_{t+1}(\langle s_{t+1}, \mathbf{z}_t \oplus \mu_{s_{t+1}|d_t} \rangle)| \\
& \leq \mathcal{O}(\kappa^{H-t+1/2} \sqrt{H!/(t+1)!} \sigma_n (1 + \sigma_y^2/\sigma_n^2)^{H-t-1/2}) \\
& \quad + \max_{s_{t+2} \in \mathcal{A}(s_{t+1})} |Q_{t+1}^*(s_{t+2}, \langle s_{t+1}, \mathbf{z}_t \oplus \mu_{s_{t+1}|d_t} \rangle) - Q_{t+1}(s_{t+2}, \langle s_{t+1}, \mathbf{z}_t \oplus \mu_{s_{t+1}|d_t} \rangle)| \\
& \leq \mathcal{O}(\kappa^{H-t+1/2} \sqrt{H!/(t+1)!} \sigma_n (1 + \sigma_y^2/\sigma_n^2)^{H-t-1/2}) + \theta_{t+1} \\
& = \mathcal{O}(\kappa^{H-t+1/2} \sqrt{H!/(t+1)!} \sigma_n (1 + \sigma_y^2/\sigma_n^2)^{H-t-1/2}) \\
& = \theta_t
\end{aligned} \tag{37}$$

where the first inequality is due to triangle inequality, the second inequality is due to (34), (8), and (33), and the last inequality is due to the induction hypothesis.

Finally, by assuming H , σ_y^2 , and σ_n^2 as constants, it follows from (37) that $\theta \triangleq \max_t \theta_t = \mathcal{O}(\kappa^{H+1/2})$ and Theorem 2 follows. \square

APPENDIX K PROOF OF THEOREM 3

We first formally discuss the implications of our tractable choice of the if condition in (9) for theoretically guaranteeing the performance of our ϵ -Macro-GPO policy π^ϵ :

I. In the likely event (with a high probability of at least $1 - \delta$) that $|Q_t(s_{t+1}, d_t) - Q_t^*(s_{t+1}, d_t)| \leq \lambda H$ for all $s_{t+1} \in \mathcal{A}(s_t)$ (Theorem 1),

$$\begin{aligned}
& |Q_t(s_{t+1}, d_t) - Q_t(s_{t+1}, d_t)| \\
& \leq |Q_t(s_{t+1}, d_t) - Q_t^*(s_{t+1}, d_t)| + |Q_t^*(s_{t+1}, d_t) - Q_t(s_{t+1}, d_t)| \\
& \leq \lambda H + \theta
\end{aligned}$$

for all $s_{t+1} \in \mathcal{A}(s_t)$ such that the first inequality is due to triangle inequality and the second inequality is due to Theorems 1 and 2. Consequently, according to (9), $Q_t^\epsilon(s_{t+1}, d_t) = Q_t(s_{t+1}, d_t)$ for all $s_{t+1} \in \mathcal{A}(s_t)$ and $\pi^\epsilon(d_t)$ thus selects the same macro-action as the policy induced by stochastic sampling (6).

II. In the unlikely event (with an arbitrarily small probability of at most δ) that $Q_t(s_{t+1}, d_t)$ (6) is unboundedly far from $Q_t^*(s_{t+1}, d_t)$ (5) (i.e., $|Q_t(s_{t+1}, d_t) - Q_t^*(s_{t+1}, d_t)| > \lambda H$) for some $s_{t+1} \in \mathcal{A}(s_t)$, $\pi^\epsilon(d_t)$ (9) guarantees that, for any selected macro-action $s_{t+1} \in \mathcal{A}(s_t)$,

$$\begin{aligned}
& |Q_t^\epsilon(s_{t+1}, d_t) - Q_t^*(s_{t+1}, d_t)| \\
& = \begin{cases} |Q_t(s_{t+1}, d_t) - Q_t^*(s_{t+1}, d_t)| & \text{if } |Q_t(s_{t+1}, d_t) - Q_t(s_{t+1}, d_t)| \leq \lambda H + \theta, \\ |Q_t(s_{t+1}, d_t) - Q_t^*(s_{t+1}, d_t)| & \text{otherwise;} \end{cases} \\
& \leq \begin{cases} |Q_t(s_{t+1}, d_t) - Q_t(s_{t+1}, d_t)| + |Q_t(s_{t+1}, d_t) - Q_t^*(s_{t+1}, d_t)| & \text{if } |Q_t(s_{t+1}, d_t) - Q_t(s_{t+1}, d_t)| \leq \lambda H + \theta, \\ \theta & \text{otherwise;} \end{cases} \\
& \leq \lambda H + 2\theta, \quad \text{by triangle inequality and Theorem 2.}
\end{aligned}$$

The above two implications of our tractable choice of the if condition in (9) are central to establishing our main result deterministically bounding the *expected* performance loss of π^ϵ relative to that of Bayes-optimal Macro-GPO policy π^* , that is, policy π^ϵ is ϵ -Bayes-optimal.

The following lemmas are needed to prove our main result here:

Lemma 5. Suppose that the observations d_t , $H \in \mathbb{Z}^+$, a budget of $\kappa(H - t)$ input locations for $t = 0, \dots, H - 1$, $\delta \in (0, 1)$, and $\lambda > 0$ are given. Then, the probability of

$$|Q_t^*(\pi^*(d_t), d_t) - Q_t^*(\pi^\epsilon(d_t), d_t)| \leq 2\lambda H$$

is at least $1 - \delta$ by setting N according to that in Theorem 1.

Proof.

$$\begin{aligned}
& Q_t^*(\pi^*(d_t), d_t) - Q_t^*(\pi^\epsilon(d_t), d_t) \\
& \leq Q_t^*(\pi^*(d_t), d_t) - Q_t(\pi^\epsilon(d_t), d_t) + \lambda H \\
& \leq \max_{s_{t+1} \in \mathcal{A}(s_t)} |Q_t(s_{t+1}, d_t) - Q_t^*(s_{t+1}, d_t)| + \lambda H \\
& \leq \lambda H + \lambda H \\
& = 2\lambda H
\end{aligned}$$

where the first and last inequalities are due to Theorem 1 and the second inequality is further due to implication I. \square

Lemma 6. Suppose that the observations d_t , $H \in \mathbb{Z}^+$, a budget of $\kappa(H - t)$ input locations for $t = 0, \dots, H - 1$, $\delta \in (0, 1)$, and $\lambda > 0$ are given. Then,

$$Q_t^*(\pi^*(d_t), d_t) - \mathbb{E}_{\pi^\epsilon(d_t)}[Q_t^*(\pi^\epsilon(d_t), d_t)] \leq 2\lambda H + 4\delta\theta$$

where θ is previously defined in Theorem 2.

Proof. By Lemma 5, the probability of $|Q_t^*(\pi^*(d_t), d_t) - Q_t^*(\pi^\epsilon(d_t), d_t)| \leq 2\lambda H$ is at least $1 - \delta$. Otherwise, the probability of $|Q_t^*(\pi^*(d_t), d_t) - Q_t^*(\pi^\epsilon(d_t), d_t)| > 2\lambda H$ is at most δ . In the latter case,

$$\begin{aligned} & |Q_t^*(\pi^*(d_t), d_t) - Q_t^*(\pi^\epsilon(d_t), d_t)| \\ & \leq |Q_t^*(\pi^*(d_t), d_t) - Q_t^\epsilon(\pi^\epsilon(d_t), d_t)| + |Q_t^\epsilon(\pi^\epsilon(d_t), d_t) - Q_t^*(\pi^\epsilon(d_t), d_t)| \\ & \leq \max_{s_{t+1} \in \mathcal{A}(s_t)} |Q_t^\epsilon(s_{t+1}, d_t) - Q_t^*(s_{t+1}, d_t)| + \lambda H + 2\theta \\ & \leq \lambda H + 2\theta + \lambda H + 2\theta \\ & = 2\lambda H + 4\theta \end{aligned} \tag{38}$$

where the first inequality is due to triangle inequality and the last two inequalities are due to implication II. Recall that π^ϵ is a stochastic policy due to its use of stochastic sampling in Q_t (6), which implies that $\pi^\epsilon(d_t)$ is a random variable. Then,

$$\begin{aligned} & Q_t^*(\pi^*(d_t), d_t) - \mathbb{E}_{\pi^\epsilon(d_t)}[Q_t^*(\pi^\epsilon(d_t), d_t)] \\ & = \mathbb{E}_{\pi^\epsilon(d_t)}[Q_t^*(\pi^*(d_t), d_t) - Q_t^*(\pi^\epsilon(d_t), d_t)] \\ & \leq (1 - \delta)(2\lambda H) + \delta(2\lambda H + 4\theta) \\ & = 2\lambda H + 4\delta\theta \end{aligned}$$

where the expectation is with respect to random variable $\pi^\epsilon(d_t)$ and the inequality follows from Lemma 5 and (38). \square

Main proof. We will give a proof by induction on t that

$$V_t^*(d_t) - \mathbb{E}_{\pi^\epsilon}[V_t^{\pi^\epsilon}(d_t)] \leq (2\lambda H + 4\delta\theta)(H - t). \tag{39}$$

When $t = H - 1$ (i.e., base case),

$$\begin{aligned} & V_{H-1}^*(d_{H-1}) - \mathbb{E}_{\pi^\epsilon}[V_{H-1}^{\pi^\epsilon}(d_{H-1})] \\ & = Q_{H-1}^*(\pi^*(d_{H-1}), d_{H-1}) - \mathbb{E}_{\pi^\epsilon}[Q_{H-1}^{\pi^\epsilon}(\pi^\epsilon(d_{H-1}), d_{H-1})] \\ & = Q_{H-1}^*(\pi^*(d_{H-1}), d_{H-1}) - \mathbb{E}_{\pi^\epsilon(d_{H-1})}[R(\pi^\epsilon(d_{H-1}), d_{H-1})] \\ & = Q_{H-1}^*(\pi^*(d_{H-1}), d_{H-1}) - \mathbb{E}_{\pi^\epsilon(d_{H-1})}[Q_{H-1}^*(\pi^\epsilon(d_{H-1}), d_{H-1})] \\ & \leq 2\lambda H + 4\delta\theta \end{aligned}$$

where the first equality is due to (3) and (5), the second equality is due to (3), the third equality is due to (5), and the inequality is due to Lemma 6. So, (39) holds for the base case. Supposing (39) holds for $t + 1$ (i.e., induction hypothesis), we will prove that it holds for $t = 0, \dots, H - 2$:

$$\begin{aligned} & V_t^*(d_t) - \mathbb{E}_{\pi^\epsilon}[V_t^{\pi^\epsilon}(d_t)] \\ & = Q_t^*(\pi^*(d_t), d_t) - \mathbb{E}_{\pi^\epsilon}[Q_t^{\pi^\epsilon}(\pi^\epsilon(d_t), d_t)] \\ & = Q_t^*(\pi^*(d_t), d_t) - \mathbb{E}_{\pi^\epsilon}[Q_t^*(\pi^\epsilon(d_t), d_t)] + \mathbb{E}_{\pi^\epsilon}[Q_t^*(\pi^\epsilon(d_t), d_t)] - \mathbb{E}_{\pi^\epsilon}[Q_t^{\pi^\epsilon}(\pi^\epsilon(d_t), d_t)] \\ & = Q_t^*(\pi^*(d_t), d_t) - \mathbb{E}_{\pi^\epsilon(d_t)}[Q_t^*(\pi^\epsilon(d_t), d_t)] + \mathbb{E}_{\pi^\epsilon}[Q_t^*(\pi^\epsilon(d_t), d_t) - Q_t^{\pi^\epsilon}(\pi^\epsilon(d_t), d_t)] \\ & \leq 2\lambda H + 4\delta\theta + \mathbb{E}_{\pi^\epsilon}[Q_t^*(\pi^\epsilon(d_t), d_t) - Q_t^{\pi^\epsilon}(\pi^\epsilon(d_t), d_t)] \\ & = 2\lambda H + 4\delta\theta + \mathbb{E}_{\pi^\epsilon}[\mathbb{E}_{z_{t+1}|\pi^\epsilon(d_t), d_t}[V_{t+1}^*(\langle \mathbf{s}_t \oplus \pi^\epsilon(d_t), \mathbf{z}_t \oplus z_{t+1} \rangle) - V_{t+1}^{\pi^\epsilon}(\langle \mathbf{s}_t \oplus \pi^\epsilon(d_t), \mathbf{z}_t \oplus z_{t+1} \rangle)]] \\ & = 2\lambda H + 4\delta\theta + \mathbb{E}_{\pi^\epsilon(d_t)}[\mathbb{E}_{z_{t+1}|\pi^\epsilon(d_t), d_t}[V_{t+1}^*(\langle \mathbf{s}_t \oplus \pi^\epsilon(d_t), \mathbf{z}_t \oplus z_{t+1} \rangle) - \mathbb{E}_{\pi^\epsilon}[V_{t+1}^{\pi^\epsilon}(\langle \mathbf{s}_t \oplus \pi^\epsilon(d_t), \mathbf{z}_t \oplus z_{t+1} \rangle)]]] \\ & \leq 2\lambda H + 4\delta\theta + \mathbb{E}_{\pi^\epsilon(d_t)}[\mathbb{E}_{z_{t+1}|\pi^\epsilon(d_t), d_t}[(2\lambda H + 4\delta\theta)(H - t - 1)]] \\ & = (2\lambda H + 4\delta\theta)(H - t) \end{aligned} \tag{40}$$

where the first and fourth equalities are due to (3) and (5), the first inequality is due to Lemma 6, and the last inequality is due to the induction hypothesis.

From (40), when $t = 0$,

$$V_0^*(d_0) - \mathbb{E}_{\pi^\epsilon}[V_0^{\pi^\epsilon}(d_0)] \leq 2H(\lambda H + 2\delta\theta).$$

Let $\epsilon = 2H(\lambda H + 2\delta\theta)$ by setting $\lambda = \epsilon/(4H^2)$ and $\delta = \epsilon/(8\theta H)$. Consequently, using Lemma 5 and $\theta = \mathcal{O}(\kappa^{H+1/2})$ previously defined in Theorem 2,

$$N = \mathcal{O}\left(\frac{\kappa^{2H}}{\epsilon^2} \log \frac{\kappa A}{\epsilon}\right).$$

APPENDIX L

ANYTIME ϵ -MACRO-GPO

A. Pseudocode

The pseudocode is described in Algorithm 1 and explained below. The essential steps of the main function Anytime- ϵ -Macro-GPO are as follows:

- 1) Preprocessing (lines 40-42): Compute $\Sigma_{s_{t+1}|s_t}$ (1), $L_{t+1}(s_{t+1})$ (Definition 1), and $Q_t(s_{t+1}, d_t)$ (8) for all s_{t+1} reachable from s_0 and $t = 0, \dots, H-1$, and set θ according to Theorem 2 (Appendix J);
- 2) Iteratively and incrementally expand the partially constructed search tree rooted at node d_0 by calling the recursive function ConstructTree (lines 44-45) so as to tighten the upper heuristic bound $\bar{V}_0^*(d_0)$ and lower heuristic bound $\underline{V}_0^*(d_0)$ of $V_0^*(d_0)$, hence reducing the gap $\omega \triangleq \bar{V}_0^*(d_0) - \underline{V}_0^*(d_0)$ (line 46); and
- 3) Compute our anytime (ω, ϵ) -Macro-GPO policy $\pi^{\omega, \epsilon}(d_0)$ according to (46) (lines 47-51).

The recursive function ConstructTree traverses down the partially constructed search tree by repeatedly selecting nodes d_t with the largest uncertainty of their corresponding values $V_t^*(d_t)$ (i.e., largest gap $\bar{V}_t^*(d_t) - \underline{V}_t^*(d_t)$ between the upper and lower heuristic bounds of $V_t^*(d_t)$ so as to tighten them) until an unexplored node is reached. Specifically, if the function ConstructTree selects an explored node d_t , then the following steps are performed:

- 1) Choose the macro-action s_{t+1} with the tightest lower heuristic bound $\underline{Q}_t^*(s_{t+1}, d_t)$ of $Q_t^*(s_{t+1}, d_t)$ (line 26);
- 2) Retrieve the samples $\{z^\ell\}_{\ell=1, \dots, N}$ previously generated by function ExpandTree at node d_t for macro-action s_{t+1} (line 27);
- 3) Recursively and incrementally expand the partially constructed sub-tree rooted at node $\langle s_{t+1}, \mathbf{z}_t \oplus z^{\ell*} \rangle$ with the largest uncertainty of its corresponding value $V_{t+1}^*(\langle s_{t+1}, \mathbf{z}_t \oplus z^{\ell*} \rangle)$ (i.e., largest gap $\bar{V}_{t+1}^*(\langle s_{t+1}, \mathbf{z}_t \oplus z^{\ell*} \rangle) - \underline{V}_{t+1}^*(\langle s_{t+1}, \mathbf{z}_t \oplus z^{\ell*} \rangle)$ between the upper and lower heuristic bounds of $V_{t+1}^*(\langle s_{t+1}, \mathbf{z}_t \oplus z^{\ell*} \rangle)$ so as to tighten them) (lines 28-29);
- 4) Use the tightened upper and lower heuristic bounds of $V_{t+1}^*(\langle s_{t+1}, \mathbf{z}_t \oplus z^{\ell*} \rangle)$ at node $\langle s_{t+1}, \mathbf{z}_t \oplus z^{\ell*} \rangle$ to refine the heuristic bounds at its siblings (see Corollary 1) by exploiting the Lipschitz continuity of V_{t+1}^* (Theorem 4) (line 30); and
- 5) Backpropagate the tightened/refined heuristic bounds at node $\langle s_{t+1}, \mathbf{z}_t \oplus z^{\ell*} \rangle$ and its siblings to that at their parent node d_t (lines 31-35).

Otherwise, the function ConstructTree selects an unexplored node d_t and constructs a “minimal” sub-tree rooted at node d_t via the function ExpandTree (line 38), the latter of which involves the following steps:

- 1) For every macro-action $s_{t+1} \in \mathcal{A}(s_t)$,
 - a) Draw N i.i.d. multivariate Gaussian vectors $\{z^\ell\}_{\ell=1, \dots, N}$ from GP posterior belief $p(z_{t+1}|s_{t+1}, d_t)$ (line 5);
 - b) For every child node $\langle s_{t+1}, \mathbf{z}_t \oplus z^\ell \rangle$, initialize the upper and lower heuristic bounds of $V_{t+1}^*(\langle s_{t+1}, \mathbf{z}_t \oplus z^\ell \rangle)$ (lines 6-8) using Theorem 2:

$$\begin{aligned}
 & |\mathbb{V}_{t+1}(\langle s_{t+1}, \mathbf{z}_t \oplus z^\ell \rangle) - V_{t+1}^*(\langle s_{t+1}, \mathbf{z}_t \oplus z^\ell \rangle)| \\
 &= \left| \max_{s_{t+2} \in \mathcal{A}(s_{t+1})} Q_{t+1}(s_{t+2}, \langle s_{t+1}, \mathbf{z}_t \oplus z^\ell \rangle) - \max_{s_{t+2} \in \mathcal{A}(s_{t+1})} Q_{t+1}^*(s_{t+2}, \langle s_{t+1}, \mathbf{z}_t \oplus z^\ell \rangle) \right| \\
 &\leq \max_{s_{t+2} \in \mathcal{A}(s_{t+1})} |Q_{t+1}(s_{t+2}, \langle s_{t+1}, \mathbf{z}_t \oplus z^\ell \rangle) - Q_{t+1}^*(s_{t+2}, \langle s_{t+1}, \mathbf{z}_t \oplus z^\ell \rangle)| \\
 &\leq \theta_{t+1}
 \end{aligned} \tag{41}$$

where the equality is due to (5) and (8), θ_{t+1} is previously defined in (36), and the last inequality follows from (35) in the proof of Theorem 2;

- c) Recursively expand/construct a “minimal” sub-tree rooted at the child node $\langle s_{t+1}, \mathbf{z}_t \oplus z^{\bar{\ell}} \rangle$ using the most likely sample $z^{\bar{\ell}}$ (lines 9-10);
- d) Use the tightened upper heuristic bound $\bar{V}_{t+1}^*(\langle s_{t+1}, \mathbf{z}_t \oplus z^{\bar{\ell}} \rangle)$ and lower heuristic bound $\underline{V}_{t+1}^*(\langle s_{t+1}, \mathbf{z}_t \oplus z^{\bar{\ell}} \rangle)$ of $V_{t+1}^*(\langle s_{t+1}, \mathbf{z}_t \oplus z^{\bar{\ell}} \rangle)$ at node $\langle s_{t+1}, \mathbf{z}_t \oplus z^{\bar{\ell}} \rangle$ to refine the heuristic bounds at its unexplored siblings (see Corollary 1) by exploiting the Lipschitz continuity of V_{t+1}^* (Theorem 4) (line 11); and
- 2) Backpropagate the tightened/refined heuristic bounds at node $\langle s_{t+1}, \mathbf{z}_t \oplus z^{\bar{\ell}} \rangle$ and its siblings to that at their parent node d_t (lines 12-16).

B. Theoretical Analysis

Our result below proves that $\bar{V}_t^*(d_t)$ and $\underline{V}_t^*(d_t)$, which are previously defined in lines 15-16 and 34-35 in Algorithm 1, are upper and lower heuristic bounds of $V_t^*(d_t)$, respectively:

Theorem 5. Suppose that the observations $d_{t'}$, $H \in \mathbb{Z}^+$, a budget of $\kappa(H-t')$ input locations for $t' = 0, \dots, H-1$, $\delta \in (0, 1)$, and $\lambda > 0$ are given. Then, the probability of

$$\underline{V}_t^*(d_t) \leq V_t^*(d_t) \leq \bar{V}_t^*(d_t) \tag{42}$$

Algorithm 1 Anytime ϵ -Macro-GPO

```

1: function ExpandTree( $t, d_t, \lambda$ )
2:   if  $t = H$  then
3:     return  $\langle 0, 0 \rangle$ 
4:   for all  $s_{t+1} \in \mathcal{A}(s_t)$  do
5:      $\{z^\ell\}_{\ell=1,\dots,N} \leftarrow$  Draw  $N$  i.i.d. multivariate Gaussian vectors from GP posterior belief  $p(z_{t+1}|s_{t+1}, d_t)$  (1)
6:     for all  $z^\ell$  do
7:        $\frac{V_{t+1}^*}{V_{t+1}^*}(\langle s_{t+1}, \mathbf{z}_t \oplus z^\ell \rangle) \leftarrow \mathbb{V}_{t+1}(\langle s_{t+1}, \mathbf{z}_t \oplus z^\ell \rangle) - \theta_{t+1}$  (41)
8:        $\frac{V_{t+1}^*}{V_{t+1}^*}(\langle s_{t+1}, \mathbf{z}_t \oplus z^\ell \rangle) \leftarrow \mathbb{V}_{t+1}(\langle s_{t+1}, \mathbf{z}_t \oplus z^\ell \rangle) + \theta_{t+1}$  (41)
9:        $\bar{\ell} \leftarrow \operatorname{argmin}_{\ell \in \{1,\dots,N\}} \|z^\ell - \mu_{s_{t+1}|d_t}\|$ 
10:       $\langle \bar{V}_{t+1}^*(\langle s_{t+1}, \mathbf{z}_t \oplus z^{\bar{\ell}} \rangle), \underline{V}_{t+1}^*(\langle s_{t+1}, \mathbf{z}_t \oplus z^{\bar{\ell}} \rangle) \rangle \leftarrow \text{ExpandTree}(t+1, \langle s_{t+1}, \mathbf{z}_t \oplus z^{\bar{\ell}} \rangle, \lambda)$ 
11:      RefineBounds( $t, d_t, s_{t+1}, \bar{\ell}$ )
12:       $R(s_{t+1}, d_t) \leftarrow \mathbf{1}^\top \mu_{s_{t+1}|d_t} + 0.5\beta \log |I + \sigma_n^{-2} \Sigma_{s_{t+1}|\mathbf{s}_t}|$ 
13:       $\underline{Q}_t^*(s_{t+1}, d_t) \leftarrow R(s_{t+1}, d_t) + N^{-1} \sum_{\ell=1}^N \frac{V_{t+1}^*}{V_{t+1}^*}(\langle s_{t+1}, \mathbf{z}_t \oplus z^\ell \rangle) - \lambda$ 
14:       $\bar{Q}_t^*(s_{t+1}, d_t) \leftarrow R(s_{t+1}, d_t) + N^{-1} \sum_{\ell=1}^N \frac{V_{t+1}^*}{V_{t+1}^*}(\langle s_{t+1}, \mathbf{z}_t \oplus z^\ell \rangle) + \lambda$ 
15:       $\underline{V}_t^*(d_t) \leftarrow \max_{s_{t+1} \in \mathcal{A}(s_t)} \underline{Q}_t^*(s_{t+1}, d_t)$ 
16:       $\bar{V}_t^*(d_t) \leftarrow \max_{s_{t+1} \in \mathcal{A}(s_t)} \bar{Q}_t^*(s_{t+1}, d_t)$ 
17:      return  $\langle \bar{V}_t^*(d_t), \underline{V}_t^*(d_t) \rangle$ 
18: function RefineBounds( $t, d_t, s_{t+1}, j$ )
19:    $\{z^\ell\}_{\ell=1,\dots,N} \leftarrow \text{RetrieveSamples}(t, d_t, s_{t+1})$ 
20:   for all  $i \neq j$  do
21:      $b \leftarrow L_{t+1}(\mathbf{s}_{t+1}) \|z^i - z^j\|$ 
22:      $\frac{V_{t+1}^*}{V_{t+1}^*}(\langle s_{t+1}, \mathbf{z}_t \oplus z^i \rangle) \leftarrow \max(\frac{V_{t+1}^*}{V_{t+1}^*}(\langle s_{t+1}, \mathbf{z}_t \oplus z^i \rangle), \frac{V_{t+1}^*}{V_{t+1}^*}(\langle s_{t+1}, \mathbf{z}_t \oplus z^j \rangle) - b)$ 
23:      $\frac{V_{t+1}^*}{V_{t+1}^*}(\langle s_{t+1}, \mathbf{z}_t \oplus z^i \rangle) \leftarrow \min(\frac{V_{t+1}^*}{V_{t+1}^*}(\langle s_{t+1}, \mathbf{z}_t \oplus z^i \rangle), \frac{V_{t+1}^*}{V_{t+1}^*}(\langle s_{t+1}, \mathbf{z}_t \oplus z^j \rangle) + b)$ 
24: function ConstructTree( $t, d_t, \lambda$ )
25:   if  $d_t$  has been explored then
26:      $s_{t+1} \leftarrow \operatorname{argmax}_{s'_{t+1} \in \mathcal{A}(s_t)} \underline{Q}_t^*(s'_{t+1}, d_t)$ 
27:      $\{z^\ell\}_{\ell=1,\dots,N} \leftarrow \text{RetrieveSamples}(t, d_t, s_{t+1})$ 
28:      $\ell^* \leftarrow \operatorname{argmax}_{\ell \in \{1,\dots,N\}} \bar{V}_{t+1}^*(\langle s_{t+1}, \mathbf{z}_t \oplus z^\ell \rangle) - \underline{V}_{t+1}^*(\langle s_{t+1}, \mathbf{z}_t \oplus z^\ell \rangle)$ 
29:      $\langle \bar{V}_{t+1}^*(\langle s_{t+1}, \mathbf{z}_t \oplus z^{\ell^*} \rangle), \underline{V}_{t+1}^*(\langle s_{t+1}, \mathbf{z}_t \oplus z^{\ell^*} \rangle) \rangle \leftarrow \text{ConstructTree}(t+1, \langle s_{t+1}, \mathbf{z}_t \oplus z^{\ell^*} \rangle, \lambda)$ 
30:     RefineBounds( $t, d_t, s_{t+1}, \ell^*$ )
31:      $R(s_{t+1}, d_t) \leftarrow \mathbf{1}^\top \mu_{s_{t+1}|d_t} + 0.5\beta \log |I + \sigma_n^{-2} \Sigma_{s_{t+1}|\mathbf{s}_t}|$ 
32:      $\underline{Q}_t^*(s_{t+1}, d_t) \leftarrow R(s_{t+1}, d_t) + N^{-1} \sum_{\ell=1}^N \frac{V_{t+1}^*}{V_{t+1}^*}(\langle s_{t+1}, \mathbf{z}_t \oplus z^\ell \rangle) - \lambda$ 
33:      $\bar{Q}_t^*(s_{t+1}, d_t) \leftarrow R(s_{t+1}, d_t) + N^{-1} \sum_{\ell=1}^N \frac{V_{t+1}^*}{V_{t+1}^*}(\langle s_{t+1}, \mathbf{z}_t \oplus z^\ell \rangle) + \lambda$ 
34:      $\underline{V}_t^*(d_t) \leftarrow \max_{s_{t+1} \in \mathcal{A}(s_t)} \underline{Q}_t^*(s_{t+1}, d_t)$ 
35:      $\bar{V}_t^*(d_t) \leftarrow \max_{s_{t+1} \in \mathcal{A}(s_t)} \bar{Q}_t^*(s_{t+1}, d_t)$ 
36:     return  $\langle \bar{V}_t^*(d_t), \underline{V}_t^*(d_t) \rangle$ 
37:   else
38:     return ExpandTree( $t, d_t, \lambda$ )
39: function Anytime- $\epsilon$ -Macro-GPO( $d_0, \epsilon, H$ )
40:   for all  $s_{t+1}$  reachable from  $s_0$  and  $t = 0, \dots, H-1$  do
41:     Compute  $\Sigma_{s_{t+1}|\mathbf{s}_t}$  (1),  $L_{t+1}(\mathbf{s}_{t+1})$  (Definition 1), and  $\mathbb{Q}_t(s_{t+1}, d_t)$  (8)
42:     Set  $\theta$  according to Theorem 2 (Appendix J)
43:      $\lambda \leftarrow 1/(4H/\epsilon + 1/(2\theta))$ ,  $\delta \leftarrow \epsilon/(8\theta H)$ 
44:     while resources permit do
45:        $\langle \bar{V}_0^*(d_0), \underline{V}_0^*(d_0) \rangle \leftarrow \text{ConstructTree}(0, d_0, \lambda)$ 
46:        $\omega \leftarrow \bar{V}_0^*(d_0) - \underline{V}_0^*(d_0)$ 
47:       for all  $s_1 \in \mathcal{A}(s_0)$  do
48:          $Q_0^{\omega\epsilon}(s_1, d_0) \leftarrow \underline{Q}_0^*(s_1, d_0)$ 
49:         if  $|Q_0^{\omega\epsilon}(s_1, d_0) - \mathbb{Q}_0(s_1, d_0)| > 2\lambda + \omega + \theta$  then
50:            $Q_0^{\omega\epsilon}(s_1, d_0) \leftarrow \mathbb{Q}_0(s_1, d_0)$ 
51:       return  $\pi^{\omega\epsilon}(d_0) \leftarrow \operatorname{argmax}_{s_1 \in \mathcal{A}(s_0)} Q_0^{\omega\epsilon}(s_1, d_0)$  (46)

```

for all tuples $\langle t, d_t \rangle$ generated at stage $t = t', \dots, H$ by Algorithm 1 is at least $1 - \delta$ by setting N according to Theorem 1.

Proof. We will give a proof by induction on t that the probability of (42) for all tuples $\langle t, d_t \rangle$ generated at stage $t = t', \dots, H$ by Algorithm 1 is at least $1 - \delta$. The base case of $t = H$ is true since $\underline{V}_H^*(d_H) = V_H^*(d_H) = \bar{V}_H^*(d_H) = 0$. Supposing (42) holds for $t + 1$ (i.e. induction hypothesis), we will prove that it holds for $t = t', \dots, H - 1$.

Similar to Lemma 3 and the main proof of Theorem 1, the probability of

$$\mathcal{U}_t(s_{t+1}, d_t) - \lambda \leq Q_t^*(s_{t+1}, d_t) \leq \mathcal{U}_t(s_{t+1}, d_t) + \lambda. \quad (43)$$

for all tuples $\langle t, s_{t+1}, d_t \rangle$ generated at stage $t = t', \dots, H - 1$ by Algorithm 1 is at least $1 - \delta$.

So, the probability of

$$\begin{aligned} & Q_t^*(s_{t+1}, d_t) \\ & \leq \mathcal{U}_t(s_{t+1}, d_t) + \lambda \\ & = R(s_{t+1}, d_t) + \frac{1}{N} \sum_{\ell=1}^N V_{t+1}^*(\langle s_{t+1}, \mathbf{z}_t \oplus z^\ell \rangle) + \lambda \\ & \leq R(s_{t+1}, d_t) + \frac{1}{N} \sum_{\ell=1}^N \bar{V}_{t+1}^*(\langle s_{t+1}, \mathbf{z}_t \oplus z^\ell \rangle) + \lambda \\ & = \bar{Q}_t^*(s_{t+1}, d_t) \end{aligned}$$

for all tuples $\langle t, s_{t+1}, d_t \rangle$ generated at stage $t = t', \dots, H - 1$ by Algorithm 1 is at least $1 - \delta$ where the first inequality follows from (43), the first equality is due to definition of $\mathcal{U}_t(s_{t+1}, d_t)$ (18), the last inequality is due to the induction hypothesis, and the last equality is due to definition of \bar{Q}_t^* (see lines 14 and 33 in Algorithm 1). It follows that the probability of $V_t^*(d_t) \leq \bar{V}_t^*(d_t)$ for all tuples $\langle t, d_t \rangle$ generated at stage $t = t', \dots, H - 1$ by Algorithm 1 is at least $1 - \delta$.

Similarly, the probability of

$$\begin{aligned} & Q_t^*(s_{t+1}, d_t) \\ & \geq \mathcal{U}_t(s_{t+1}, d_t) - \lambda \\ & = R(s_{t+1}, d_t) + \frac{1}{N} \sum_{\ell=1}^N V_{t+1}^*(\langle s_{t+1}, \mathbf{z}_t \oplus z^\ell \rangle) - \lambda \\ & \geq R(s_{t+1}, d_t) + \frac{1}{N} \sum_{\ell=1}^N \underline{V}_{t+1}^*(\langle s_{t+1}, \mathbf{z}_t \oplus z^\ell \rangle) - \lambda \\ & = \underline{Q}_t^*(s_{t+1}, d_t) \end{aligned}$$

for all tuples $\langle t, s_{t+1}, d_t \rangle$ generated at stage $t = t', \dots, H - 1$ by Algorithm 1 is at least $1 - \delta$ where the first inequality is due to (43), the first equality is due to definition $\mathcal{U}_t(s_{t+1}, d_t)$ (18), the last inequality is due to the induction hypothesis, and the last equality is due to definition of \underline{Q}_t^* (see lines 13 and 32 in Algorithm 1). It follows that the probability of $V_t^*(d_t) \geq \underline{V}_t^*(d_t)$ for all tuples $\langle t, d_t \rangle$ generated at stage $t = t', \dots, H - 1$ by Algorithm 1 is at least $1 - \delta$. \square

Our next result justifies why the function RefineBounds (lines 18-23) in Algorithm 1 can use the tightened heuristic bounds at nodes $\langle s_{t+1}, \mathbf{z}_t \oplus z^\ell \rangle$ and $\langle s_{t+1}, \mathbf{z}_t \oplus z^{\ell^*} \rangle$ to refine the heuristic bounds at their siblings (lines 11 and 30) by exploiting the Lipschitz continuity of V_{t+1}^* (Theorem 4), as explained previously in Appendix L-A:

Corollary 1. Suppose that the observations $d_{t'}$, $H \in \mathbb{Z}^+$, a budget of $\kappa(H - t')$ input locations for $t' = 0, \dots, H - 1$, $\delta \in (0, 1)$ and $\lambda > 0$ are given. Then, the probability of

$$\underline{V}_t^*(\langle s_t, \mathbf{z}_{t-1} \oplus z^j \rangle) - L_t(s_t) \|z^i - z^j\| \leq V_t^*(\langle s_t, \mathbf{z}_{t-1} \oplus z^i \rangle) \leq \bar{V}_t^*(\langle s_t, \mathbf{z}_{t-1} \oplus z^j \rangle) + L_t(s_t) \|z^i - z^j\|$$

between any pair of tuples $\langle t, \langle s_t, \mathbf{z}_{t-1} \oplus z^i \rangle \rangle$ and $\langle t, \langle s_t, \mathbf{z}_{t-1} \oplus z^j \rangle \rangle$ for $i, j = 1, \dots, N$ generated at stage $t = t' + 1, \dots, H$ by Algorithm 1 is at least $1 - \delta$ by setting N according to Theorem 1.

Proof.

$$\begin{aligned} & V_t^*(\langle s_t, \mathbf{z}_{t-1} \oplus z^i \rangle) \\ & \leq V_t^*(\langle s_t, \mathbf{z}_{t-1} \oplus z^j \rangle) + L_t(s_t) \|z^i - z^j\| \\ & \leq \bar{V}_t^*(\langle s_t, \mathbf{z}_{t-1} \oplus z^j \rangle) + L_t(s_t) \|z^i - z^j\| \end{aligned}$$

where the first inequality is a direct consequence of Theorem 4 in Appendix H and the second inequality is due to Theorem 5.

$$\begin{aligned} & V_t^*(\langle s_t, \mathbf{z}_{t-1} \oplus z^i \rangle) \\ & \geq V_t^*(\langle s_t, \mathbf{z}_{t-1} \oplus z^j \rangle) - L_t(s_t) \|z^i - z^j\| \\ & \geq \underline{V}_t^*(\langle s_t, \mathbf{z}_{t-1} \oplus z^j \rangle) - L_t(s_t) \|z^i - z^j\|. \end{aligned}$$

where the first inequality is a direct consequence of Theorem 4 in Appendix H and the second inequality is due to Theorem 5. \square

Similar to Theorem 1, our result below derives a probabilistic guarantee on the approximation quality of $\underline{Q}_t^*(s_{t+1}, d_t)$:

Theorem 6. Suppose that the observations d_t , $H \in \mathbb{Z}^+$, a budget of $\kappa(H - t)$ input locations for $t = 0, \dots, H - 1$, $\delta \in (0, 1)$, and $\lambda > 0$ are given and Algorithm 1 terminates at $\omega \triangleq \bar{V}_0^*(d_0) - \underline{V}_0^*(d_0)$ (see line 46 in Algorithm 1). Then, the probability of $|\underline{Q}_t^*(s_{t+1}, d_t) - Q_t^*(s_{t+1}, d_t)| \leq 2\lambda + \omega$ for all $s_{t+1} \in \mathcal{A}(s_t)$ is at least $1 - \delta$ by setting N according to Theorem 1.

Proof. It follows directly from Theorem 5 that the probability of

$$|V_0^*(d_0) - \underline{V}_0^*(d_0)| \leq \omega \quad (44)$$

is at least $1 - \delta$. In general, supposing the planning horizon is reduced to $H - t$ stages for $t = 0, \dots, H - 1$, (44) is equivalent to

$$|V_t^*(d_t) - \underline{V}_t^*(d_t)| \leq \omega \quad (45)$$

by shifting the indices of $V_0^*(d_0)$ and $\underline{V}_0^*(d_0)$ in (44) from 0 to t so that they start at stage t instead. Then, the probability of

$$\begin{aligned} & |\underline{Q}_t^*(s_{t+1}, d_t) - Q_t^*(s_{t+1}, d_t)| \\ & \leq |\underline{Q}_t^*(s_{t+1}, d_t) - \mathcal{U}_t(s_{t+1}, d_t)| + |\mathcal{U}_t(s_{t+1}, d_t) - Q_t^*(s_{t+1}, d_t)| \\ & \leq \lambda + \left| \left(\frac{1}{N} \sum_{\ell=1}^N V_{t+1}^*(\langle s_{t+1}, \mathbf{z}_t \oplus z^\ell \rangle) - \sum_{\ell=1}^N \underline{V}_{t+1}^*(\langle s_{t+1}, \mathbf{z}_t \oplus z^\ell \rangle) \right) + \lambda \right| \\ & \leq 2\lambda + \frac{1}{N} \sum_{\ell=1}^N |V_{t+1}^*(\langle s_{t+1}, \mathbf{z}_t \oplus z^\ell \rangle) - \underline{V}_{t+1}^*(\langle s_{t+1}, \mathbf{z}_t \oplus z^\ell \rangle)| \\ & \leq 2\lambda + \omega \end{aligned}$$

for all $s_{t+1} \in \mathcal{A}(s_t)$ is at least $1 - \delta$ where the first and the third inequalities are due to triangle inequality, the second inequality follows from (43), definition of $\mathcal{U}_t(s_{t+1}, d_t)$ (18), and definition of \underline{Q}_t^* (see lines 13 and 32 in Algorithm 1), and the last inequality is due to (45). \square

We will now give an anytime analogue/variant of our nonmyopic adaptive ϵ -Macro-GPO policy π^ϵ (9), which we call the $\langle \omega, \epsilon \rangle$ -Macro-GPO policy $\pi^{\omega\epsilon}$:

$$\begin{aligned} \pi^{\omega\epsilon}(d_t) & \triangleq \operatorname{argmax}_{s_{t+1} \in \mathcal{A}(s_t)} Q_t^{\omega\epsilon}(s_{t+1}, d_t) \\ Q_t^{\omega\epsilon}(s_{t+1}, d_t) & \triangleq \begin{cases} \underline{Q}_t^*(s_{t+1}, d_t) & \text{if } |\underline{Q}_t^*(s_{t+1}, d_t) - Q_t^*(s_{t+1}, d_t)| \leq 2\lambda + \omega + \theta, \\ Q_t(s_{t+1}, d_t) & \text{otherwise;} \end{cases} \end{aligned} \quad (46)$$

for stages $t = 0, \dots, H - 1$ where $Q_t(s_{t+1}, d_t)$ and θ are previously defined in (8) and Theorem 2, respectively. The implications of the tractable choice of the if condition in (46) for theoretically guaranteeing the performance of our $\langle \omega, \epsilon \rangle$ -Macro-GPO policy $\pi^{\omega\epsilon}$ are similar to that of our ϵ -Macro-GPO policy π^ϵ (9):

I. In the likely event (with an arbitrarily high probability of at least $1 - \delta$) that $|\underline{Q}_t^*(s_{t+1}, d_t) - Q_t^*(s_{t+1}, d_t)| \leq 2\lambda + \omega$ for all $s_{t+1} \in \mathcal{A}(s_t)$ (Theorem 6), $|\underline{Q}_t^*(s_{t+1}, d_t) - Q_t(s_{t+1}, d_t)| \leq |\underline{Q}_t^*(s_{t+1}, d_t) - Q_t^*(s_{t+1}, d_t)| + |Q_t^*(s_{t+1}, d_t) - Q_t(s_{t+1}, d_t)| \leq 2\lambda + \omega + \theta$ for all $s_{t+1} \in \mathcal{A}(s_t)$, by triangle inequality and Theorems 2 and 6. Consequently, according to (46), $Q_t^{\omega\epsilon}(s_{t+1}, d_t) = \underline{Q}_t^*(s_{t+1}, d_t)$ for all $s_{t+1} \in \mathcal{A}(s_t)$ and $\pi^{\omega\epsilon}(d_t)$ thus selects the same macro-action as the policy induced by $\underline{Q}_t^*(s_{t+1}, d_t)$ (see lines 13 and 32 in Algorithm 1).

II. In the unlikely event (with an arbitrarily small probability of at most δ) that $\underline{Q}_t^*(s_{t+1}, d_t)$ (see lines 13 and 32 in Algorithm 1) is unboundedly far from $Q_t^*(s_{t+1}, d_t)$ (5) (i.e., $|\underline{Q}_t^*(s_{t+1}, d_t) - Q_t^*(s_{t+1}, d_t)| > 2\lambda + \omega$) for some $s_{t+1} \in \mathcal{A}(s_t)$, $\pi^{\omega\epsilon}(d_t)$ (46) guarantees that, for any selected macro-action $s_{t+1} \in \mathcal{A}(s_t)$,

$$\begin{aligned} & |\pi^{\omega\epsilon}(d_t) - Q_t^*(s_{t+1}, d_t)| \\ & = \begin{cases} |\underline{Q}_t^*(s_{t+1}, d_t) - Q_t^*(s_{t+1}, d_t)| & \text{if } |\underline{Q}_t^*(s_{t+1}, d_t) - Q_t(s_{t+1}, d_t)| \leq 2\lambda + \omega + \theta, \\ |Q_t(s_{t+1}, d_t) - Q_t^*(s_{t+1}, d_t)| & \text{otherwise;} \end{cases} \\ & \leq \begin{cases} |\underline{Q}_t^*(s_{t+1}, d_t) - Q_t(s_{t+1}, d_t)| & \text{if } |\underline{Q}_t^*(s_{t+1}, d_t) - Q_t(s_{t+1}, d_t)| \leq 2\lambda + \omega + \theta, \\ \theta & \text{otherwise;} \end{cases} \\ & \leq 2\lambda + \omega + 2\theta, \end{aligned} \quad (47)$$

by triangle inequality and Theorem 2.

The above implications are central to proving our next result bounding the *expected* performance loss of $\pi^{\omega\epsilon}$ relative to that of Bayes-optimal Macro-GPO policy π^* , that is, policy $\pi^{\omega\epsilon}$ is $\langle \omega, \epsilon \rangle$ -Bayes-optimal:

Lemma 7. Suppose that the observations d_t , $H \in \mathbb{Z}^+$, a budget of $\kappa(H - t)$ input locations for $t = 0, \dots, H - 1$, $\delta \in (0, 1)$, and $\lambda > 0$ are given. Then, the probability of

$$|Q_t^*(\pi^*(d_t), d_t) - Q_t^*(\pi^{\omega\epsilon}(d_t), d_t)| \leq 2\lambda + 2\omega$$

is at least $1 - \delta$ by setting N according to that in Theorem 1.

Proof.

$$\begin{aligned} & Q_t^*(\pi^*(d_t), d_t) - Q_t^*(\pi^{\omega\epsilon}(d_t), d_t) \\ & \leq Q_t^*(\pi^*(d_t), d_t) - \underline{Q}_t^*(\pi^{\omega\epsilon}(d_t), d_t) + 2\lambda + \omega \\ & \leq |Q_t^*(\pi^*(d_t), d_t) - \underline{Q}_t^*(\pi^{\omega\epsilon}(d_t), d_t)| + 2\lambda + \omega \\ & = |Q_t^*(\pi^*(d_t), d_t) - \max_{s_{t+1} \in \mathcal{A}(s_t)} \underline{Q}_t^*(s_{t+1}, d_t)| + 2\lambda + \omega \\ & = |V_t^*(d_t) - \underline{V}_t^*(d_t)| + 2\lambda + \omega \\ & \leq \omega + 2\lambda + \omega \\ & = 2\lambda + 2\omega \end{aligned}$$

where the first inequality is due to Theorem 6, the first equality is further due to implication I discussed just after (46), the second equality is due to the definitions of V_t^* (5) and \underline{V}_t^* (see lines 15 and 34 in Algorithm 1), and the last inequality is due to (45). \square

Lemma 8. Suppose that the observations d_t , $H \in \mathbb{Z}^+$, a budget of $\kappa(H - t)$ input locations for $t = 0, \dots, H - 1$, $\delta \in (0, 1)$, and $\lambda > 0$ are given. Then,

$$Q_t^*(\pi^*(d_t), d_t) - \mathbb{E}_{\pi^{\omega\epsilon}(d_t)}[Q_t^*(\pi^{\omega\epsilon}(d_t), d_t)] \leq 2\lambda + 2\delta\lambda + 2\omega + 4\delta\theta$$

where θ is previously defined in Theorem 2.

Proof. By Lemma 7, the probability of $|Q_t^*(\pi^*(d_t), d_t) - Q_t^*(\pi^{\omega\epsilon}(d_t), d_t)| \leq 2\lambda + 2\omega$ is at least $1 - \delta$. Otherwise, the probability of $|Q_t^*(\pi^*(d_t), d_t) - Q_t^*(\pi^{\omega\epsilon}(d_t), d_t)| > 2\lambda + 2\omega$ is at most δ . In the latter case,

$$\begin{aligned} & |Q_t^*(\pi^*(d_t), d_t) - Q_t^*(\pi^{\omega\epsilon}(d_t), d_t)| \\ & \leq |Q_t^*(\pi^*(d_t), d_t) - Q_t^{\omega\epsilon}(\pi^{\omega\epsilon}(d_t), d_t)| + |Q_t^{\omega\epsilon}(\pi^{\omega\epsilon}(d_t), d_t) - Q_t^*(\pi^{\omega\epsilon}(d_t), d_t)| \\ & \leq \max_{s_{t+1} \in \mathcal{A}(s_t)} |Q_t^{\omega\epsilon}(s_{t+1}, d_t) - Q_t^*(s_{t+1}, d_t)| + 2\lambda + \omega + 2\theta \\ & \leq 2\lambda + \omega + 2\theta + 2\lambda + \omega + 2\theta \\ & = 4\lambda + 2\omega + 4\theta \end{aligned} \tag{48}$$

where the first inequality is due to triangle inequality and the last two inequalities are due to (47) (i.e., implication II). Recall that $\pi^{\omega\epsilon}$ is a stochastic policy due to its use of stochastic sampling in \underline{Q}_t^* (see lines 13 and 32 in Algorithm 1), which implies that $\pi^{\omega\epsilon}(d_t)$ is a random variable. Then,

$$\begin{aligned} & Q_t^*(\pi^*(d_t), d_t) - \mathbb{E}_{\pi^{\omega\epsilon}(d_t)}[Q_t^*(\pi^{\omega\epsilon}(d_t), d_t)] \\ & = \mathbb{E}_{\pi^{\omega\epsilon}(d_t)}[Q_t^*(\pi^*(d_t), d_t) - Q_t^*(\pi^{\omega\epsilon}(d_t), d_t)] \\ & \leq (1 - \delta)(2\lambda + 2\omega) + \delta(4\lambda + 2\omega + 4\theta) \\ & = 2\lambda + 2\delta\lambda + 2\omega + 4\delta\theta \end{aligned}$$

where the expectation is with respect to random variable $\pi^{\omega\epsilon}(d_t)$ and the inequality follows from Lemma 7 and (48). \square

Theorem 7. Suppose that the observations d_0 , $H \in \mathbb{Z}^+$, a budget of κH input locations, and an arbitrarily user-specified loss bound $\epsilon > 0$ are given and Algorithm 1 terminates at $\omega \triangleq \bar{V}_0^*(d_0) - \underline{V}_0^*(d_0)$ (see line 46 in Algorithm 1). Then, $V_0^*(d_0) - \mathbb{E}_{\pi^{\omega\epsilon}}[V_0^{\pi^{\omega\epsilon}}(d_0)] \leq 2\omega H + \epsilon$ by setting θ according to Theorem 2, $\delta = \epsilon/(8\theta H)$ and $\lambda = 1/(4H/\epsilon + 1/(2\theta))$ in Theorem 1 to yield

$$N = \mathcal{O}\left(\frac{\kappa^{2H}}{\epsilon^2} \log \frac{\kappa A}{\epsilon}\right).$$

Proof. We will give a proof by induction on t that

$$V_t^*(d_t) - \mathbb{E}_{\pi^{\omega\epsilon}}[V_t^{\pi^{\omega\epsilon}}(d_t)] \leq (2\lambda + 2\delta\lambda + 2\omega + 4\delta\theta)(H - t). \tag{49}$$

When $t = H - 1$ (i.e., base case),

$$\begin{aligned} & V_{H-1}^*(d_{H-1}) - \mathbb{E}_{\pi^{\omega\epsilon}}[V_{H-1}^{\pi^{\omega\epsilon}}(d_{H-1})] \\ & = Q_{H-1}^*(\pi^*(d_{H-1}), d_{H-1}) - \mathbb{E}_{\pi^{\omega\epsilon}}[Q_{H-1}^{\pi^{\omega\epsilon}}(\pi^{\omega\epsilon}(d_{H-1}), d_{H-1})] \\ & = Q_{H-1}^*(\pi^*(d_{H-1}), d_{H-1}) - \mathbb{E}_{\pi^{\omega\epsilon}(d_{H-1})}[R(\pi^{\omega\epsilon}(d_{H-1}), d_{H-1})] \\ & = Q_{H-1}^*(\pi^*(d_{H-1}), d_{H-1}) - \mathbb{E}_{\pi^{\omega\epsilon}(d_{H-1})}[Q_{H-1}^*(\pi^{\omega\epsilon}(d_{H-1}), d_{H-1})] \\ & \leq 2\lambda + 2\delta\lambda + 2\omega + 4\delta\theta \end{aligned}$$

where the first equality is due to (3) and (5), the second equality is due to (3), the third equality is due to (5), and the inequality is due to Lemma 8. So, (49) holds for the base case. Supposing (49) holds for $t + 1$ (i.e., induction hypothesis), we will prove that it holds for $t = 0, \dots, H - 2$:

$$\begin{aligned}
& V_t^*(d_t) - \mathbb{E}_{\pi^{\omega^\epsilon}}[V_t^{\pi^{\omega^\epsilon}}(d_t)] \\
&= Q_t^*(\pi^*(d_t), d_t) - \mathbb{E}_{\pi^{\omega^\epsilon}}[Q_t^{\pi^{\omega^\epsilon}}(\pi^{\omega^\epsilon}(d_t), d_t)] \\
&= Q_t^*(\pi^*(d_t), d_t) - \mathbb{E}_{\pi^{\omega^\epsilon}}[Q_t^*(\pi^{\omega^\epsilon}(d_t), d_t)] + \mathbb{E}_{\pi^{\omega^\epsilon}}[Q_t^*(\pi^{\omega^\epsilon}(d_t), d_t)] - \mathbb{E}_{\pi^{\omega^\epsilon}}[Q_t^{\pi^{\omega^\epsilon}}(\pi^{\omega^\epsilon}(d_t), d_t)] \\
&= Q_t^*(\pi^*(d_t), d_t) - \mathbb{E}_{\pi^{\omega^\epsilon}(d_t)}[Q_t^*(\pi^{\omega^\epsilon}(d_t), d_t)] + \mathbb{E}_{\pi^{\omega^\epsilon}}[Q_t^*(\pi^{\omega^\epsilon}(d_t), d_t) - Q_t^{\pi^{\omega^\epsilon}}(\pi^{\omega^\epsilon}(d_t), d_t)] \\
&\leq 2\lambda + 2\delta\lambda + 2\omega + 4\delta\theta + \mathbb{E}_{\pi^{\omega^\epsilon}}[Q_t^*(\pi^{\omega^\epsilon}(d_t), d_t) - Q_t^{\pi^{\omega^\epsilon}}(\pi^{\omega^\epsilon}(d_t), d_t)] \\
&= 2\lambda + 2\delta\lambda + 2\omega + 4\delta\theta \\
&\quad + \mathbb{E}_{\pi^{\omega^\epsilon}}[\mathbb{E}_{z_{t+1}|\pi^{\omega^\epsilon}(d_t), d_t}[V_{t+1}^*(\langle \mathbf{s}_t \oplus \pi^{\omega^\epsilon}(d_t), \mathbf{z}_t \oplus z_{t+1} \rangle) - V_{t+1}^{\pi^{\omega^\epsilon}}(\langle \mathbf{s}_t \oplus \pi^{\omega^\epsilon}(d_t), \mathbf{z}_t \oplus z_{t+1} \rangle)]] \\
&= 2\lambda + 2\delta\lambda + 2\omega + 4\delta\theta \\
&\quad + \mathbb{E}_{\pi^{\omega^\epsilon}(d_t)}[\mathbb{E}_{z_{t+1}|\pi^{\omega^\epsilon}(d_t), d_t}[V_{t+1}^*(\langle \mathbf{s}_t \oplus \pi^{\omega^\epsilon}(d_t), \mathbf{z}_t \oplus z_{t+1} \rangle) - \mathbb{E}_{\pi^{\omega^\epsilon}}[V_{t+1}^{\pi^{\omega^\epsilon}}(\langle \mathbf{s}_t \oplus \pi^{\omega^\epsilon}(d_t), \mathbf{z}_t \oplus z_{t+1} \rangle)]]] \\
&\leq 2\lambda + 2\delta\lambda + 2\omega + 4\delta\theta + \mathbb{E}_{\pi^{\omega^\epsilon}(d_t)}[\mathbb{E}_{z_{t+1}|\pi^{\omega^\epsilon}(d_t), d_t}[(2\lambda + 2\delta\lambda + 2\omega + 4\delta\theta)(H - t - 1)]] \\
&= (2\lambda + 2\delta\lambda + 2\omega + 4\delta\theta)(H - t)
\end{aligned} \tag{50}$$

where the first and fourth equalities are due to (3) and (5), the first inequality is due to Lemma 8, and the last inequality is due to the induction hypothesis.

From (50), when $t = 0$,

$$V_0^*(d_0) - \mathbb{E}_{\pi^{\omega^\epsilon}}[V_0^{\pi^{\omega^\epsilon}}(d_0)] \leq 2H(\lambda + \delta\lambda + \omega + 2\delta\theta) = 2\omega H + 2H(\lambda + \delta\lambda + 2\delta\theta).$$

Let $\epsilon = 2H(\lambda + \delta\lambda + 2\delta\theta)$ by setting $\lambda = 1/(4H/\epsilon + 1/(2\theta))$ and $\delta = \epsilon/(8\theta H)$. Consequently, using Lemma 7 and $\theta = \mathcal{O}(\kappa^{H+1/2})$ previously defined in Theorem 2,

$$N = \mathcal{O}\left(\frac{\kappa^{2H}}{\epsilon^2} \log \frac{\kappa A}{\epsilon}\right).$$

□

APPENDIX M AUXILIARY RESULTS

Lemma 9. $L_t(\mathbf{s}_t) = \mathcal{O}(\kappa^{H-t+1/2} \sqrt{H!/t!} (1 + \sigma_y^2/\sigma_n^2)^{H-t})$ for $t = 0, \dots, H - 1$.

Proof. Using Definition 1 followed by Lemma 10,

$$\begin{aligned}
& L_t(\mathbf{s}_t) \\
&= \max_{\mathbf{s}_{t+1} \in \mathcal{A}(\mathbf{s}_t)} \sqrt{\kappa} \alpha(\mathbf{s}_{t+1}) + L_{t+1}(\mathbf{s}_{t+1}) \sqrt{1 + \alpha(\mathbf{s}_{t+1})^2} \\
&= (\sqrt{\kappa} + L_{t+1}(\mathbf{s}_t \oplus \mathbf{s}_{t+1}^*)) \mathcal{O}(\kappa \sqrt{t+1} (1 + \sigma_y^2/\sigma_n^2))
\end{aligned} \tag{51}$$

for $t = 0, \dots, H - 1$ where $\mathbf{s}_{t+1}^* \triangleq \operatorname{argmax}_{\mathbf{s}_{t+1} \in \mathcal{A}(\mathbf{s}_t)} L_{t+1}(\mathbf{s}_t \oplus \mathbf{s}_{t+1})$.

We will now give a proof by induction on t . When $t = H - 1$ (i.e., base case), since $L_H(\mathbf{s}_H) = 0$ (Definition 1), it follows from (51) that $L_{H-1}(\mathbf{s}_{H-1}) = \mathcal{O}(\kappa^{3/2} \sqrt{H} (1 + \sigma_y^2/\sigma_n^2))$. Supposing Lemma 9 holds for $t + 1$ (i.e., induction hypothesis), we will prove that it holds for $0 \leq t < H - 1$:

$$\begin{aligned}
& L_t(\mathbf{s}_t) \\
&= (\sqrt{\kappa} + \mathcal{O}(\kappa^{H-t-1/2} \sqrt{H!/(t+1)!} (1 + \sigma_y^2/\sigma_n^2)^{H-t-1})) \mathcal{O}(\kappa \sqrt{t+1} (1 + \sigma_y^2/\sigma_n^2)) \\
&= \mathcal{O}(\kappa^{H-t+1/2} \sqrt{H!/t!} (1 + \sigma_y^2/\sigma_n^2)^{H-t})
\end{aligned}$$

where the first equality follows from (51) and the induction hypothesis. □

Lemma 10. $\alpha(\mathbf{s}_{t+1}) = \mathcal{O}(\kappa \sqrt{t+1} (1 + \sigma_y^2/\sigma_n^2))$ for $t = 0, \dots, H - 1$ where the function α is previously defined in Lemma 1.

Proof. Let $\Xi\Lambda\Xi^\top$ be an eigendecomposition of the symmetric and positive definite $\Sigma_{\mathbf{s}_t\mathbf{s}_t}$ where Ξ is a matrix whose columns comprise an orthonormal basis of eigenvectors of $\Sigma_{\mathbf{s}_t\mathbf{s}_t}$ and Λ is a diagonal matrix with positive eigenvalues of $\Sigma_{\mathbf{s}_t\mathbf{s}_t}$. From the definition of the function α in Lemma 1,

$$\begin{aligned}
& \alpha(\mathbf{s}_{t+1})^2 \\
&= \|\Sigma_{\mathbf{s}_{t+1}\mathbf{s}_t} \Sigma_{\mathbf{s}_t\mathbf{s}_t}^{-1}\|_F^2 \\
&= \|\Sigma_{\mathbf{s}_{t+1}\mathbf{s}_t} \Xi\Lambda^{-1}\Xi^\top\|_F^2 \\
&= \text{Tr}(\Sigma_{\mathbf{s}_{t+1}\mathbf{s}_t} \Xi\Lambda^{-1}\Xi^\top \Xi\Lambda^{-1}\Xi^\top \Sigma_{\mathbf{s}_t\mathbf{s}_{t+1}}) \\
&= \text{Tr}(\Sigma_{\mathbf{s}_{t+1}\mathbf{s}_t} \Xi\Lambda^{-2}\Xi^\top \Sigma_{\mathbf{s}_t\mathbf{s}_{t+1}}) \\
&= \text{Tr}(\Sigma_{\mathbf{s}_{t+1}\mathbf{s}_t} \Xi(\xi^{-2}I)\Xi^\top \Sigma_{\mathbf{s}_t\mathbf{s}_{t+1}}) - \text{Tr}(\Sigma_{\mathbf{s}_{t+1}\mathbf{s}_t} \Xi(\xi^{-2}I - \Lambda^{-2})\Xi^\top \Sigma_{\mathbf{s}_t\mathbf{s}_{t+1}}) \\
&\leq \text{Tr}(\Sigma_{\mathbf{s}_{t+1}\mathbf{s}_t} \Xi(\xi^{-2}I)\Xi^\top \Sigma_{\mathbf{s}_t\mathbf{s}_{t+1}}) \\
&= \xi^{-2} \text{Tr}(\Sigma_{\mathbf{s}_{t+1}\mathbf{s}_t} \Sigma_{\mathbf{s}_t\mathbf{s}_{t+1}}) \\
&= \xi^{-2} \|\Sigma_{\mathbf{s}_{t+1}\mathbf{s}_t}\|_F^2 \\
&= \mathcal{O}(\kappa^2(t+1)(1 + \sigma_y^2/\sigma_n^2)^2)
\end{aligned} \tag{52}$$

where ξ is the smallest eigenvalue in Λ , the second equality is due to $\Sigma_{\mathbf{s}_t\mathbf{s}_t}^{-1} = \Xi\Lambda^{-1}\Xi^\top$, the third and seventh equalities are due to $\|\Phi\|_F^2 = \text{Tr}(\Phi\Phi^\top)$ for any matrix Φ (see Section 10.4.3 in [41]), the fourth equality follows from the orthonormality of Ξ , the fifth equality is due to linearity of trace, the inequality is due to the positive semidefinite $(\xi^{-2}I - \Lambda^{-2})$ since ξ^{-2} is the largest eigenvalue in Λ^{-2} , and the last equality follows from (a) $\|\Sigma_{\mathbf{s}_{t+1}\mathbf{s}_t}\|_F^2 = \mathcal{O}(\kappa^2(t+1)(\sigma_y^2 + \sigma_n^2)^2)$ since every prior covariance is not more than $\sigma_y^2 + \sigma_n^2$ and the length of \mathbf{s}_t is $\mathcal{O}(\kappa(t+1))$ and (b) $\xi \geq \sigma_n^2$ since $(\Sigma_{\mathbf{s}_t\mathbf{s}_t} - \sigma_n^2 I)$ is positive semidefinite and hence $\xi - \sigma_n^2$ is nonnegative. \square